TEKNILLINEN KORKEAKOULU

Sähkö- ja tietoliikennetekniikan osasto

Veli Voipio

Wideband Patch Antenna Array Techniques for Mobile Communications

Lisensiaatintutkimus, joka on jätetty opinnäytteenä tarkastettavaksi tekniikan lisensiaatin tutkintoa varten Espoossa 20.10.1998

Työn valvoja

Professori Pertti Vainikainen

Työn toinen tarkastaja

TkT Anssi Toropainen

Helsinki University of Technology **Abstract of the licentiate thesis**

Author: Veli Voipio

Name of the thesis: Wideband patch antenna array techniques for mobile communications

Date: October 20, 1998 **Number of pages:** 109

Department: Department of Electrical and Communications Engineering

Professorship: S-26 Radio Engineering

Supervisor: Professor Pertti Vainikainen

Instructor: D.Sci (Tech.) Anssi Toropainen

The adaptive antenna systems for mobile communications require most likely small antenna arrays. The exact requirements are not known yet, but some background information was possible to collect: The spatial filter adaptation process can attenuate interferences that are much stronger than the desired signal, but for initial detection of the desired signal it is beneficial to have low sidelobes and a single main beam with beamwidth of about 10°.

Four main areas are studied: a small wide bandwidth patch antenna, a patch antenna with high separation of two polarizations, how to decrease mutual coupling, and how to make use of depth in an antenna array.

The 3D FDTD electromagnetic simulation method was used successfully in obtaining mutual coupling, radiation pattern and impedance bandwidth information.

The wideband patch antenna is based on thick substrate which gave new challenges for the design, because of the inductance caused by the probe feed. The problems were solved, and a design method is suggested. A wide impedance bandwidth, 35% was reached. A byproduct was a concept of the antenna fed patch antenna. Its precise operation is a subject of further study.

The half-wave stacked patch antenna was developed for sufficient bandwidth (10%) and cross-polarization separation for the wideband radio channel sounding. A concept of dielectric feed was developed to further reduce the cross-polar level, and the result was cross-polarization separation of better than 20 dB over ±57° angular range in the implemented prototype.

Two ways to reduce the mutual coupling were studied by simulations: a metal wall between antenna elements, and a dielectric wall between the elements. The metal wall proved to be useless, because the vertical component of the electric field crosses the wall. The dielectric partially conductive wall decreased the mutual coupling 16 dB, but changed the radiation pattern, reduced efficiency and increased the cross-polar level. Therefore neither of these methods was used in the further development of the array. Increasing the element spacing from $0.5 \cdot \lambda$ to $0.7 \cdot \lambda$ is suggested.

The effect of depth in an antenna array was studied in the case of a cylindrical array. It was shown theoretically that there are advantages in suitable depth and phasing. One example is an array of 35 elements that has 12.1° beamwidth and sidelobe level below 20 dB. It has a comparable radiation pattern and smaller size than an omnidirectionally scanning arrangement of six panels of seven-element linear antenna arrays made of similar antenna elements.

Keywords: Adaptive antenna, array antenna, FDTD, mobile communications, patch antenna

Teknillinen korkeakoulu **Tiivistelmä lisensiaatintutkimuksesta**

Tekijä: Veli Voipio

Työn nimi: Laajakaistainen mikroliuska-antenniryhmä liikkuvalle tietoliikenteelle

Päivämäärä: 20.10.1998 **Sivumäärä:** 109

Osasto: Sähkö- ja tietoliikennetekniikan osasto

Professuuri: S-26 Radiotekniikka

Työn valvoja: Professori Pertti Vainikainen

Työn ohjaaja: TkT Anssi Toropainen

Siirtyvän tietoliikenteen adaptiivinen antenni muodostetaan todennäköisiseti pienikokoisesta antenniryhmästä. Täsmällisiä vaatimuksia ei vielä tiedetä, mutta oli mahdollista koota taustatietoa: Adaptiivinen tilasuodatin voi vaimentaa häiriöitä jotka ovat huomattavasti haluttua signaalia voimakkaampia. Jotta haluttu signaali voidaan havaita, antennilla tulisi olla matala sivukeilataso ja yksi pääkeila, jonka leveys on noin 10°.

Työssä on tutkittu neljää pääasiallista aihetta: pientä laajakaista-antennia, mikroliuska-antennia, joka erottelee kaksi polarisaatiota hyvin, keskinäiskytkennän vähentämistä, ja antenniryhmän syvyyden hyväksikäyttöä.

Työssä on käytetty kolmiulotteista FDTD-tyypistä sähkömagneettista simulointi-menetelmää jota käytettiin tuloksellisesti seuraavissa simuloinneissa: keskinäis-kytkentä, suuntakuvio, impedanssikaistanleveys.

Laajakaistainen mikroliuska-antenni perustuu paksun substraatin käyttöön, josta seurasi suunnitteluvaikeuksia pitkän keskijohdinsyötön aiheuttaman induktanssin takia. Suunnitteluongelmiin löydettiin ratkaisu, ja suunnittelumenetelmä esitellään. Laaja 35% impedanssikaistanleveys saavutettiin. Sivutuotteena syntyi antenni-syötetyn mikroliuska-antennin käsite, joka antaa aihetta jatkotutkimuksiin.

Jotta saavutettaisiin riittävä kaistanleveys (10%) ja ristipolarisaatioerottelu laajakaistaista kanavaluotausta varten, kehitettiin kaksikerroksinen puolen aallon mikroliuska-antenni. Ristipolarisaation vähentämiseksi edelleen muunnettiin antennin syöttö dielektrisen kappaleen välityksellä tapahtuvaksi. Rakennetun prototyypin polarisaatioerottelu on parempi kuin 20 dB yli ±57° keilauskulman alueella.

Keskinäiskytkennän vähentämiseksi tutkittiin kahta mahdollisuutta simulointien avulla: metalliseinä ja dielektrinen seinä antennielementtien välillä. Metalliseinä ei toiminut odotetusti, koska sähkökentän vertikaalinen komponentti ylittää seinän. Dielektrinen osittain johtava seinä vähensi keskinäiskytkentää 16 dB, mutta muutti suuntakuviota, alensi hyötysuhdetta ja lisäsi ristipolarisaatiota. Siksi kumpaakaan menetelmää ei otettu käyttöön antenniryhmissä. Elementtivälin lisäämistä $0{,}5\cdot\lambda$:sta $0{,}7\cdot\lambda$:aan ehdotetaan.

Sylinteriantenniryhmän avulla tutkittiin, kuinka antenniryhmän syvyyttä voi käyttää hyväksi. Laskelmien avulla osoitettiin, että sopivilla syvyyseroilla ja vaiheistuksella voi saavuttaa etuja. Esimerkkinä tarkastellaan 35 elementin ryhmää jolla on 12.1° keilanleveys ja sivukeilataso alle 20 dB. Ryhmä on pienempikokoinen kuin vastaavalla säteilykuviolla varustettu kuudesta suorasta antenniryhmästä koottu ympärikeilaava rakenne, kun kussakin ryhmässä on seitsemän samanlaista elementtiä kuin sylinteriryhmässä.

Avainsanat: Adaptiivinen antenni,ryhmäantenni, FDTD, siirtyvä tietoliikenne, mikroliuska-antenni

Preface

This thesis work has been carried out in Radio Laboratory at Institute of Radio Communications (IRC), Helsinki University of Technology (HUT), in a project called MAST funded by Technology Development Centre Finland (TEKES), Nokia, Sonera, and Finnet Group. I express my gratitude for having had the opportunity to participate in the project.

I would like to thank to professor Pertti Vainikainen for his guidance and suggestions concerning the work and D.Sc.(Tech.) Anssi Toropainen for his comments and professor Antti Räisänen for the opportunity to do postgraduate studies in this subject and Professor Keijo Nikoskinen for various help. I also thank M.Sc.(Tech.) Kimmo Kalliola, M.Sc.(Tech.) Jani Ollikainen, Lic.Sc.(Tech.) Päivi Haapala, M.Sc.(Tech.) Pauli Aikio and Lic.Sc.(Tech.) Heikki Valmu, and other colleagues at Radio laboratory of HUT for help and useful insights. I thank the technicians, particularly Eino Kahra and Lorenz Schmuckli for making antenna prototypes, and Harri Frestadius for the groundwork for the drawings. I thank Wihuri fund and Savo high technology fund for scholarships. Also I thank Mikkeli Polytechnic for the opportunity to use their radio laboratory and computer programs.

Thanks to my wife Heli for support, my son Teemu for patience and my son Riku in helping to solve computing problems.

Helsinki, October 20, 1998

Veli Voipio

Table of contents

Abbreviations

3D	Three-Dimensional
CDMA	Code Division Multiple Access
DSP	Digital Signal Processing
FDTD	Finite Difference Time Domain method
FEM	Finite Element Method
GSM	Global System for Mobile communications
HUT	Helsinki University of Technology
I	In-phase component
IRC	Institute of Radio Communications
LEO	Low Earth Orbiting satellite system
LMS	Least Mean Squares
MoM	Method of Moments
PCS	Personal Communication System
PEC	Perfect Electric Conductor
Q	Quadrature component
RF	Radio Frequency
SDMA	Space Division Multiple Access
TDMA	Time Division Multiple Access
TLM	Transmission Line Matrix
UHF	Ultra High Frequency band 300...3000 MHz
UMTS	Universal Mobile Telecommunication Services

Symbols

A	area
a_n	complex excitation amplitude of the n^{th} element
BER	bit error rate
BW	bandwidth
C	capacitance
C_A	capacitance of the antenna patch equivalent circuit
C_S	capacitance of the substrate capacitor
C_{SG}	capacitance between the lower plate of the substrate capacitor and ground
CF	cost factor
c	speed of light
d	distance between elements, element spacing
	distance between capacitive plates
f	frequency
E	magnitude of the electric field strength, components, E_x, E_y, E_z
$E(\hat{u})$	electric field strength to the direction of the unit vector $\hat{u}$
E_i	electric field strength towards the direction i
E_d	desired electric field strength towards the direction
f	frequency
$g_n(\hat{u})$	directivity of the n^{th} element in the direction of $\hat{u}$
h	thickness of the substrate, height of the patch antenna from the ground
I	Interference power
i	index
i_a	starting direction for the cost calculation around the main beam
i_b	ending direction for the cost calculation around the main beam
J	current density, components J_x, J_y, J_z
K	(frequencies available in a cell)/(frequencies allocated for the cellular operator)
k	wave number $2\pi/\lambda$
L	inductance
L_A	inductance of the antenna patch equivalent circuit
L_p	probe inductance
L_{ret}	return loss
l	horizontal length of the patch antenna
N	Number of antenna elements

n	element number (positive integer)
p	distance of the probe from the short
Q	resonator quality factor
Q_r	antenna radiation Q
r	radius
$\vec{r}_n$	position vector
R	resistance
R_A	resistance of the antenna patch equivalent circuit = radiation resistance
R_{Max}	maximum resistance
S	standing wave ratio
S_{11}	reflection from port 1
S_{21}	coupling from port 1 to port 2
SLL	sidelobe level
$SINR$	signal-to interference and noise ratio
$\hat{u}$	unit vector
w	width of the patch antenna
X_P	$j\cdot\ \omega\cdot\ L_P$
XPD	cross polarization discrimination
XPI	cross polarization isolation
XPL	cross polarization level
Z	impedance
Z_A	patch impedance
ε_r	relative permittivity
θ	elevation angle (*theta* in some computer printouts)
λ	wavelength
ρ	reflection coefficient
σ	conductivity
Φ	azimuth angle (*fi* in some computer printouts)
ω	angular frequency $2\cdot\ \pi\cdot\ f$

1. Introduction

The number of users of mobile communications is growing fast and there is a need to increase the channel capacity in dense user areas and to increase the range of the cells in sparsely populated areas. The mobile communications make use of the UHF frequency range, which is suitable in many aspects, but still does not allow enough channels to the users. The cellular system technology with power control and the time-division multiple access (TDMA) and the code division multiple access (CDMA) technologies already improve channel capacity significantly. In addition to those, the control of the antenna radiation pattern is seen as a very promising way to improve the capacity of the cellular systems. Also the International Telecommunications Union is promoting the use of adaptive antennas [32].

The antenna radiation pattern can be controlled electronically if an antenna array is used [57]. Therefore there is a need to develop antenna arrays and antenna elements for the arrays that could serve in an adaptively controlled antenna system for mobile communications and for the radio channel sounder in the research of mobile communications [37].

When developing a radio system using the array pattern control, one should be aware of the delay spread and the angular spread of the signals. These both can be measured with the help of an antenna array, where the amplitude and phase of the received pulses are measured and stored by a channel sounder system, giving the angles and timing of the received pulses. The adaptive antennas use similar arrays and elements as the channel sounder, so the sounder antenna array is included in this study.

The first scope is to research patch antenna elements. One requirement is sufficient bandwidth and another is small size [50]. An additional requirement is the ability to separate two polarizations. That ability could be also utilized in base stations, mobile sets and channel sounding. The second scope is to examine array designs made of patch antenna elements. The antenna array is required to have a narrow beam and low sidelobes, and as small physical size as reasonably possible [80].

The thesis is organized as follows: Chapter 2 presents the topics related to the adaptive array systems in general and highlights aspects related to the antenna array design. Chapter 3 describes the research scheme. Chapter 4 describes the design of three types of antenna elements. Chapter 5 describes design aspects of antenna arrays: reducing the mutual coupling with a wall between elements and a means of utilizing the depth in an antenna array.

2. Introduction to the adaptive antennas

Aspects of adaptive antenna systems affecting the design of the elements and the array are described in this chapter. A more detailed overview is given in [86]. The system requirements are described in Chapter 3.

2.1 Definitions

The basic definitions are found in Kraus [42]. An *adaptive antenna* can steer the beam towards the existing signal and generate nulls towards undesired signals. This is done it by means of internal feedback control while the antenna system is operating. On page 497: “Also, by suitable processing, performance may be further enhanced, giving *simulated patterns* of higher resolution and lower sidelobes. In addition, by appropriate sampling and digitizing the signals at the terminals of each element and processing them with a computer, a very intelligent *smart antenna* can, in principle be built.” Digital beamforming antennas can simultaneously direct *multiple* beams.

Smart antenna and intelligent antenna are sometimes alternative names for the adaptive antenna. Commercial ads use the term “smart” quite liberally, and a “smart antenna” may not be anything else than an antenna with several narrow switched beams.

Physically an adaptive antenna looks very much like an ordinary antenna, but has built-in control electronics and software. The adaptive antenna has an antenna array as input unit, and the array properties can be designed with known methods for many array configurations [12], [31].

Adaptive antennas are easiest to implement in land mobile base stations and in vehicle installed units. Handheld systems have size limitations. The future satellite systems could make use of the digital beamforming antennas, both in satellites [4], and in land fixed and mobile units [33]. Especially in the LEO systems the array antenna with signal processing compensates the changes of the direction of the communication caused by the movements of the satellites and the mobile [52].

2.2 Antenna system aspects

2.2.1 Diversity

The multipath propagation leads to correlated interference that causes fading. Diversity helps to overcome the effects of fading by providing two or more uncorrelated received signals of the transmitted signal [70].

Diversity reception requires appropriate combination. Selection combining is the simplest method and maximal ratio combining is the most efficient method [70]. Channel equalization can be seen as implicit multipath diversity combining. RAKE receiver multipath reception can be used in CDMA spread spectrum systems to alleviate the effects of frequency selective fading within the bandwidth [65][69][79].

Path diversity or macrodiversity can be considered in some cases. In this method, multiple base stations communicate with one mobile [64].

2.2.2 Beamforming: pointing and nulling

Beam switching is a simple way to add functionality. Electronic beam steering (beam pointing) does the same. Adaptive beamforming is a more advanced process: the antenna generates one or more beams towards the desired signal, and nulls toward the undesired signals. In that sense the adaptive antenna is also a spatial filter [13], [14], [25].

The type of the channel gives requirements the design of the antenna beam and null widths [11]. If the angular separation of two mobiles is small, the adaptive antenna can place a null between the two mobiles in order to maximize the separation [48]. Normally the nulls in an antenna radiation pattern are quite narrow [28]. If *N* is the number of elements, the degree of freedom is *N-1*, which means that *N-1* interferers can be canceled. In mobile communications the path angular spread is wider than the width of the nulls. The solution is to place multiple nulls to cover the interfering signal path angle, but then there are less nulls available for the rest of the interferers. The position of the nulls changes with frequency, which is a problem in wideband systems [26].

Superresolution is a DSP technique. The beam is like an inverted null, and that kind of beam is very narrow. The disadvantage is that superresolution is sensitive to noise, unknown sensor gain and phase variations across the array aperture [22].

Superdirectivity or supergain could be considered in mobile sets. In that case the antenna array is small. However, these techniques require accurate driver units to control the currents in the elements. Some currents are very high, so the power consumption rules out the use of superdirectivity in practice [42].

2.2.3 Adaptivity

Adaptivity in general is means that the system can improve its performance in the course of time [24]. The adaptive antenna uses all signal information available from antenna elements, seen as arbitrarily positioned sensors. The process can be seen as beamforming, but also as optimal combining or spatial filtering of the signals received by different antenna elements. The goal of the adaptation process is to minimize the bit error rate using digital signal processing.

The adaptive antenna can constructively use multipath signals coming from different directions and path delays. This corresponds to the idea of having several antenna beams to receive one user channel. An equalizer or a RAKE receiver are also needed.

Man-made noise and the interference by other mobile units tend to be directional [43]. This helps to identify interference sources, so that interference cancellation can be implemented. In CDMA systems the users are separated by codes, which means that the interference cancellation techniques can be used to cancel the interference caused by other users [15], [51]. Multiuser detection is a more developed form of it [61]. Spatial interference cancellation means that if a strong interference is coming from the same direction as the desired signal - and is also

simultaneously coming from a different direction, it can be used to cancel itself. Therefore the detection of the desired signal becomes easier.

2.2.4 Direction of arrival and distance estimation

The direction of arrival can be estimated if the antenna array parameters are well known. These parameters should also be regularly checked and the system consequently calibrated.

If two pulses come from the same direction, they can be separated by distance. Increasing the bandwidth of the signal increases the accuracy. However, the location is very difficult to interpret in the urban area because of the possible lack of the line-of-sight signal, and because of the time and angular dispersion caused by the diffraction and multipath propagation. With continuous signals this effect cannot be used directly, but the space-time processing in multiuser detection makes use of it [65].

In macrodiversity systems the location of the mobiles can be determined by triangulation.

2.2.5 Adaptation in transmitting

The adaptive transmitting antenna can control both the phase and the amplitude of the signal fed to each element, so it is capable to replicate the received signal pattern exactly when transmitting. However, in most systems the transmission frequency is different than the received frequency, and consequently the interference situation in transmission is not the same as in reception. In addition to that, different frequencies in the uplink and downlink radio paths don't correlate in multipath environment. Therefore this method is not useful.

The reflections that cause the strong components of the angular spread and negligible delay spread, are near the receiving end, both in downlink and uplink transmissions. It is not useful to reproduce those near reflection components in the transmission when most likely a single narrow beam towards the main signal direction will work better [17].

If the adaptive system can estimate the direction of arrival of the received signal from the mobile, then it is possible to point a single antenna beam towards the mobile, without any specific beamforming or adaptation.

The use of the time-division duplex (TDD) has also been suggested for CDMA. TDD means that the same frequency is used in the transmission and the reception, in different time slots. Then only the base station needs to estimate the received channel impulse response and the mobile can have a simpler receiver. When transmitting, the base station multiplies the signal to be sent to a user by the time-inverted complex conjugate of the received channel impulse response. This is a kind of "Pre-RAKE" system. In TDD it is also possible to allocate time slots asymmetrically, provided that the channel does not change too rapidly.

2.2.6 Channel characterization

The mobile radio channel is unpredictable because of the movement of the mobile unit and other objects. It is also subject to weather conditions and to the

interference caused by other users. The main outdoor phenomena are: path loss caused by the distance, shadowing for the non-line-of-sight situations, fading caused by the multipath effects, and the Doppler effect caused by the movement of the mobile [1], [16].

The multipath effect is caused by reflections. The reflections cause various delays in the received signal. One consequence of the multipath propagation is that the waves arrive from different directions to the receiving antenna. The variation of the received delays is called delay spread, and the variation of the arrival angles is called angular spread.

Since the radio waves are reflected at different points of the radio channel, there are several paths in the radio channel. That causes delay spread and angular spread in the channel. There is also delay spread and angular spread within the paths, called path delay spread and path angular spread [45].

Regarding wireless LAN systems indoors, there are several multipath components in progress and the first reflections are almost equally strong. In addition to that, for example fan propellers may cause fast-changing Doppler effects.

Two plane waves with different polarizations propagate differently. Therefore the antenna system can make use of the polarization diversity [74].

The radio channel behavior should be well known in order to design an optimal adaptive antenna system. Various statistical rules of thumb are available, computer simulations are being done, and theories are developed [40].

The most accurate information comes from the actual measurements. One example of a measuring system is the fast wideband channel sounder which is under development at IRC [39]. Channel modeling is discussed in [90].

Channel simulation is one possible way to find insight to the channel behavior. Ray tracing is used in microcell environments [29]. In indoor systems in small rooms the FDTD method has been used [72].

For this research the important values for design of the array can be obtained from [45]. That data applies to suburban situations, but it is useful as a starting point. The path angular spread is 5˚, and a 10˚ beam will include most beams in suburban areas. In suburban areas there is normally a main peak, not necessarily in the line-of-sight direction. Cross-polarization discrimination XPD = 6...10 dB and a 10 dB discrimination limit between main path and other paths is sufficient for the antenna [45]. In fixed radio links XPD = 45 dB in ideal conditions, but degrades under adverse transmission conditions [16].

2.2.7 Cellular network system aspects

The adaptive antenna makes it possible to use space division multiple access (SDMA). It means that the system can allocate the same channel (frequency and time slot) for several users in the same cell, and all cells can use the full frequency range allocated to the operator. This could change the nature of the network planning. SDMA may work in larger outdoor cells, but not in indoor cells, when there are several equally strong multipaths. An adaptive antenna may still be useful in indoor cells, helping in CDMA detection.

The multiuser detection also helps in interference canceling [23], and the multiuser detection system can co-operate with the adaptive antenna array control system. In addition to SDMA and multiuser detection, one can add more intelligence in the network. For example the vehicle locations or movements can be predicted to some extent, and that information could be added to speed up the antenna adaptation process.

2.3 Building blocks of the current adaptive antenna systems

2.3.1 Antenna structures

The array structure could be linear, planar, circular, cylindrical, or spherical. A spherical array or a cylindrical array with a ground plane may be feasible if the antenna element is directional, like a microstrip patch antenna element [58]. The array can be sparse (having wide element spacing), since the adaptive processing can minimize the effects of the grating lobes.

The antenna array inherently has some space diversity because of the size. On the other hand, increasing the size just to achieve diversity gain is normally not practical in cellular systems using compact base stations.

The array should have antennas in two orthogonal polarizations with sufficient cross-polarization discrimination in order to make use of the polarization diversity.

Mobile handheld antennas, like in the personal handheld phones, palmtop or laptop computers cause limitations in adaptive antenna design. The physical size of the handheld units is small, but the antenna array system works better if it is large.

Mobile vehicular antenna setup has various limitations and possibilities [21]: Cars may need to be designed so that the antennas are hidden and as well placed in favorable positions from the communications point of view. For trucks the positioning of antenna is much easier because large surfaces and sufficient height is available.

2.3.2 Transceiver technology in adaptive antennas

The phased array antenna can direct the beam electronically. This is based on the ability to control the amplitude and phase of the individual antenna elements. The scan angle depends on the phasing and the element spacing compared to the wavelength. Amplitude control is implemented using amplifiers with gain control, or with digital multiplication. The phase control is more complicated [8].

The phase shifting can be done using analog phase shifters but this technique works well for one beam only. The trend in the beamforming technology implementation is from RF phase shifting to baseband digital signal processing [55]. In the reception by digital beamforming an I/Q demodulator is normally used to preserve the phase information of the baseband signal, and the analog baseband signal can be converted digital to provide the digital signal for several beamforming processes. Then the phase shift and amplitude are controlled numerically. A similar technique can be used in transmission.

For wideband arrays a delay-controlled array is better than a phased array. In a phase-controlled array there is a grating effect: the beam and null directions are slightly different at different frequencies, because the element spacing compared to the wavelength varies with frequency. Delay control can be implemented using delay lines, similar as equalizers, or it can be implemented as digital signal processing [26].

2.3.3 Adaptive control

One way to describe the operation of the adaptive antenna is that the signals received by the elements are multiplied with complex weights and then added together in order to produce a spatially filtered signal. The gain and the phase shifts in the signals from the different elements are determined by a signal processor control unit. The control unit assigns the values for the weights for each channel. The control unit can be preprogrammed, but normally it uses appropriate search algorithms (like LMS) or neural networks [55], [43]. This search makes the process adaptive, which means that the performance of the filter improves with time.

In current adaptive antennas the control unit uses a multidimensional search algorithm to maximize the signal to interference and noise ratio. In digital systems it means minimizing the bit error rate (BER). When seen as a beamforming process, the algorithm sets the nulls towards the interferences while the main beam stays towards the signal direction as much as possible.

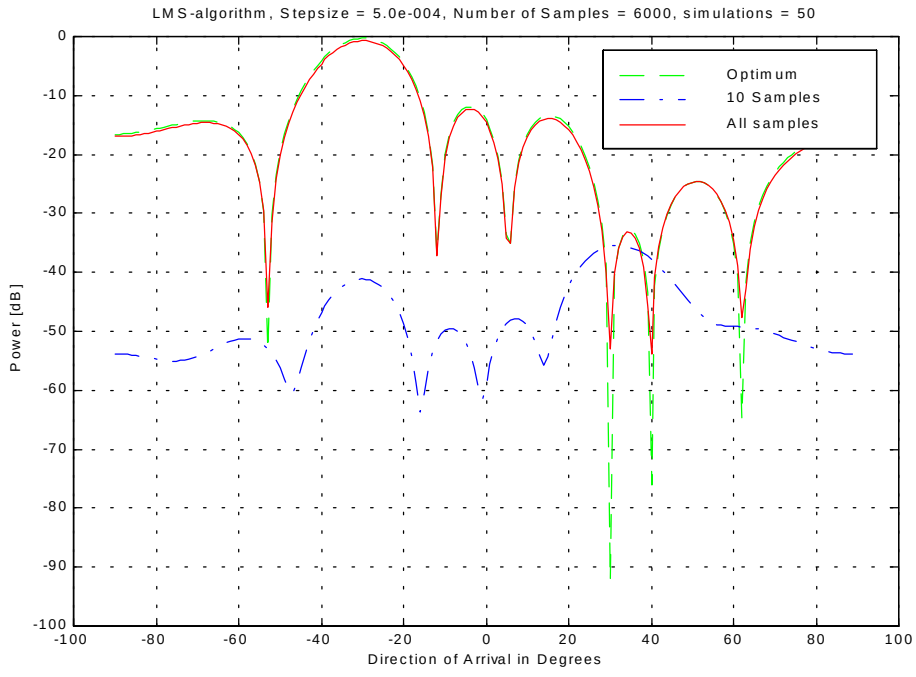

Figure 1. An example of LMS beamforming, calculated as an exercise. The beamform after 10 simulations is shown, and the beamform after all the simulations is shown. The beamform can be seen approaching the optimum beamform. The desired signal is coming from the -30° direction. The interference 1 is coming from the 30° direction and it is 25 dB above the signal level. The interference 2 is coming from the 40° direction and it is 15 dB above the signal level. The array is linear and has 7 elements.

A key point here is that the interfering signals can be far stronger than the desired signal and the system can still adapt, Figure 1. In that figure the adaptive antenna adjusts low gains ("nulls") towards the interferers, and the highest gain towards the desired signal as close as possible. There are two interfering signals, 25 dB and 15 dB above the signal level, nevertheless, the final signal to interference ratio (*SINR*) is 15 dB. However, low sidelobes are needed to help the beamforming system to initially detect the desired signal, and that has an effect to the array structure and element design.

2.4 Commercial approaches and academic research groups in the area of adaptive antennas

Some commercial enterprises in the field of the adaptive antenna arrays:

- ArrayComm (Intellicell, PCS 1900 trial in 1996 http://www.arraycomm.com/products/pindex.html/
- Celwave (12-beam switched beam base station, adaptive SmartSystem base station) http://www.celwave.com/
- ERA Technology http://www.era.co.uk/div80/bc82/smartant/tsunami2/t2trials.htm/
- Hagenuk (with EU project Tsunami) [81]
- Metawave (12-beam switched beam), http://www.metawave.com/
- Mitsubishi (doing research in digital beamforming antennas)
- NorTel (SmartBTS base station) http://www.nortel.com/home/press/1995b/ntbts44.html
- Rafael (in USA and Israel)
- Raytheon (DIVERSITY) http://www.raytheon.com/
- Sinclair, http://www.sinctech.com/
- Thomson (adaptive antenna, AMSAR project).

Some active research groups in the field of the adaptive antenna array:

- Aalborg University, Denmark – Center for Personkommunikation (EU project Tsunami) [10], http://www.kom.auc.dk/CPK/
- MacMaster University, Canada – Wireless Technology Group (CRL project, John Litva) [55], http://www.crl.mcmaster.ca/
- Royal Institute of Technology, Sweden, http://www.s3.kth.se/
- Stanford University, USA, California - Smart antenna research group, http://www-isl.stanford.edu/groups/SARG/
- TU-Wien, Austria (Joseph Fuhl), http://www.tuwien.ac.at/nthft/
- University of Bristol, UK – Center for Communications Research, http://www.fen.bris.ac.uk/elec/research/ccr/ccr.html/
- University of Kaiserlautern, Germany – Research Group for RF Communications, http://www.e-technik.uni-kl.de/
- University of Kansas, USA – Kansas Integrated Phased Array Antenna, http://www.trio.ca/asp-1.htm/
- University of Texas at Austin, USA – Telecommunications and Information Systems engineering, http://www.ece.utexas.edu/projects/tise/

- Virginia Tech, USA – Center for wireless Telecommunications [70], http://www.cwt.vt.edu/ – Mobile and Portable Radio Research Group, http://www.mprg.ee.vt.edu/

Related sources of information:

- IMT-2000 http://www.imt-2000.com/
- Adaptive antennas http://www.webproforum.com/arraycomm/

3. Research scheme

3.1 Setting

3.1.1 Requirements for adaptive antenna arrays and elements in the mobile communications environment

The adaptive antenna array is an complex and intrinsically large item. On the contrary, any antenna for mobile communications should be small and also reasonably priced. The size limitation is most urgent in handheld mobile units. The laptop computer, vehicular installations and the base station have some more space for an antenna array or for unrestrained antenna positions.

Base stations need wideband antennas. A wideband antenna tends to be large due to the laws of the antenna radiation physics. A mobile unit could use a small electronically tunable narrowband antenna.

UMTS may need bandwidth of 20% (1880...2280 MHz). Including DCS-1800 would increase the bandwidth requirement to 28%. Some applications may use only part of the available bandwidth, but since the duplex distance is 190 MHz, the minimum bandwidth is 10% [36]. The typical return loss requirement is at least 10 dB for base stations and 6 dB for mobile handsets. The requirement for the channel sounder at IRC is 2154 MHz carrier frequency and 100 MHz (5%) bandwidth. The conventional patch antennas have only a narrow bandwidth, therefore special techniques are needed here to achieve the required bandwidth.

Reducing the size of a directive antenna is difficult, because the directivity is inversely proportional to the dimensions of the antenna system.

The total coverage of the array depends on situation, some situations need omnidirectional coverage, and wall installations need 180° coverage. At the base station the antenna often should have sectorized coverage. The antenna array should be able to scan within the sector. Therefore a sectorized planar antenna array and cylindrical array should be considered here.

The base station antenna element for this study should be able to separate two polarizations, and this is also desirable in the antenna in the mobile unit. $XPD >$ 20 dB between ±30° was taken as design goal, based on section 2.2.6.

The antenna array should have low level of sidelobes and narrow beamwidth which help to find a low level signal among stronger interferers, before the interference canceling process takes place. The backlobes should be minimized because most reflections come from the rear of the antenna [9]. Sidelobe and backlobe levels should be at least –10 dB, preferably –20 dB.

The beamwidth of 10° may be narrow enough for a base station antenna, since the path angular spread is roughly 10° [45]. For the research purposes the beamwidth could be made narrower, if easily achievable. For a linear array a reasonable scan angle is needed, at least ±30°. In the cylindrical antenna array it is often sufficient to cover the scanning angle by commutating. It is also useful to study some modified geometries.

Antenna arrays normally have problems related to mutual coupling, which is researched here.

The adaptive antenna has a complex electronic control system, but this doesn't seem to be the issue, since the development in microelectronics and computer software alleviates the situation.

Reasonable costs and easy manufacture with adequately tight tolerances are required in practical applications. Therefore this research pays attention to those aspects, although is not tied to that restriction.

3.1.2 Antenna system nonidealities

As a technical system the antenna has many nonidealities which can be divided in the following categories: element position errors, mutual coupling, mismatches, quantization in digital conversion and receiver nonlinearity [55].

The element position can be $\lambda/10$ off its intended position without affecting too much the performance of the array. A total failure of an element does not prevent the array from the beamforming operation, it just degrades [46]. The misalignment of the elements reduces the polarization separation of the array.

Three assumptions are often used in antenna array calculations: 1. Currents or fields are proportional to applied excitations, 2. The distribution of current or aperture field is the same for each radiator, 3. The distribution does not change as the array is scanned [58]. In practice, the mutual coupling between radiating elements results in both modification of the element radiation pattern and also variations in the element feeding which together distort the array pattern. In scanned arrays, these effects are scan angle sensitive [35]. These affect the scanning bandwidth and the maximum scanning angle.

The mutual coupling should be minimized by hardware design or compensated by software. According to Southall [75] adaptive control or neural systems can compensate an uncalibrated structure in the reception. This calibration data is useful when doing the adaptive transmission.

Design, manufacturing and installation tolerances affect the performance of the antennas. There are variations in the size, material (especially substrates), position (also direction, rotation), form (soldering can deform straight plates), component tolerances and joints. Corrosion can affect joints electrically after the antenna is taken in use. These cause variations in the antenna element impedance and radiation pattern, both causing radiation pattern variations in the array.

Surface waves are not expected to cause problems when using an "air-substrate" antenna [58]. Some kind of traveling wave may emerge in the periodic structures in the antenna array .

Power handling capability can become a problem when using microstrip feeders, because of the high conductor loss in the strip. The plastic foam substrate may boost the internal thermal effects.

The joints between two different metals can cause nonlinear effects. Also corroded joints cans cause nonlinear effects. Nonlinear effects cause third-order intermodulation which can be disturbing in power transmission.

When the antenna array is installed there are certain errors that are just part of the normal operation. The temperature range where the antenna has to function can be wide and the antenna dimensions vary with the temperature. The heat caused by direct sunshine can change the operating characteristics of and active antenna, or even deform the antenna structure. Wind forces can cause vibration, bending and misdirection. The feeder connections can corrode. The antenna system has to be designed to endure those conditions.

Tilting the antenna downwards will help in snow, ice and rain problems. The warming caused by antenna transmitter power alleviates these effects. Any structures, vegetation, or moving objects around the base station antennas can change the radiation pattern. A radome protects from corrosion caused by the climate or pollutive gases to some extent. Vehicle use will cause shock, vibration, temperature cycling and moisture on antennas. Thunderbolts are common, so the antenna should be protected, especially in towers.

3.2 Research subjects

This study concentrates on antenna elements and on the theoretical study of cylindrical array as main topics. Some initial study of mutual coupling is also done. Attention is paid to effects and other topics mentioned in 3.1 when significant.

3.2.1 Elements for the base station antenna array

A triangular quarter-wave antenna element with walls was chosen for research, and a quarter-wave rectangular patch, because they are smaller than half-wave patch antennas, both with probe feeds, Figure 51.

Increasing the thickness of substrate increases the bandwidth, since the radiating aperture at the end of the patch increases, and radiated energy increases compared to stored energy. Increasing the width of the patch has the same effect. Lowering the substrate permittivity ε_r helps to increase the size of the patch antenna, thus increasing the bandwidth. In other words, increasing the volume of the antenna increases the bandwidth [59].

Another way to increase the bandwidth is to add resonators [3], for example by adding another patch on top of the main patch. This kind of structure is called stacked patch antenna [67].

When a good separation of the two polarizations is required and the size is not the major limitation, a half-wave patch antenna is better than a quarter-wave patch antenna. A reasonable bandwidth is also required, therefore the stacked patch antenna element was found to be a feasible structure ([2], [7], [19]) for research. The probe feed was chosen for this research because of the simplicity of construction.

3.2.2 Microstrip patch antennas for the mobile unit

The focus in the research is on the antenna elements for the base stations, but observations are made if the same elements can be used in mobile units as well.

The mobile handset does not have room for a proper array unless the wavelength is below 10mm. In the current 2GHz frequency range it is possible to mount two quarter-wave patch antennas in a handset. With appropriate signal processing a significant improvement of the reception of the desired signal is possible, either by utilizing available space diversity or polarization diversity [18]. The human hearing system can be considered as an analogical case: when listening to a speaker in a crowd where many persons are speaking it is possible to detect the speaker. It is much more difficult to listen with one ear covered.

It is possible to implement polarization diversity within one antenna element. Antennas with good separate reception of two polarizations tend to be large. If there are two small quarter-wave patch antennas in a handset, the polarization separation of the element can be low, but they can still provide polarization diversity, even with one feed in each antenna. One possible way of implementation is to place the patch antennas so that they point to opposite directions and the polarization is controlled by the phase difference of the feeds.

3.2.3 Array structures

The linear array is the most commonly used antenna array. The element spacing of $\lambda/2$ or less gives an unambiguous beam in a linear array, but the main beam becomes wider when scanning angles are large. If the element spacing is wider, the main beam becomes narrower, but there will be grating lobes in addition to sidelobes. For example in a linear array the element spacing can be $0.7\cdot\ \lambda$ with the scanning angle less than ±30°, so that the grating lobes don't grow higher than sidelobes. Because the scanning angle is limited in practical applications, one choice is to use several panels of linear arrays to cover a wider scan angle. Six panels produce a hexagonal arrangement for omnidirectional scanning, and is resembles a cylindrical array so much that the question is whether a more optimal array can be made using a cylindrical array. Therefore a cylindrical array was taken under study here.

Making use of the sparse element spacing and the depth in an array became an attractive subject and was studied theoretically in this research. Because the cylindrical array has depth and a regular form, that array was taken under research in this project. Two types of element patterns were used: omnidirectional and directive, resembling a stacked patch pattern. Two kinds of optimizations were used: the optimal combinations of array radius and element number, and the optimal element weights.

In a mobile communication system, particularly in CDMA, there are several interferers quite evenly scattered around the receiver. Therefore it is not feasible to design the antenna to have the ability produce deep nulls like in the military systems, section 2.2.2.

The mutual coupling needs attention in an antenna array. It changes the radiation pattern of the elements, active impedance, scanning angle of the array, and the cross-polarization separation. Normally the changes are disadvantageous to the operation of the array. This is a wide area for research. Some initial study was done in lowering the mutual coupling in section 5.2. In digital beamforming antennas the mutual coupling can be compensated numerically [76].

The antenna design needs to be optimized for the environment in which it is to operate. Especially if the base station is wall-mounted, the designer should pay attention to the conductivity and permittivity of the wall materials [41]. In this study the environment was assumed to be free space.

3.3 Methods

3.3.1 General

The research in this thesis is limited to the electromagnetic structure of the antennas. The literature research was conducted to find out the current knowledge. Computer simulations were used in the following way: a FDTD program was used to simulate the patch antennas and mutual coupling, and the MathCad and Matlab programs were used for the array radiation pattern optimization.

Prototypes of the antenna elements were built, and the input impedance versus frequency and the radiation patterns in both polarizations were measured [5],[20]. The facility for the radiation efficiency measurement was not available at the time when the prototyping was done, but since the antennas were predominantly made of relatively thick metal plates no major losses were expected.

The antenna measurements were done in the IRC Radio laboratory anechoic chamber of Helsinki University of Technology. The measurements were done using the vector network analyzer HP 8792C and the antenna positioner Flam & Russell AE200, controller Flam & Russell 8502 by the Flam & Russell program "Automated antenna measurement workstation" program version 7.00. The reference horn for the measurements was Flam Microwave Instruments FMI 08240-10. The accuracy of that system is assumed to be ± 1 dB.

3.3.2 Computer calculation and simulation

There are many electromagnetic simulation methods for computers, and many of them are useful in antenna calculations [60]. The patch antennas of this research have a thick substrate and therefore the structure is 3-dimensional. The 2-dimensional patch programs were not used after some initial testing.

The finite element method (FEM) works well for 3-D calculations, but impedance calculations are done separately for each frequency. Therefore it is too slow for the wideband antenna design.

In the finite difference time domain (FDTD) method the time and space are discretized, and the calculations are done in time domain [44]. This method simulates the electromagnetic field in sequential timesteps, hence waves can be visualized and transients can be plotted. It calculates the input impedance versus frequency in one simulation. FDTD has difficulties with curved surfaces, but patch antennas used in this study fit to a rectangular grid. Patch currents need to be checked in certain cases to find out various modes of operation at different frequencies. This is straightforward when using a FDTD method. For these reasons FDTD was chosen the main simulator for the element design.

The RemCom XFDTD program version 2.21e was used. The conducting surfaces and cables were modeled using PEC (perfect electric conductor), because the use

of the accurate model for the metal surfaces did not increase the accuracy of the calculations.

The grid for the calculations is square. The cubes making the grid are called voxels (= "volume pixel"). The material values (conductivity, permittivity, permeability) can be individually assigned to the grid lines or "sticks" forming the edges of the voxels.

The smaller the voxels, the higher maximum frequency can be simulated. For example with 1 mm voxel size the maximum frequency is 30 GHz. The impedance calculations are accurate only when the pixel size is small compared to the wavelength, under $\lambda/100$. In this simulation the voxel size is $\lambda/140$ (except the first simulations, Figure 9, where it was $\lambda/56$).

When the impedance is calculated according to frequency, the FDTD program uses a Gaussian pulse (modulated Gaussian pulse for shorted patch antennas 1 GHz as modulation frequency) as the excitation, and the frequency response is obtained in one sweep. The calculation is done is steps, and the more calculation steps, the smaller the frequency steps in the frequency response. For example, 8000 calculation steps and a 1 mm grid result in 7.5 MHz frequency steps. When the radiation pattern, field patterns or mutual coupling are calculated, the FDTD program uses a sine wave excitation at the desired frequency. In that case the calculations must be done until the steady state is reached, 2000 steps were used in these simulations.

The program does not calculate the coupling between two antennas (S_{21}) automatically. Therefore a 50Ω line resistor was used as a load in the receiving antenna feed when calculating the coupling between antenna feeds. The S_{21} was calculated using the field strength at the load converted to the voltage over the load. The accuracy of the S_{21} calculations in this way remains to be verified.

In an electromagnetic simulation, connecting the feed to the system can be challenging, [66]. A simple line feed [41] was used here, and the results in impedance matching were directly applicable to the prototype manufacturing.

The array calculations were made by relatively simple self-made code using MathCad or MatLab (Appendices A...H). The code makes use of the equation (1), similar to equation (10) in [38], or equation (1) in [84] to calculate the array far field radiation pattern when the element patterns, element positions and element attitudes are known:

$$E(\hat{u}) = \sum_{n=1}^{N} a_n \cdot e^{jk\,\vec{r}_n \cdot \hat{u}}\, g_n(\hat{u}), \qquad (1)$$

where $E(\hat{u})$ is the electric field strength to the direction of the unit vector $\hat{u}$, n is the number of elements, $\vec{r}_n$ is the position vector and a_n is the complex excitation amplitude of the n^{th} element, $k = 2\pi/\lambda$ is the wave number when λ is the wave-length and $g_n(\hat{u})$ is the directivity of the n^{th} element in the direction of the unit vector $\hat{u}$.

4. Antenna elements

This chapter describes the antenna element research. In Section 4.1 a solution is described for triangular quarter-wave patch with walls. Sections 4.2, 4.3 and 4.4.describe research on rectangular quarter-wave patches. Sections 4.5, 4.6 and 4.7 describe research on stacked half-wave patch antennas.

4.1 Triangular quarter-wave patch antenna with metallic walls

When there is a need to make a patch antenna that can receive two polarizations separately, the half-wave patch antenna with two feeds is an obvious solution as implemented in Section 4.7. Since one of the goals of this research was to look for small array antenna solutions, one objective was to find out how two polarizations can be received using quarter-wave patch antennas.

After some initial testing it was found out, that having two feeds to produce two separable polarizations in a quarter-wave antenna is difficult. Since we are interested in the small antenna structures, we are interested in the resonance mode that produces the lowest frequency in the antenna structure. Because the shorting joint is shared for both polarizations, all the currents go through the same shorting joint, and the longest path for the currents excited by two different feeds is the same. Therefore the shorted patch has a tendency to produce only one mode of resonance and hence only one polarization at the lowest resonating frequency.

In the beginning of the design it was supposed that with two separate quarter-wave patch antennas it could be possible to save up to 75% of the space required by the half-wave patch antenna if the quarter-wave patches are triangular, each taking 1/8 of the area of the half-wave patch. Because the elements would be positioned close to each other, there was an idea to use metal walls between elements. The effect of the walls is studied in paragraph 5.2.1.

Consequently, a prototype of a triangular shorted patch antenna with walls was made. The tip of the patch is in the center of the square, which allows flexible positioning of the squares in two polarizations in the array as in Figure 51 in section 5.1.2. The element is made of one single copper plate 0.5 mm thick cut and bent into shape and soldered at the corners. The probe feed is added under the patch, and the resulting prototype is shown is in Figure 2.

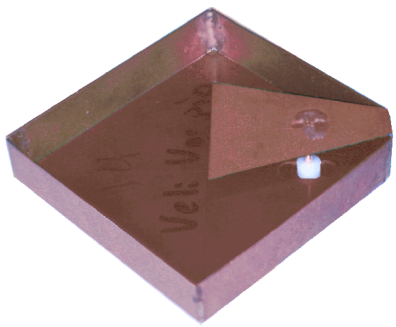

Figure 2. Triangular patch antenna on a square walled ground.

The dimensions are: The patch width is 24 mm at the tip, is 4 mm at the short and the patch length is 30 mm. The probe is located in the center line of the patch at 13 mm from the short. The patch is located on a square ground plate of 50x50 mm^2, the surrounding wall is 10 mm high. The shorted end of the patch is joined to the wall at the edge of the ground plate.

Because the antennas are close to each other the mutual coupling became high. The wall around the antenna aimed to reduce the mutual coupling did not work as expected, see paragraph 5.2.1. The cross-polarization separation of the element is also low, Figure 6.

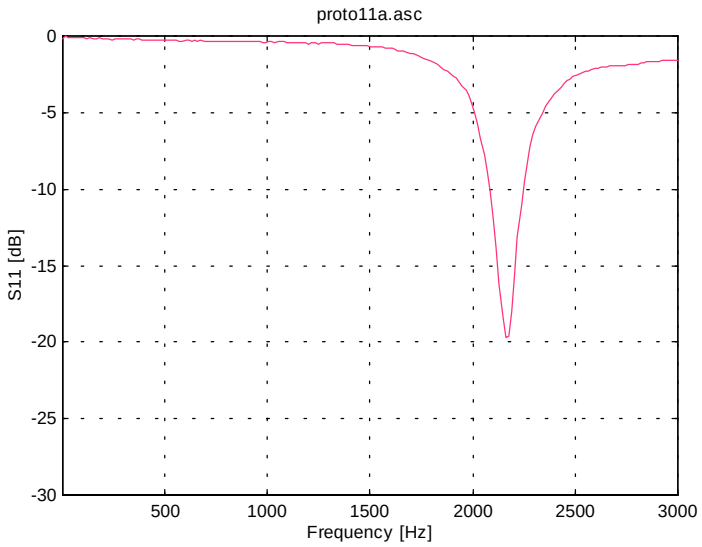

Figure 3. Reflection coefficient of the triangular antenna

Figure 3 shows the reflection coefficient as a function of frequency. The –10 dB reflection coefficient corresponds to 10 dB return loss, and consequently the bandwidth filling the criteria L_{ret} > 10 dB is 9.6%, which is sufficient for the antenna in UMTS systems and for the measurement purposes in channel sounding.

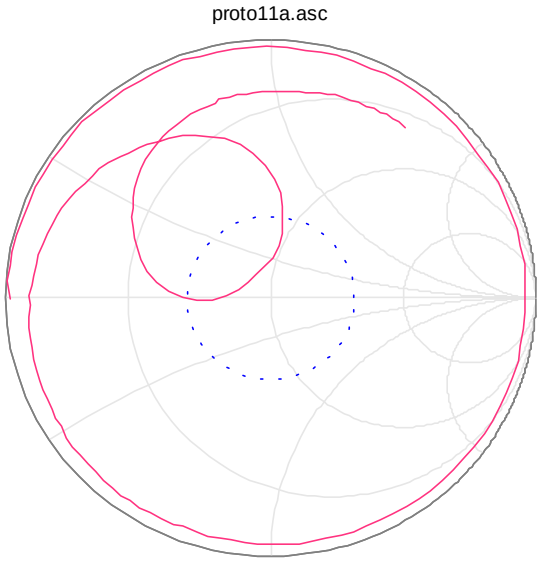

Figure 4. Measured impedance on the Smith chart of the triangular antenna

Figure 4 indicates that the antenna has two resonances. The ground plate resonance was tested by placing lossy material connecting the ground between the feed point and the corner opposite to the feed point and the lossy material damped the second resonance significantly. The distance of the path of the current between the feed point and the top of the wall in the corner opposite to the feed point is 67 mm which is close to the quarter-wave length. This means that the structure meant as ground plate also resonates. The designer of the antenna must be aware of that possibility and check possible ground plate resonances, or box resonances in handheld units.

Figure 5 and Figure 6 show the radiation patterns of the antenna in E-plane and H-plane. They are as can be expected, except that the cross-polar level in H-plane is high, because of the long probe.

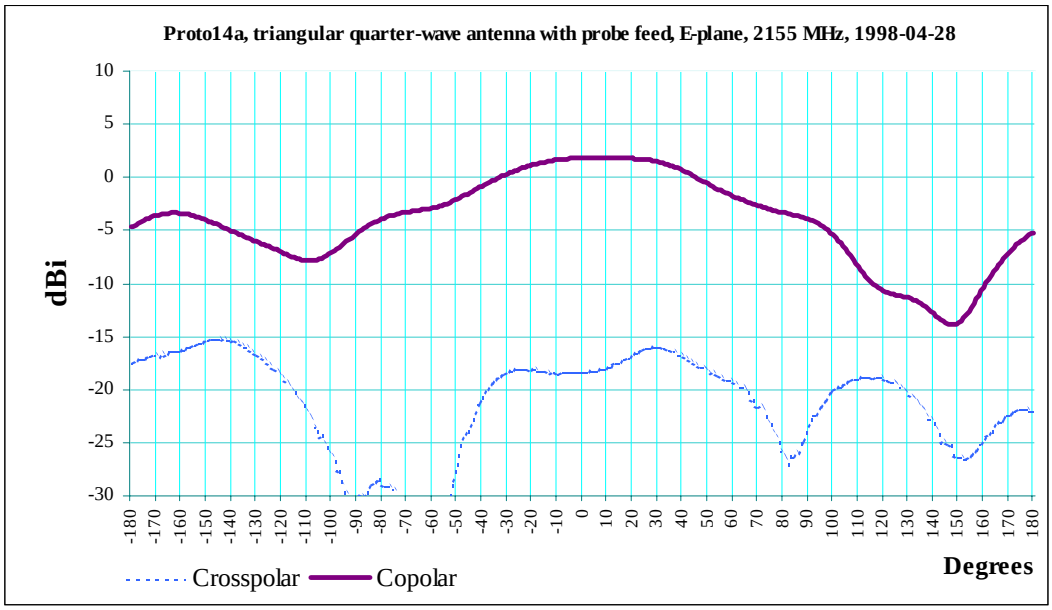

Figure 5. Measured radiation pattern of the triangular antenna in E-plane.

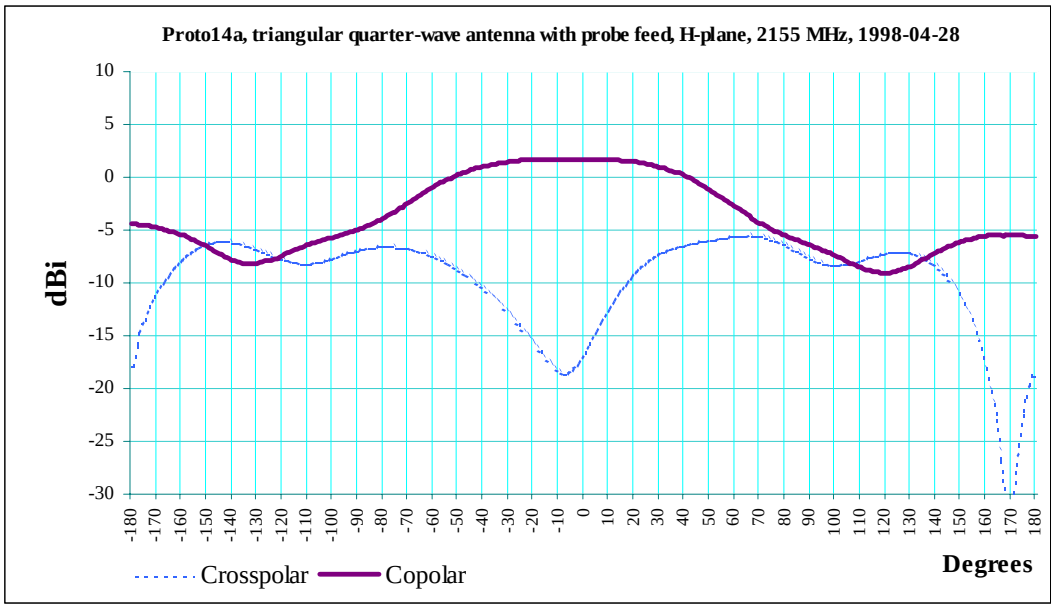

Figure 6. Measured radiation pattern of the triangular antenna in H-plane.

The antenna is good in many aspects: the right frequency and sufficient bandwidth are achieved with a simple structure without a matching capacitor. The problems come from the mutual coupling effects due to the shared shorting point.

4.2 Quarter-wave patch antenna design procedure with long probe feed

The matching of the antenna in the previous section was achieved in the conventional way by changing the position of the probe. The inductance of the probe was compensated by the capacitance causing another resonance in that antenna structure. In this section the focus is on patch antennas having a single resonant structure with long probe, and it is described how the high inductive reactance caused by the long probe can be compensated.

A quarter-wave patch antenna has a metal patch above the metal ground plate and the patch is shorted at one end, Figure 7. The patch consists of the part that is parallel to the ground plate and the shorting part. The probe feed is the center conductor of the coaxial connector above the ground plate.

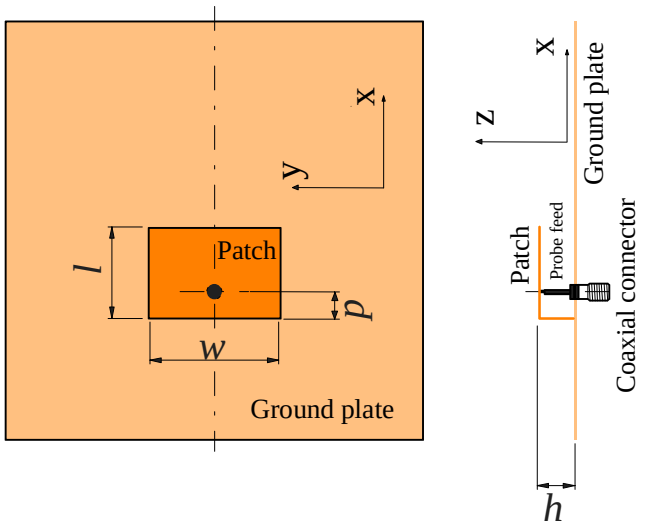

*Figure 7. The structure of a rectangular quarter-wave (shorted) patch antenna. **w** is the width of the patch, **h** is the thickness (height) of the substrate and also the length of the probe above the ground, **l** is the length of the patch, and **p** is the distance of the probe from the shorted end of the patch. The material is 0.5 mm thick copper. The axes are shown for both drawings. The E-plane is in xz-plane, and the H-plane is in yz-plane. The angle θ is the deviation from the z-axis, and the angle φ is positive towards the positive x-direction in E-plane and towards the positive y-direction in H-plane.*

In this work a wide bandwidth is required and it can be achieved by using a thick substrate [94]. Designing a patch antenna with a thick substrate turned out to be different from conventional patch antenna design. The first efforts in the design did not seem to show a consistent behavior. The conventional theory regarding the patch length and matching impedance do not take the inductance of the probe into account, which displaces the matching point of the patch [47].

The cross-polarization discrimination is another problem in patch antennas with thick substrates if a long probe feed is used. The inductance problem and the cross-polarization problem can be alleviated with the aperture feed. Aperture fed antennas are suitable for mass production [94]. In thick substrates the coupling

may become a problem, and also the back radiation can be high in aperture fed antennas.

In this study the probe feed was chosen, because it is simple to implement in prototypes and the direct galvanic contact is preferred by industrial manufacturers. A new design approach was developed for the design of patch antennas with thick substrate. The method is actually quite simple, because the patch resonance and the probe inductance are treated separately. The idea is to exclude the inductive reactance $X_P = j \cdot \omega \cdot L_P$ of the probe, Figure 8, from the initial analysis. The patch resonance is due to the patch impedance Z_A alone, and it can be analyzed separately, based on the patch radiation properties.

The length of the patch will determine the desired patch resonant frequency. As a first estimate, the length of the patch is the quarter-wave length at that frequency. The length corresponding the quarter wave is the sum of the height of the patch (h) and the length (l) of the patch, $\lambda/4=h+l$. In practice the frequency is slightly lower than $f=c/(4 \cdot (h+l))$, because of the stray field at the radiating end of the patch. The electrical length of the patch is increased by the stray field at the radiating end of the patch, and this effect is enhanced by height of the substrate. Therefore the next step is to shorten the patch.

When measuring or simulating, one should pay attention to the resistance curve, which is the real part of the impedance $\mathrm{Re}(Z_A(f)) = \mathrm{Re}(Z_{Tot}(f))$, provided the measuring point is calibrated at the ground plate surface level. The frequency point where the resistance is at highest is the patch resonant frequency [47]. The quarter-wave patch resonance is a parallel resonance (Figure 1) when fed with a probe. At patch resonance the impedance of the parallel reactive part is infinite, so the resistive part is equal to the radiation resistance. At that point the reactance should normally be zero, but in a probe-fed patch there is a positive reactive component caused by the probe inductance. This probe inductance will change the reflection coefficient so that the frequency point of the lowest reflection coefficient does not match the resonant frequency of the patch.

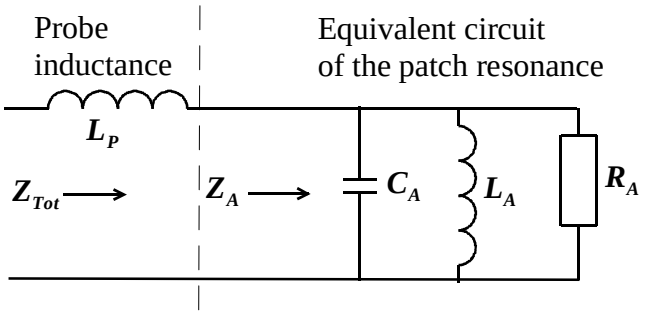

Figure 8. Equivalent circuit of the antenna divided to the probe inductance part and patch resonator. L_p is the probe inductance, R_A is the radiation resistance, L_A and C_A are the inductive and capacitive parts of the antenna resonant circuit. Z_A is the impedance of the patch only and Z_{Tot} is the total impedance of the antenna.

If the resonant frequency is too low, the length of the patch should be reduced and vice versa. It is important to define the length of the patch correctly as the first step, because the rest of the design is based on it.

The position of the probe determines the radiation resistance. Moving the probe towards the radiating end increases the radiation resistance. The probe should be positioned so that the real part of the antenna impedance Re(Z_A) (= Re(Z_{Tot}) at the resonant frequency) is about 90Ω at the resonance. This is done anticipating the series-parallel double resonant matching at L_{ret} > 10 dB, where Re(Z)$_{Max} \leq$ 100 Ω, Figure 8.

Increasing the diameter of the probe feed will reduce the inductance. The matching capacitor is still often needed to compensate for the inductive reactance caused by the probe. This is normally necessary only if the patch antenna is of the single patch resonator type and has a thick substrate.

4.3 Examples of design of the quarter-wave patch

4.3.1 Matching the patch antenna impedance

The design was based on the 2154 MHz frequency , because then the antennas are compatible with the channel sounder at IRC [39]. The structure of the antenna is shown in Figure 7. In this simulation a 2.5 mm grid was used, which is useful for initial calculations although the accuracy of the impedance suffers. The patch length l = 22.5 mm and substrate thickness h = 10 mm give a resonant frequency of 2140 MHz which is close enough to 2154 MHz. The width w = 35 mm, and the position of the probe p = 7.5 mm from the short, which give 55Ω resistive part of the impedance at patch resonance. The voxel here is 2.5 mm, therefore the result is not closer to 90Ω. The FDTD grid pattern representation is in Figure 9.

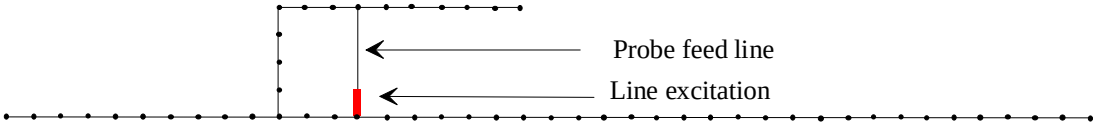

Figure 9. The FDTD grid pattern. The figure is a cross-section cut along the central x-line. The black lines represent x-directional PEC lines and the dots represent the y- and z-directional PEC lines. l = 22.5 mm, h = 10 mm, w = 35 mm, p = 7.5 mm. The grid is 2.5 mm.

Figure 10 is a screen image copy of the FDTD simulator output. The red line is the real part of the antenna input impedance (always positive) and the green line is the imaginary part. This version of the simulator does not give the Smith chart directly, but in this analysis the resistance-reactance plot is useful. The peaks in the resistance curve indicate the patch resonances, because they are single parallel resonances. It means that at this point of the analysis attention is paid only to the radiation resonance, excluding the other components like the probe inductance which affect the reflection coefficient, which is of interest in the later stage of the analysis.

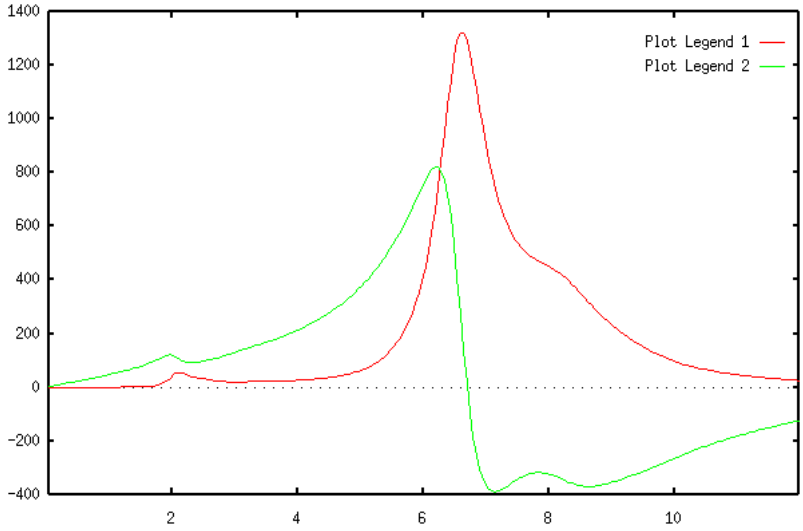

Figure 10. Resistance (always positive) and reactance curves of a simulated patch antenna. l = 22.5 mm, h = 10 mm, w = 3 5mm, p = 7.5 mm. x-axis is frequency in GHz, y-axis is resistance and reactance in Ω.

As can be seen, there is a resonance near 2 GHz, and another one near 6 GHz, which correspond the primary ($\lambda/4$) and tertiary ($3\cdot \lambda/4$) resonances. The secondary resonance does not exist in shorted quarter-wave resonators. The third resonance near 8 GHz is probably caused by the probe and stray capacitance. The 10GHz resonance ($5\cdot \lambda/4$) and higher resonances is not visible.

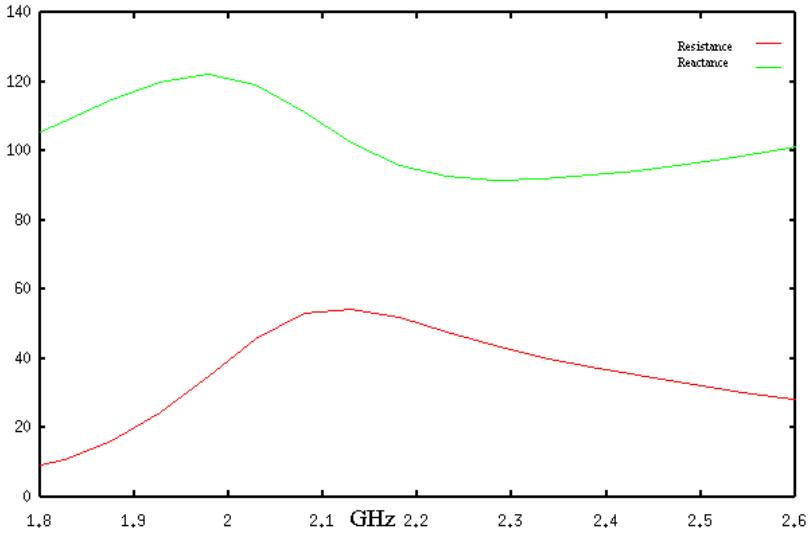

Figure 11. Resistance (always positive) and reactance curves of the same simulated patch antenna as in Figure 10, a close-up around the desired frequency 2154 MHz. l = 22.5 mm, h = 10 mm, w= 35 mm, p = 7.5 mm. x-axis is frequency in GHz, y-axis is resistance and reactance in Ω.

Figure 11 is a close-up from the Figure 10. The natural patch resonance value is visible, and the additional reactance caused by the probe is apparent, causing a positive reactance component.

Figure 12 shows a similar patch antenna simulated using a finer voxel of 1 mm, and using a capacitor to compensate the positive reactance component. The capacitor is modeled as in Figure 29. The shape of the resistance curve does not change, and the reactance curve is lowered so much that it is zero at the resonance point. The capacitor compensates the inductive reactance. It also increases the

bandwidth by forming a coupled second resonance at the same frequency as the patch resonant frequency.

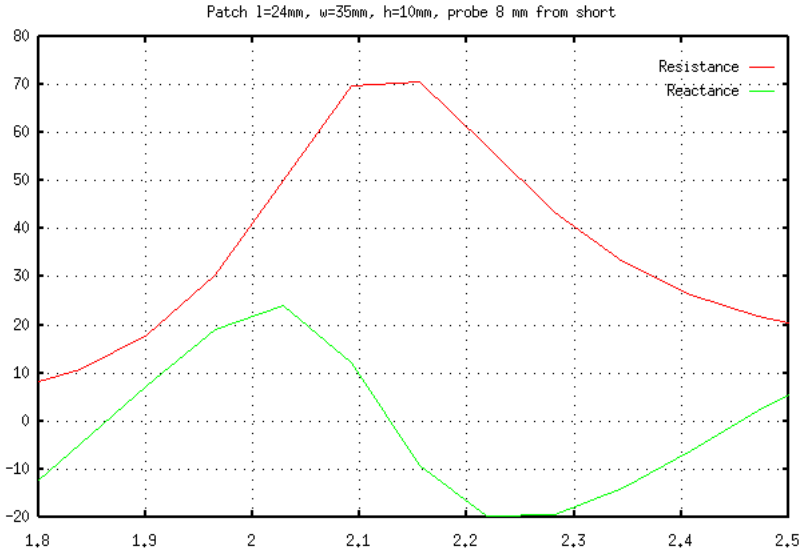

Figure 12. Resistance (always positive) and reactance curves of a simulated patch antenna. Matching capacitor added. l = 24 mm, h = 10 mm, w = 37 mm, p = 8 mm, ε_r = 7.6, the capacitor plate area A = 4 mm^2, distance between plates d = 1 mm, Figure 29. Capacitor =0.27 pF. Probe inductance L_p = 20.3 nH. x-axis is frequency in GHz, y-axis is resistance and reactance in Ω.

4.3.2 Reducing the cross-polarization with the capacitor in the probe

Figure 13 is an output of a simulation. On the left it shows the x-directional (Figure 7) current distribution on the quarter-wave patch top. The figure on the right shows the z-directional electric field strength in the same situation. The sides produce the cross-polarized component of the electric field in a quarter-wave antenna. In contrast, in a half-wave antenna the currents are in opposite phases at the radiating ends of the antenna, and that reduces the cross-polarized component, especially in the z-direction.

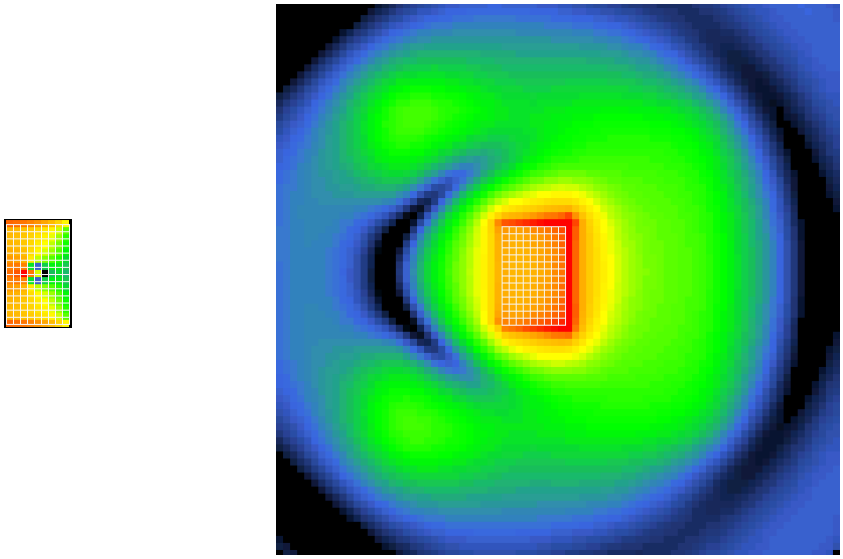

Figure 13. Two illustrations of FDTD simulations: field patterns, red strongest, black weakest. Left: x-directional current density J_x (horizontal axis). The current concentrates at the sides and in the middle. Right: electric field strength E_z (the direction of the field is perpendicular to the page) The main field is at the radiating end of the patch. The fields at the sides cause the cross-polarization. l = 22.5 mm, h = 10 mm, w = 35 mm, p = 7.5 mm.

The probe inductance can be compensated with a capacitor in the feed line, like in Figure 29. Figure 15 and Figure 16 show the simulated radiation patterns without the capacitor, and with the capacitor in the probe. The cross-polar level *XPL* = 0 dB in Figure 15, and *XPL* = -6 dB in Figure 16, so the capacitor increases the cross-polar separation. Figure 15 and Figure 16 are screen printouts from the FDTD program. The vertical scale is different in the figures. The copolar gain is 1 dBi in Figure 15 and 3 dBi in Figure 16. The increase of the gain can be explained by the reduction of the cross-polarization.

The FDTD grid pattern representation is in Figure 14:

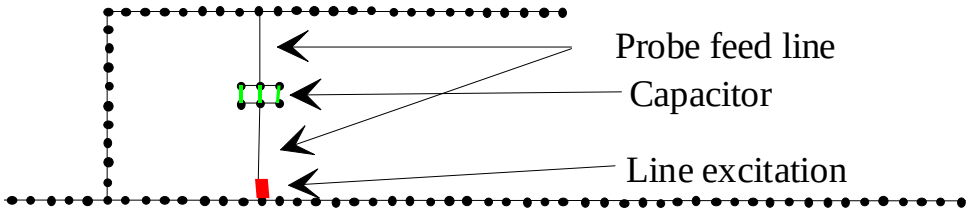

Figure 14. The FDTD grid pattern. The figure is a cross-section cut along the central x-line, the ground plane only partly shown.. The black lines represent x-directional PEC lines and the dots represent the y- and z-directional PEC lines. The green lines represent the insulator in the capacitor, ε_r = 7.6, length of capacitor edge 2 mm. l = 24 mm, h = 10 mm, w = 37 mm, p = 8 mm. The grid is 1 mm.

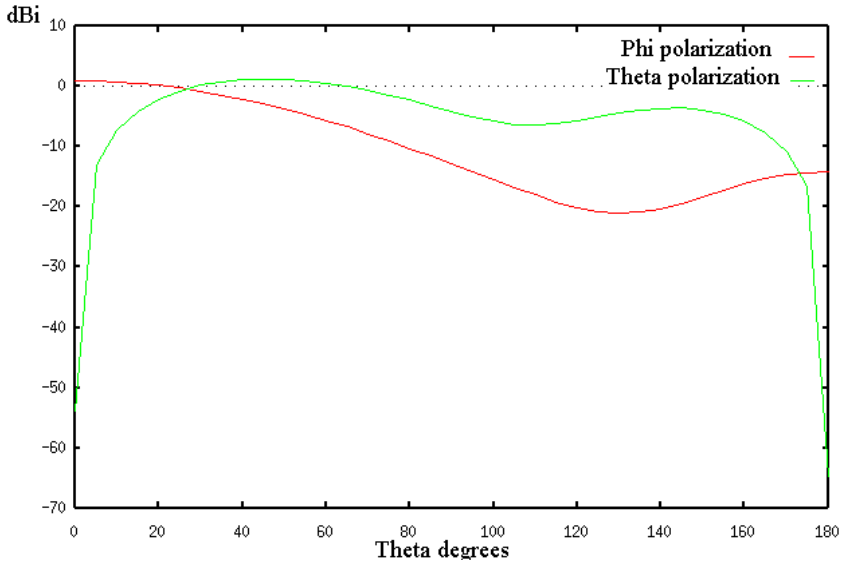

Figure 15 H-plane radiation pattern with dimensions of l = 22.5 mm, h = 10 mm, w = 35 mm, p = 7.5 mm, no capacitor in a quarter-wave patch. Red line (high at 0°) is the copolar radiation pattern, green for cross-polar. With no capacitor the cross-polarization discrimination is over 10 dB between ±8° deviation. (There is symmetry on both sides of 0°, therefore only one side of the radiation pattern is shown.).

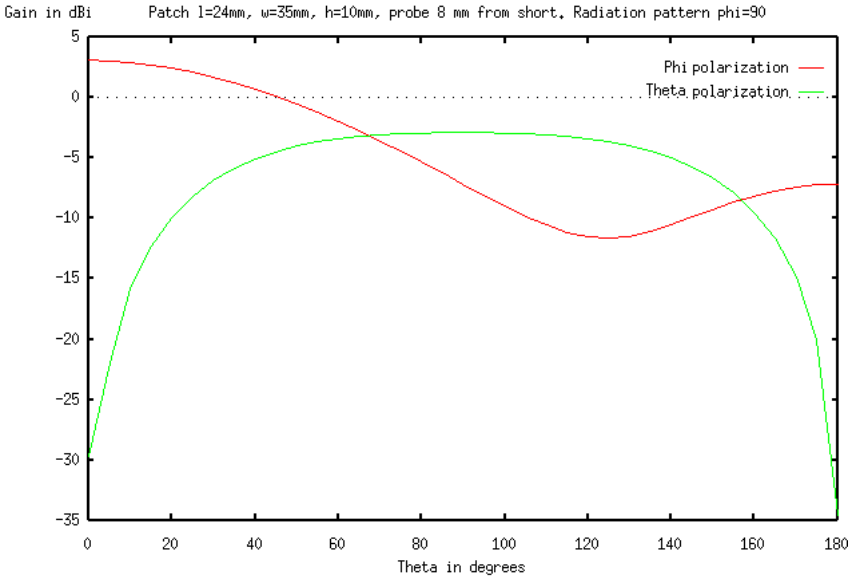

Figure 16. H-plane radiation pattern with dimensions of l = 24 mm, h = 10 mm, w = 37 mm, p = 8 mm, ε_r = 7.6, A = 4 mm^2, d = 1 mm. with capacitor in a quarter-wave patch. Red line (high at 0°) is the copolar radiation pattern, green for cross-polar. With the capacitor the cross-polarization discrimination is over 10 dB between ±24° deviation. (There is symmetry on both sides of 0°, therefore only one side of the radiation pattern is shown.)

One can study the effect of the capacitor in the middle of the probe by monitoring the changes in the H-plane radiation pattern in the simulation. The capacitance required for the matching is C = 0.27 pF, so one can deduce that the inductance caused by the probe is L_p = 20.3 nH at 2154 MHz. In Figure 16 the *XPD* is 9 dB better at 20° direction than in Figure 15. In Figure 16 *XPD* is over 10 dB between ±24° deviation while in Figure 15 *XPD* is over 10 dB only between ±7°. The improvement of *XPD* is due to the capacitor.

This effect needs further study. Nevertheless the cross-polarization separation was not high enough, and another type of patch was chosen for the development, Section 4.5.

4.4 Wideband patch antenna prototype

The goal of the research discussed in this section was to achieve as wide bandwidth as possible for the antenna element compared to the volume in wavelengths. One way to increase the bandwidth is to add resonators in the feed circuit, but that adds to the space needed by the antenna with the feeder circuit. Instead, the resonant structure can be placed within the antenna volume itself. This was the idea of the previous section and it is further developed in this section.

4.4.1 Antenna structure

A small quarter-wave patch antenna with the impedance bandwidth of 35% was constructed. The antenna has a probe feed with an integrated capacitor to compensate for the probe inductance or to produce a dual-resonant structure [88].

The proposed antenna is a quarter-wave rectangular microstrip patch antenna with a thick air substrate (Figure 17 and Figure 18). The material of the patch is 0.5 mm thick copper plate and the ground 1 mm thick copper plate so that the

structure is solid enough with the air substrate. The antenna has a capacitor in the middle or top of the probe.

Two possible configurations have been studied. In the first version the capacitor consisted of a chip capacitor (or several in series in order to achieve a suitable capacitance). Here the capacitor functions as the matching capacitor described in 4.3.

In the second version the capacitor was made of a piece of Duroid 5880 low-permittivity ε_r = 2.33 substrate material having metal on both sides (Figure 19). Therefore the structure of the antenna resembles a stacked patch antenna. The substrate functions also as a coupling capacitor for the feed. There are similarities between the proposed structure and that in [82] and [83]. The main difference is the short-circuited quarter-wave structure.

To separate the types of capacitors in the following text, the terms *substrate capacitor* (large material dimensions, called large volume capacitor in the simulations) and *chip capacitor* (small dimensions) are used when a difference must be made.

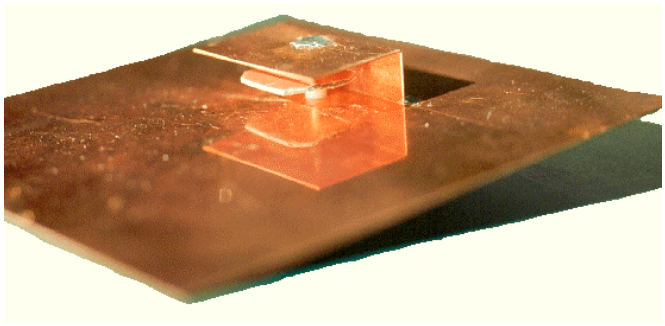

Figure 17. Structure of the prototype antenna

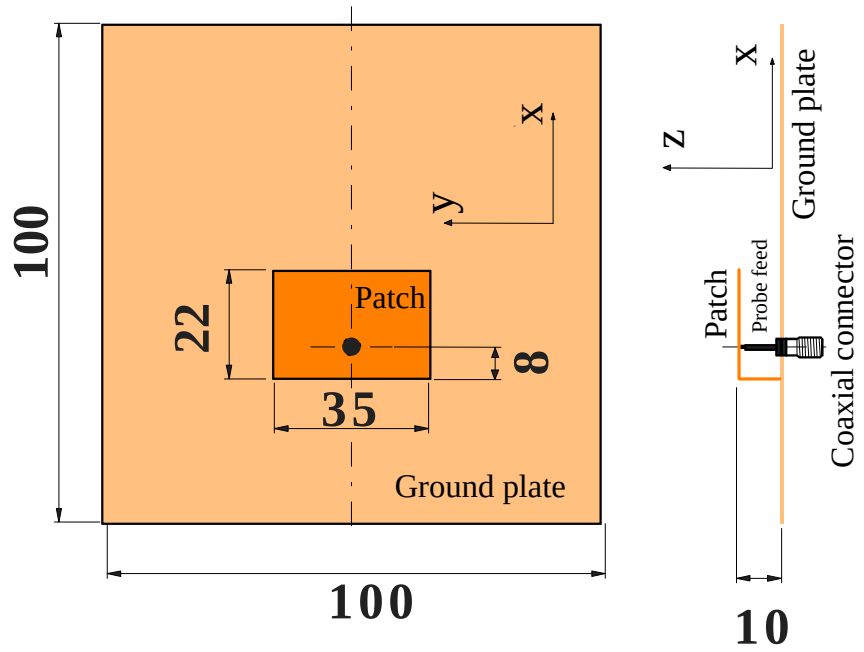

Figure 18. Dimensions of the prototype antenna before installing the capacitor (in mm).The axes are same as in Figure 7.

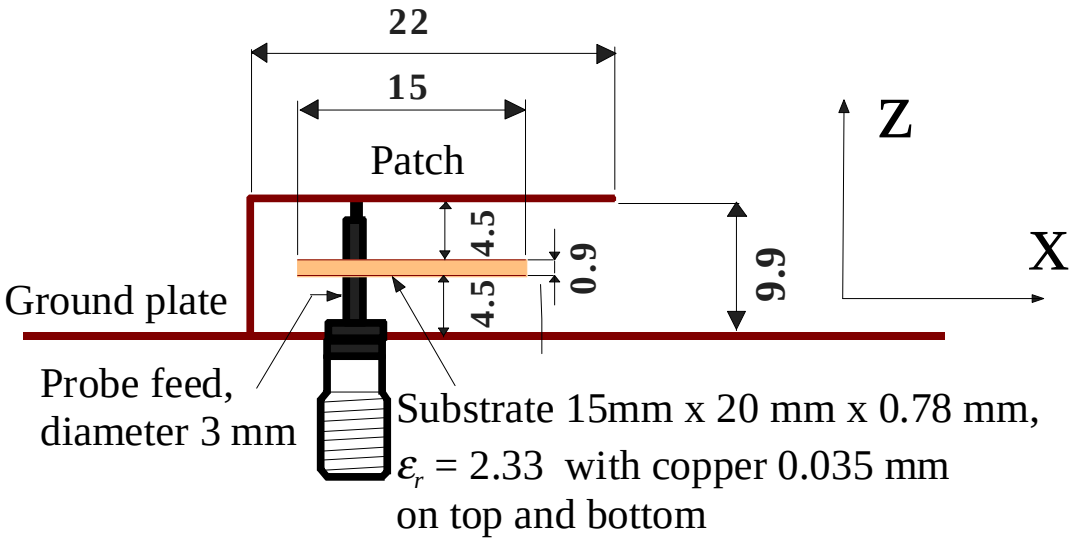

Figure 19. An close-up of Figure 18 with the substrate capacitor in the middle of the probe.

4.4.2 Measured properties

The measured reflection coefficient for the antenna version with the substrate capacitor is given in Figure 20 and the input impedance in Figure 21.

Figure 20. Measured reflection coefficient.

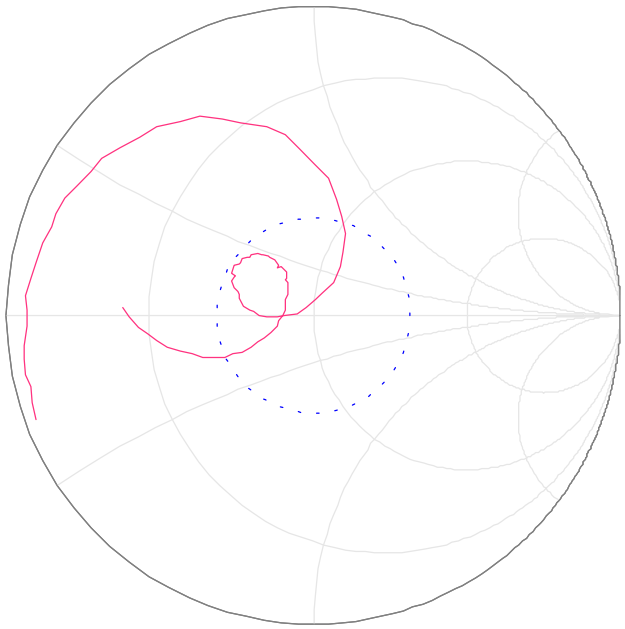

Figure 21. Measured input impedance. The small circle in the center is the –10 dB reflection coefficient circle.

The impedance bandwidth for the 10 dB return loss is 35 %. From Figure 21 it can be noticed that the matching was not totally optimal and somewhat larger bandwidth can be obtained by moving the probe towards the end of the patch. That will increase the antenna impedance and move the loop as close to the center as possible.

On the basis of a measurement without the capacitor the inductance of the probe of the prototype was estimated to be 7 nH. Thus using the frequency 2400 MHz (the center frequency of the radiating frequency band) the respective capacitance is 0.55 pF. When a 0.67 pF (±20%) chip capacitor was used to replace the substrate capacitor a 10 dB bandwidth of 31% was obtained. The simulated inductance is different in 4.3.2 which indicates that the probe was modeled too thin (diameter 1 mm) in the simulation.

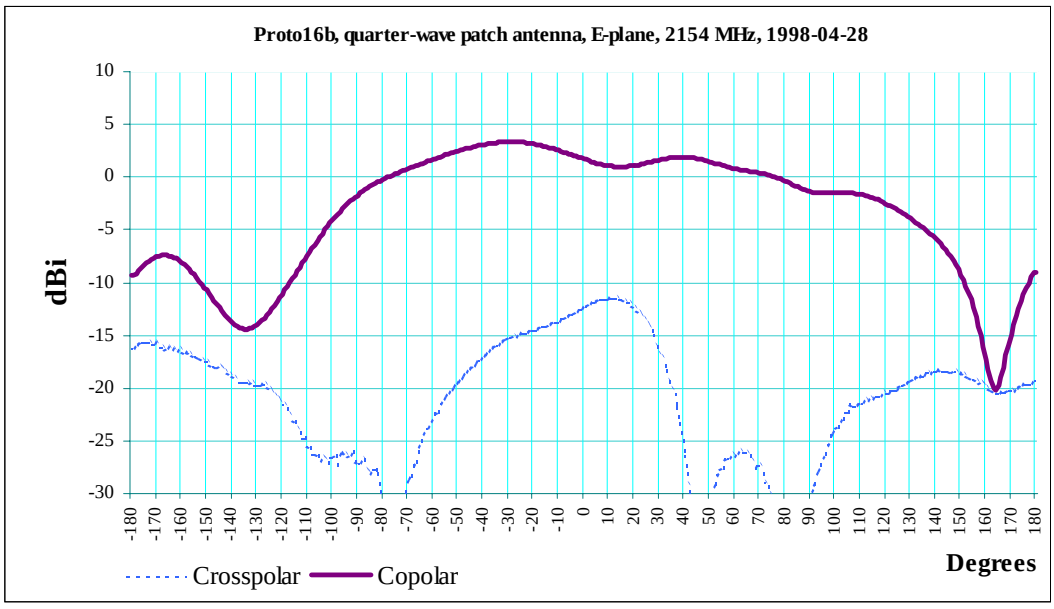

Figure 22. Measured radiation pattern in E-plane, maximum is 3.3 dBi

The measured radiation patterns for the antenna with substrate capacitor are shown in Figure 22 and Figure 23. It can be seen that the radiation pattern is fairly omnidirectional. Gain is 3.3 ± 1 dBi, Section 3.3.1. The maximum cross-polar value in H-plane is as high as the maximum copolar value in H-plane. This means that the matching circuit radiates and therefore the bandwidth is wider than with the chip capacitor. Regarding E-plane, the radiation from the matching circuit is copolar, and it adds to the patch copolar radiation pattern.

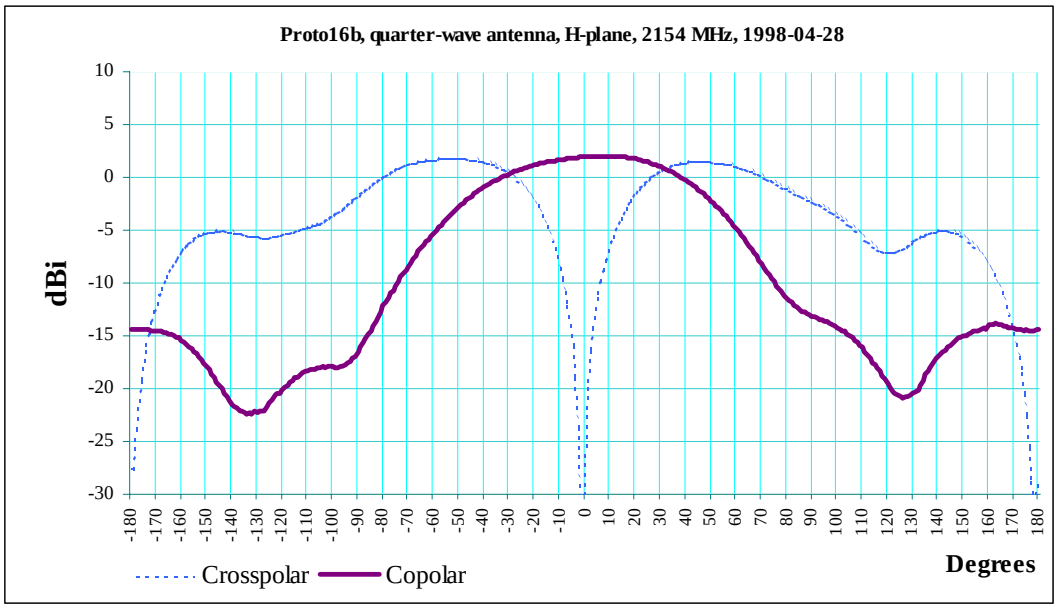

Figure 23. Measured radiation pattern in H-plane

4.4.3 Theory of operation of the patch antenna with substrate capacitor

Figure 24 shows that the measured resistance peaks are approximately at frequencies 2055 MHz and 2655 MHz. The radiation patterns are measured at those frequencies because these points suggest the radiation resonance points of the two resonance modes, although not accurately, because the resonances are coupled.

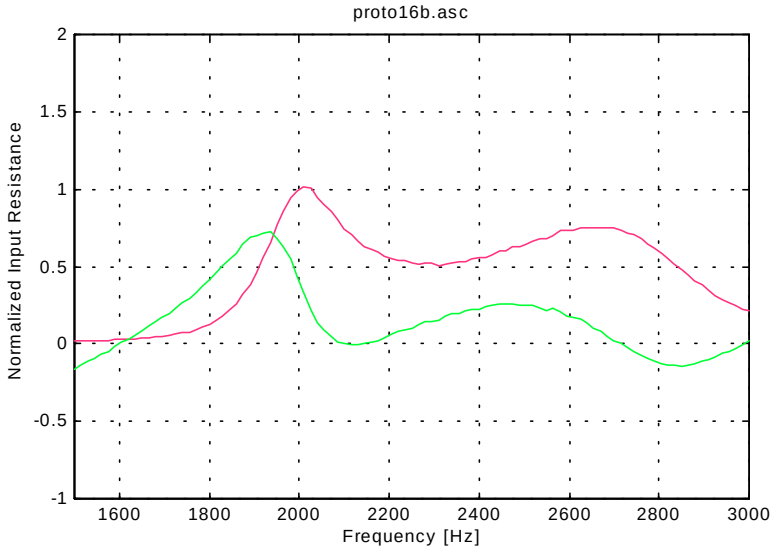

Figure 24.Measured impedance, real part (the line which is positive only) and imaginary part

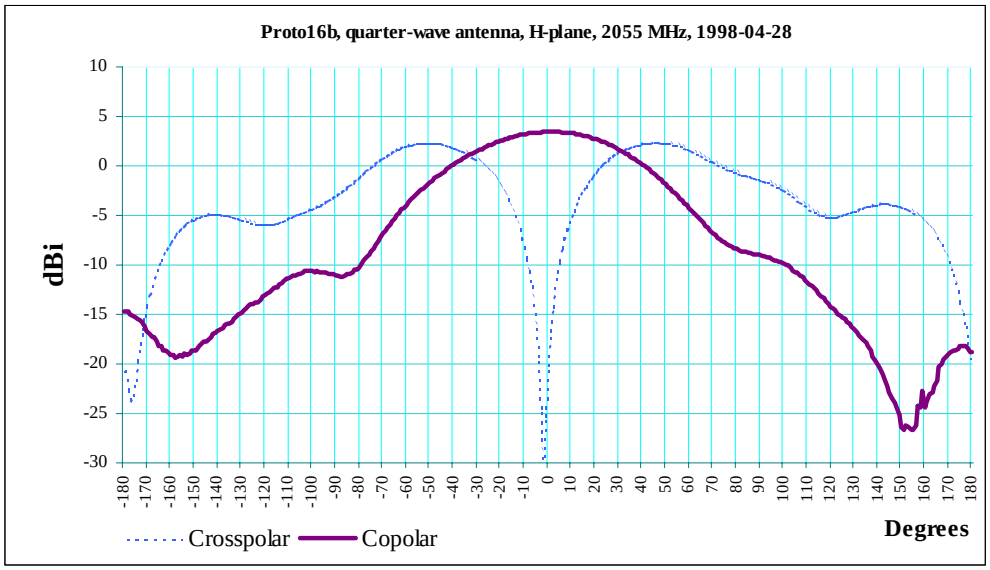

Figure 25. Radiation pattern in H-plane at 2055 MHz (in E-plane the maximum copolar gain is 4.3 dBi).

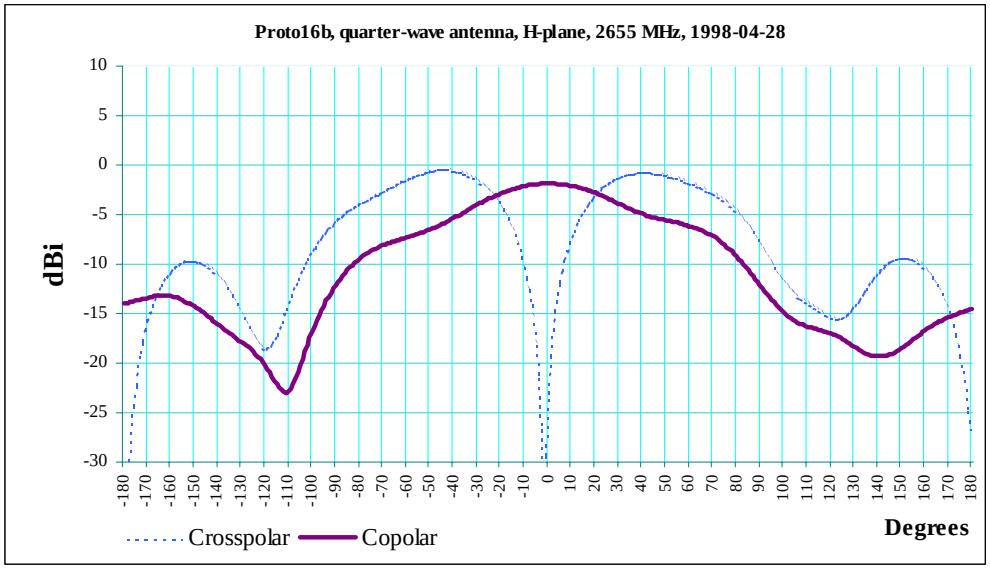

Figure 26. Radiation pattern in H-plane at 2655 MHz (in E-plane the maximum copolar gain is 2.3 dBi, the direction of the maximum gain is different from Figure 26).

The relative cross-polarized level increases when the frequency increases in Figure 25 and Figure 26. This indicates monopole/dipole operation of the probe, Figure 28. At the same time the ordinary patch antenna pattern is visible in Figure 25 and Figure 26, indicating some patch antenna operation, Figure 27. The lower resonance frequency corresponds to the resonance of the patch antenna size. The higher resonance frequency corresponds to the probe antenna resonance.

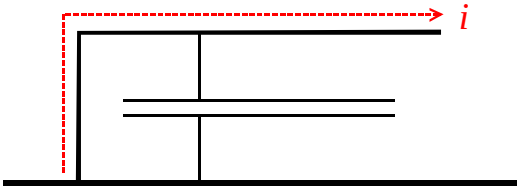

Figure 27. Ordinary resonating current (dotted line) in a quarter-wave antenna.

In the prototype with substrate capacitor the capacitance of the substrate capacitor is far too high (5pF) to be the matching capacitance. It works as a coupling capacitance. The currents of this resonance mode are sketched in Figure 28, and this resonance mode is a series resonance like in monopoles. Therefore the capacitance in the air between the substrate metal ground plane must be the capacitive load of the monopole antenna.

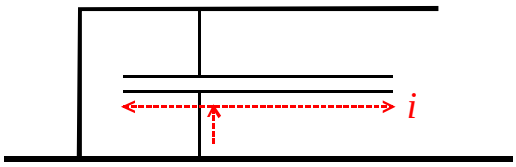

Figure 28. Capacitively loaded monopole resonating current (dotted line).

In this structure additional resonance modes can exist. For example moving the substrate capacitor forth and back changed the bandwidth significantly, which indicates a stacked patch mode. The simulations providing the current patterns show the J_x and J_y in separate illustrations, so it is difficult to make conclusions without special postprocessing and visualization. The lumped circuit equivalent models did not work with reasonable values. The antenna volume is small, so the coupling between the resonance modes is tight, therefore further analysis of the antenna is complicated.

4.4.4 Computer simulations with chip capacitor

In FDTD simulations, a 28.8% bandwidth (L_{ret} = 10 dB) was reached, Figure 30 and Figure 31. The antenna dimensions were w = 36 mm and l = 22 mm. The capacitor was modeled in the middle of the probe (Figure 29, Figure 14), ε_r = 7.0, capacitor surface A = 4 mm^2, distance between plates d = 1 mm, so C = 0.25pF. The probe was modeled as a line of PEC, which corresponds 1 mm diameter in 1 mm voxels. The excitation was modeled as a line excitation between the ground surface and probe bottom.

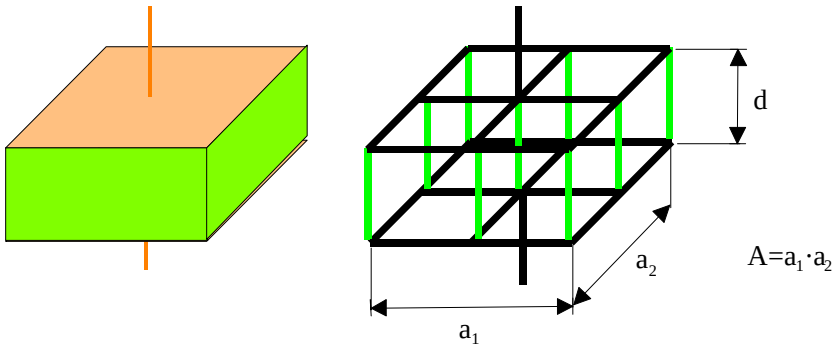

Figure 29. The modeling of the capacitor (left) in FDTD (right). The black lines correspond to the PEC. The green lines correspond to the dielectric material. The black vertical lines above and below the capacitor show part of the probe to indicate the points of connection.

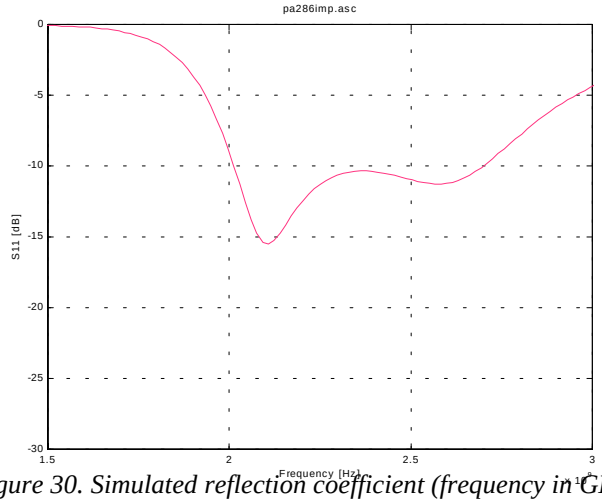

Figure 30. Simulated reflection coefficient (frequency in GHz).

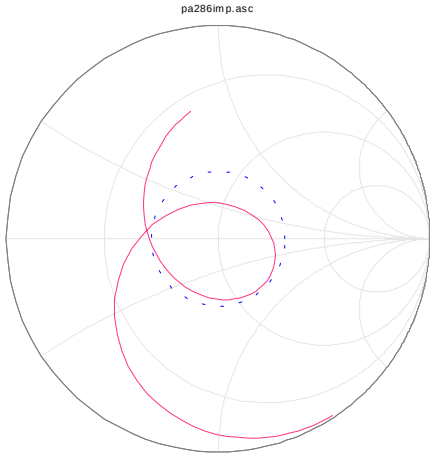

Figure 31. Simulated input impedance.

In Figure 30 and Figure 31 the input impedance was closer to optimum than in the prototype. The bandwidth is narrower than in the prototype. The prototype may have some losses that increase the bandwidth. The capacitor used in this simulation is small in volume, the horizontal surface was 4 mm^2, corresponding to the chip capacitor. Another simulation with a large volume capacitor (a simplified model corresponding the substrate capacitor) resulted in the same bandwidth, although the electrical current patterns were quite different. The large volume capacitor model could be refined in further research.

4.4.5 Observations

Comparable impedance bandwidths from 20 to 35 % have been obtained with aperture coupled antenna [66].

The resistance curve in Figure 11 shows that the patch resonance bandwidth where L_{ret} > 10 dB is 15.2% (between the frequency points where $R < 0.7 \cdot R_{Max}$, R_{Max} is the maximum value in the resistance curve) and thus the Q_r-value is 4.4, calculated from $Q=(S-1)/(BW \cdot \sqrt{S})$ [49]. The standing wave ratio S = 1.92 at L_{ret} = 10 dB.

The bandwidth with the double resonance with the substrate capacitor is 35% which is exactly 2.3 times 15.2% when L_{ret} > 10 dB [27].

The antenna bandwidth is normally compared to volume in wavelengths. Formulas relating volume and bandwidth are found in [59] and tables in [30].

When comparing the bandwidth to volumes directly the wavelength at lowest resonant frequency (at L_{ret} = 10 dB) was used (1970 MHz for the antenna of this study). For this antenna the bandwidth compared to the volume in wavelengths is 15960 [%/λ^3]. Comparison is made to the antenna in [92] where BW = 10.1%, w = 15 mm, l = 17.5 mm, h = 12.5 mm. For that antenna the bandwidth compared to the volume in wavelengths (at 1710 MHz frequency) is 16500 [%/λ^3] which is slightly (3%) better than achieved here.

When using the theory in [59], the geometrical mean frequency (2360 MHz) was used. Therefore the radius which can cover the whole antenna in Figure 18 is 21.2 mm or 0.167· λ. Then the theoretical lower limit of the Q_r-value (radiation quality factor) is 1.81 for that antenna. The resulting maximum theoretical bandwidth is 37% (L_{ret} > 10 dB) which is slightly more (5%) than actually achieved here.

The losses can increase the bandwidth, but the above 3 GHz the return loss approaches zero which indicates that the losses in the antenna are small. The antenna is made of 0.5 mm thick copper which has low losses. The substrate material permittivity is low (ε_r = 2.33) and it has low losses.

The antenna is comparable with other antennas approaching the theoretical limit of bandwidth versus volume in wavelengths.

4.4.6 Findings

Measured and simulated results for a resonant-fed thick quarter-wave patch were studied. The bandwidth obtained in the measurements was 35 %. The simulated bandwidth was clearly lower than the measured bandwidth, which indicates that model used in simulation needs improvements, particularly in the modeling of the probe. The performance of the prototype can also be improved by optimizing the dual-resonant input impedance.

The antenna bandwidth can be widened by using resonators. In this antenna the feed is modified to a radiating resonator within the antenna volume: it is actually an antenna-fed patch. Compared to the conventional method of having the second resonating circuit separately outside the antenna, this method reduces the total size of the antenna structure. The structure gives a possibility to experiment in creating a third resonance. It would be a patch resonance, formed on top metal of the substrate capacitor.

The antenna could be used in cellular base stations when wide bandwidth is required and polarization separation is not necessary. The antenna could be modified for mobile handsets for example by using a substrate material of higher permittivity and by reducing the height. These modifications would shrink the size of the antenna but would also reduce the bandwidth, typically proportional to volume. By using this design it is possible to modify the antenna to an almost smallest possible antenna for the required bandwidth (10%...28%, depending on the individual case). The main problem is the radiation pattern and polarization change with frequency. This is normally not desirable and therefore further analysis and development of this structure was not seen necessary.

4.5 Half-wave stacked patch antenna

There is a need to have antennas with wide bandwidth and high polarization purity that can receive both polarizations separately for base stations and for the channel sounder measurements. The half-wave patch antenna has inherently lower cross-polarized level than a quarter-wave antenna. A thick substrate is needed for the wide bandwidth, but when using the probe feed the polarization purity is lost. A solution is to use a patch on a thin substrate, and another patch with a thicker substrate on top of the lower patch as a second resonator to widen the bandwidth. The lower patch is fed by a short probe which does not cause too much cross-polarization. The result is called stacked half-wave patch antenna [67].

In a half-wave patch it is possible to excite two separate polarizations simultaneously, in orthogonal directions. Therefore two feeds can used for the same antenna, one fore each polarization. When both polarizations are received with the same antenna element the location for each polarization is same, which is an advantage in channel sounder measurements.

The antenna was designed for the 2154 MHz center frequency and for ±50 MHz bandwidth (with return loss $L_{ret} > 10$ dB). The polarization isolation is planned to be comparable with other antennas designed for good polarization isolation, Section 4.6.1.

One purpose of this section is to investigate whether the FDTD simulation is a valid tool for antenna design [87]. The investigation is done in this section because the antenna under consideration has high requirements regarding cross-polarization separation and also because the impedance matching of the coupled resonant structure of a stacked patch antenna is a critical task.

4.5.1 Antenna structure

The antenna is made of two half-wave patches on top of each other above the ground plate, Figure 32 and Figure 33. The patches are made of 0.5 mm thick copper plate. The dimension of the lower patch d_1 = 60 mm, and the dimension of upper patch d_2 = 54 mm. The lower patch is connected to two probe feeds through an 1pF matching capacitor. The ground plate dimensions are 100x100 mm^2. Lower patch is 2 mm above the ground plate and the upper patch is 5 mm above the upper plate and 7.5 mm above ground plate because of the 0.5 mm thickness of the lower plate.

The simulated antenna had otherwise same dimension except the top plate (d_2) was 56 mm, since it gave more similar results to the measured ones than the 54 mm size. It is still within the accuracy of the FDTD simulator at 1 mm voxel cube and the prototyping tolerance of ±0.5 mm.

The parameters for the simulation were set in the following way: The material in the simulator representing the copper of the prototype is perfect electric conductor. The use copper as the material in the model did not make any real difference in the results, it only slowed down the calculations. The excitation is a line excitation between the bottom end of the feed probe and the ground surface. The load corresponds to a vertical (z-directional) line made of a σ = 20 S/m material. In the 1 mm grid the length of the load is 1 mm and the cross-section is 1

mm^2, which results to a 50Ω resistance. The load is in the corresponding place as the excitation (line feed) in the transmitting antenna: one end connected to the bottom end of the probe and the other end connected to the surface of the ground plane.

The voxel cube size is 1mm which corresponds the design unit of the prototype. The calculation consists of a 32 timesteps wide Gaussian pulse in order to get wideband impedance calculation for the frequencies between 0.1...30GHz. In order to get impedance values at relatively small frequency intervals (7.5 MHz), a relatively high number (8000) of iteration steps were used. Short frequency intervals are needed to see the double resonance in the output.

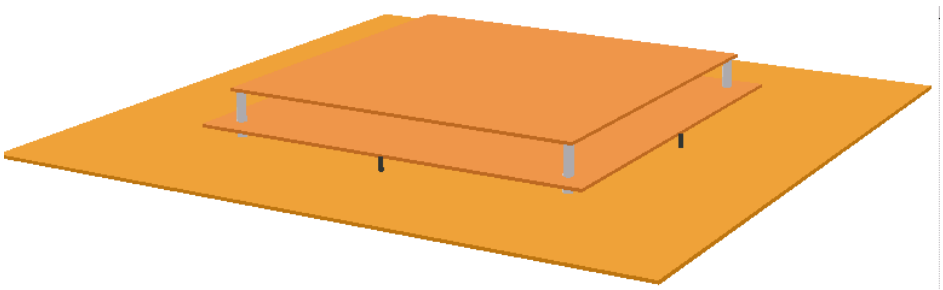

Figure 32. Antenna structure: capacitors black, supports gray.

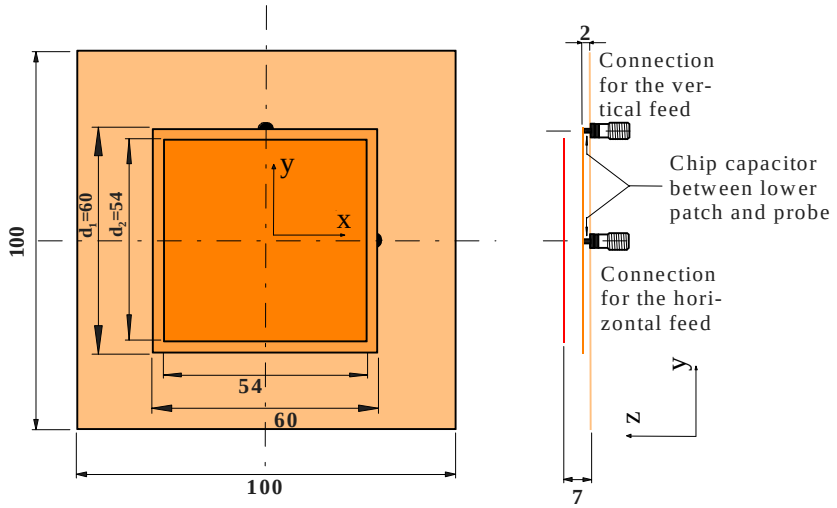

Figure 33. The dimensions of the antenna (in mm) The active feed in the simulations and measurements here is on the y-axis in the radiation pattern plots. Therefore the E-plane is in yz-plane, and the H-plane is in xz-plane. The angle is the deviation from the z-axis, and the angle is positive towards the positive y-direction in E-plane and towards the positive x-direction in H-plane.

The FDTD grid pattern representation is in Figure 34.

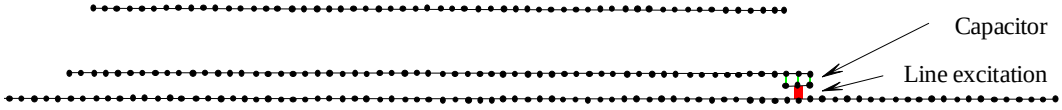

Figure 34. The FDTD grid pattern. The figure is a cross-section cut along the central y-directional line. The ground plate is only partially shown. The black lines represent y-directional PEC lines and the dots represent the x-directional PEC lines. The green lines represent the insulator in the capacitor, ε_r = 30, length of capacitor edge 2 mm. C = 1.1 pF. The grid is 1 mm.

4.5.2 Impedance matching

The reflection coefficient in Figure 35 shows that the antennas are similar both in measured and simulated cases. The center frequency is about the same. The measured 10 dB bandwidth is wider (10%) than the simulated bandwidth (4.8%).

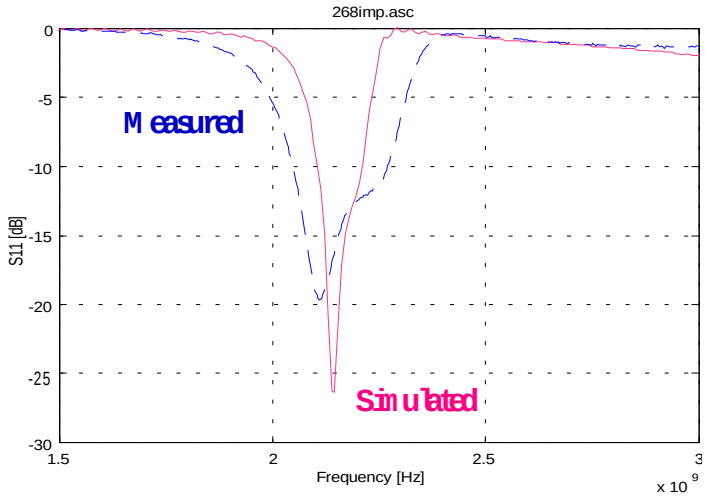

Figure 35. Reflection coefficient.

4.5.3 Impedance on Smith chart

When the impedance is shown on a Smith chart, it reveals the form of the double resonance of this type of antenna, both in the measured and the simulated impedance with the same frequency sweep. The small circle in the center in the chart is the 10 dB return loss circle. The impedance plot should reside inside the –10 dB return loss circle in order to achieve the widest bandwidth fulfilling the criterion of 10 dB return loss.

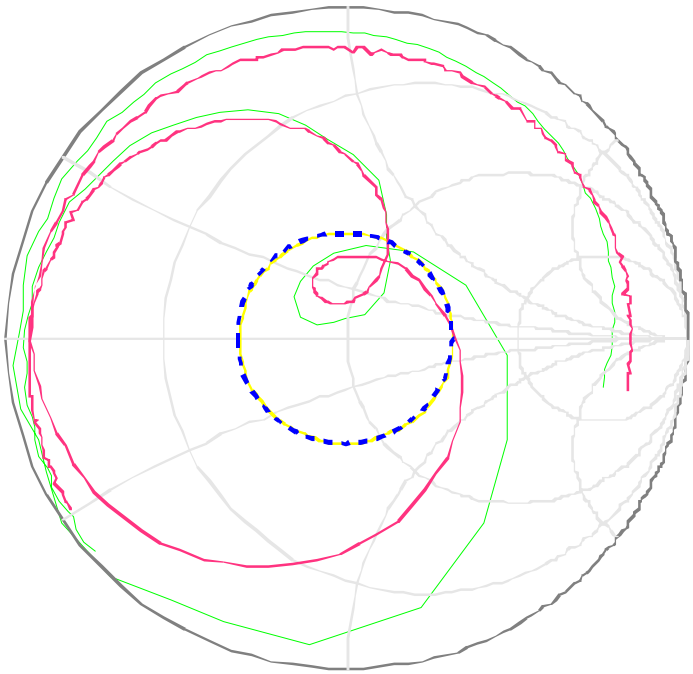

Figure 36. Simulated impedance between 1442...3867 MHz on Smith chart (Green curve, larger loop). Measured impedance between 1500 ...3000 MHz on Smith chart (Red curve, smaller loop).

The reference plane of the simulation was moved 20 mm (0.143· λ at 2143 MHz in the air) towards the generator so that the simulated and measured impedance are positioned having the measured loop completely inside the simulated loop. The SMA connector (with Teflon insulation) in the measurement corresponds 15 mm (0.107· λ at 2143 MHz in the air) rotation. From Figure 36 one can see that the measurement and the simulation agree very well in the shape of the impedance curve. The small differences are caused by prototyping tolerances in the prototype and the simplifications made in the simulation model, and the model voxel size.

Neither curve show an optimal matching, but this type of antenna is easy to tune, because the upper and lower patches are connected with plastic nuts and bolts. The tuning is done by adding or removing washers under the lower and upper patches, or by replacing the lower or upper patch with a patch of different size.

4.5.4 Radiation pattern in H-plane

If there are problems in the cross-polarization separation, it will be most apparent in the H-plane radiation pattern. Therefore only the H-plane radiation pattern is under study here, Figure 37 and Figure 38.

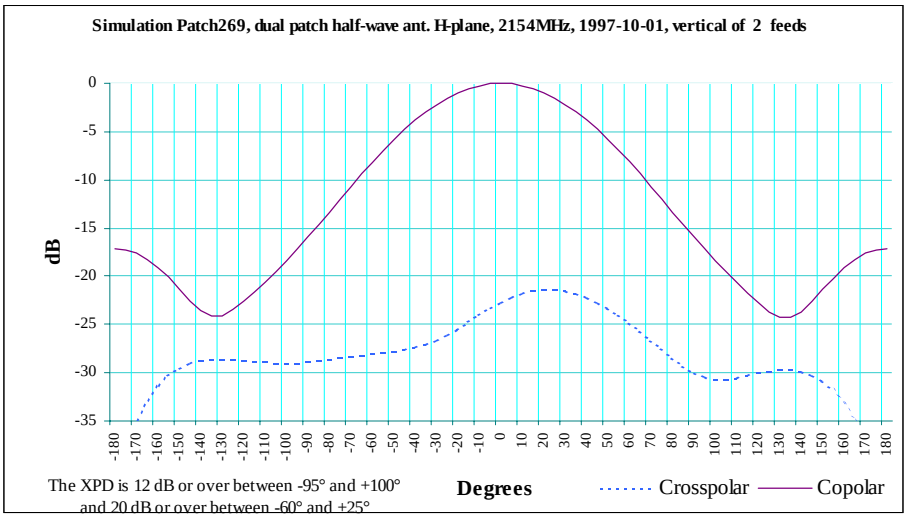

Figure 37. Simulated radiation pattern of the stacked patch antenna, H-plane. Normalized dB-scale. The simulation included the 50 Ω resistance at the second feed.

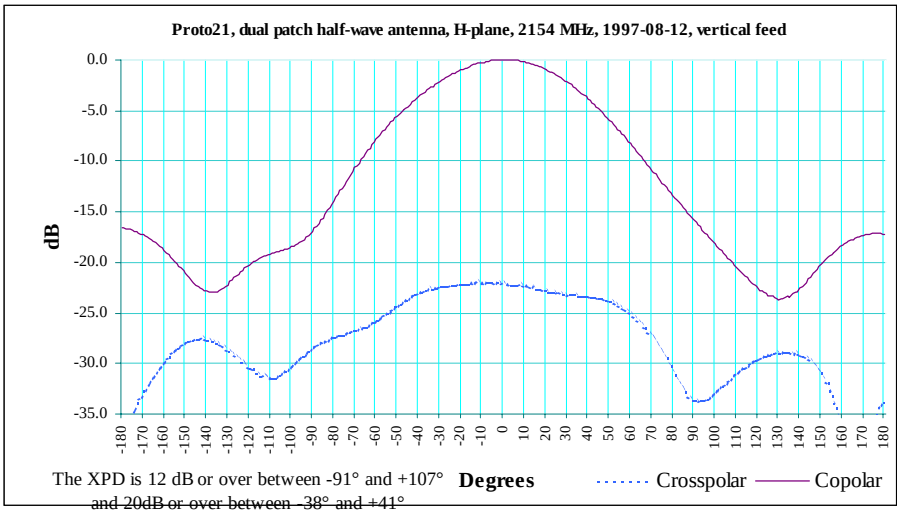

Figure 38. Measured radiation pattern of the stacked patch antenna, H-plane. Normalized dB-scale. The measurement included the 50 Ω resistance at the second feed.

The isolation between feed ports in the same antenna patch $|S_{21}|$ (inverse of cross-polarization isolation *XPI*) was measured and it is 21dB at 2154 MHz.

An initial check of mutual coupling between two antennas having ground plates beside each other (100x100 mm^2 ground plate corresponds $0.7\cdot\ \lambda$) gave -24 dB at 2154 MHz. These values of *XPI* and mutual coupling are satisfactory, although some improvement would be desirable.

The similarity of the measurements and simulations is apparent. FDTD is useful when designing prototypes and when evaluating the effect of changes in the design before modifying the prototype.

4.6 Dielectric feed

The antenna is fed using a probe which is essentially the center conductor of the coaxial cable where the outer conductor or shield is cut at the level of the ground. The capacitor between the probe and the lower patch of the stacked patch antenna is mainly used as a matching capacitor, to counteract the effect of the inductance caused by the feeder probe. The capacitor also reduces the length of the probe, thus reducing the cross-polarization. The stacked patch antenna design also requires positioning the probe at the edge of the lower patch, so it is easier to position the capacitor there during construction. In this section the idea of a matching capacitor is developed to a dielectric coupling system, electrically resembling the aperture coupled feed.

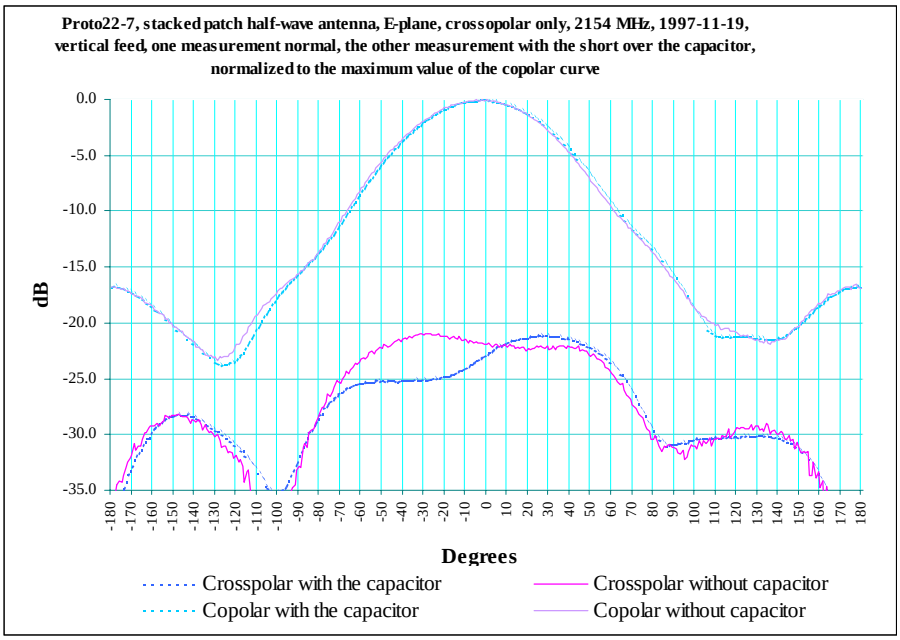

Figure 39. Effect of the capacitor in a half-wave stacked patch antenna. Normalized dB-scale.

Figure 39 shows the effect of a chip capacitor. The capacitor improves the *XPD* to some extent. The effect of the capacitor depends on its position and orientation. To make best use of the capacitor, the capacitor's plates should be parallel to the patch.

4.6.1 Comparison and theoretical limit of the cross-polarization separation

Antennas designed for good polarization isolation have cross-polarization separation over 20 dB within the 3 dB beamwidth [62] or maximal cross-polar level 17 dB below the maximum co-polarized value of the antenna [63]. The values in [34] can be used as general references: *XPD* is 18…24 dB for circular patches, *XPD* is 24…45 dB for a rectangular patch. The reference horn used in the measurements has *XPD* = 40 dB in broadside direction which can be considered as upper limit for *XPD* achievable.

The cross-polar isolation (*XPI*) is similar as the coupling between the ports S_{21}, if the ports are feeds for orthogonal polarizations. The absolute values are same but *XPI* is always positive. Values of over 30 dB are often specified [54]. *XPI* = 35 dB was reached in [54]. *XPI* > 24 dB was reached in C-band in [68]. This is a simple measure, but it does not tell what is the cross-polar separation into various directions, for example the *XPI* = 35 dB in the antenna in [54] but *XPD* is only 17 dB at 50° in azimuth plane, which is slightly less than in the antenna of this study.

4.7 Half-wave stacked patch antenna with dielectric feed

The dimensions of the antenna are shown in Figure 40 and a close-up of the feed is shown in Figure 41. The basic structure is the stacked patch antenna [67], and the feed connector is same, but the probe is as short as possible, and a substrate with metal on both sides forms the feeder dielectric feed, or feeder capacitor.

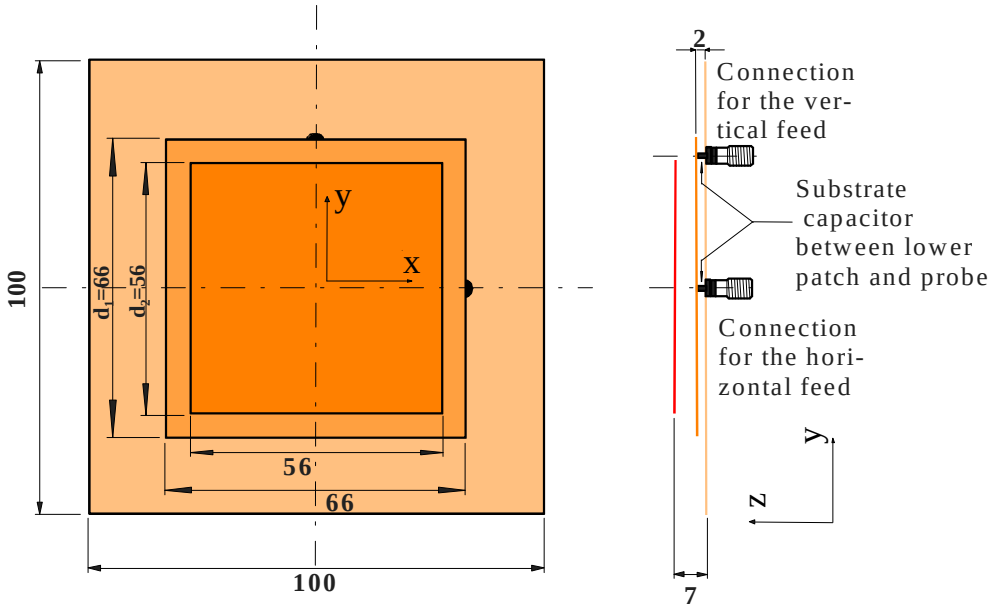

Figure 40. Half-wave stacked antenna with dielectric feed. Dimensions in mm. The active feed is in y-axis in the radiation pattern plots. Therefore the E-plane is in yz-plane, and the H-plane is in xz-plane. The angle is the deviation from the z-axis, and the angle is positive towards the positive y-direction in E-plane and towards the positive x-direction in H-plane.

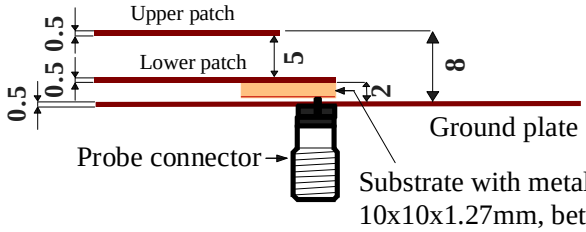

Substrate with metal on top and bottom, dimensions 10x10x1.27mm, between the probe tip and the lower patch in pressure contact. ε_r = 2.33. C = 1.62 pF. Probe protruding 0.7 mm above the surface.

Figure 41. Enlargement of Figure 40 at the feed point showing the structure of dielectric feed. The FDTD grid pattern representation is in Figure 42.

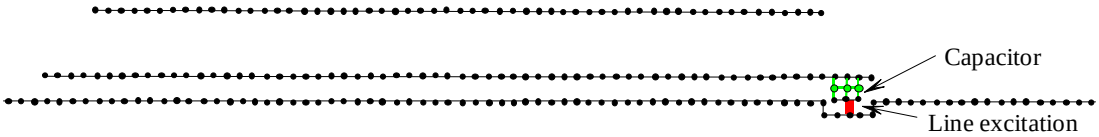

Figure 42. The FDTD grid pattern. The figure is a cross-section cut along the central y-line, the ground plate only partially shown.. The black lines represent y-directional PEC lines and the dots represent the x-directional PEC lines. The green lines and dots represent the insulator in the capacitor in z- and x-axis, ε_r = 100, length of capacitor edge 2 mm. C = 1.77 pF. The grid is 1 mm.

The dielectric feed was implemented by dielectric plate placed between the lower plate of the antenna and the top of the center of the coaxial cable. The dimensions of the plate are 2x3x1.27mm. The dimensions of the lower patch were 64x64 mm^2 in the simulation, because that produced the same impedance match as the 66x66 mm^2 patch in the prototype. This is within the step size in the simulations using 1 mm voxel cube because the patch is symmetrical so the step size is 2 mm. In the construction the distance of the lower plate from the ground is critical, because the relative changes in the prototyping tolerance are high.

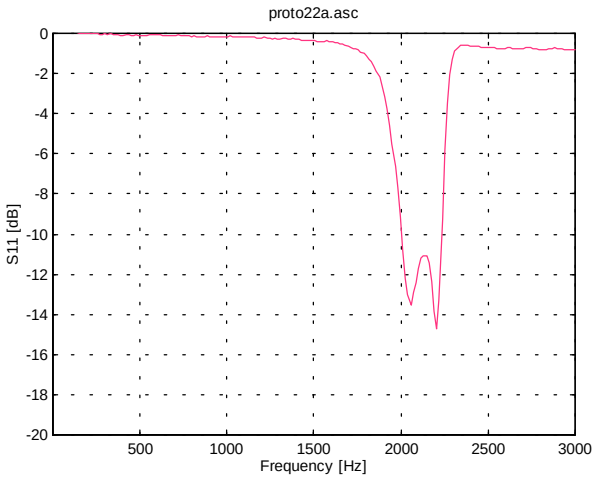

Figure 43. Measured reflection coefficient.

The bandwidth with L_{ret} = 10 dB is 11.2%, Figure 43. From Figure 44 one can conclude that the matching of the double resonance is not perfect, because the loop does not go around the center of the Smith chart, and bandwidth can be increased if necessary.

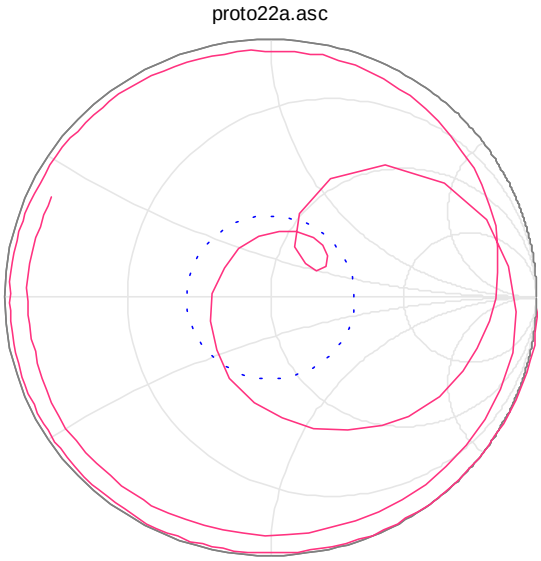

Figure 44. Measured impedance on Smith chart.

One has to be very precise when positioning the antenna in the measurement of the crosspolarization. The cross-polarized level is very low and it will increase if the antenna rotates a few degrees around the *z*-axis.

Figure 45 and Figure 46 show the radiation patterns of the antenna in E-plane and H-plane. In E-plane the *XPD* > 20 dB between -72°...+41° scanning angles. In H-plane *XPD* > 20 dB between -57°...+78° scanning angle. This exceeds the requirements of the the antenna (*XPD* > 20dB between ±30°, section 3.1.1). The gain is 6.6±1 dBi and the beamwidth is 60° in E-plane and in 70° H-plane.

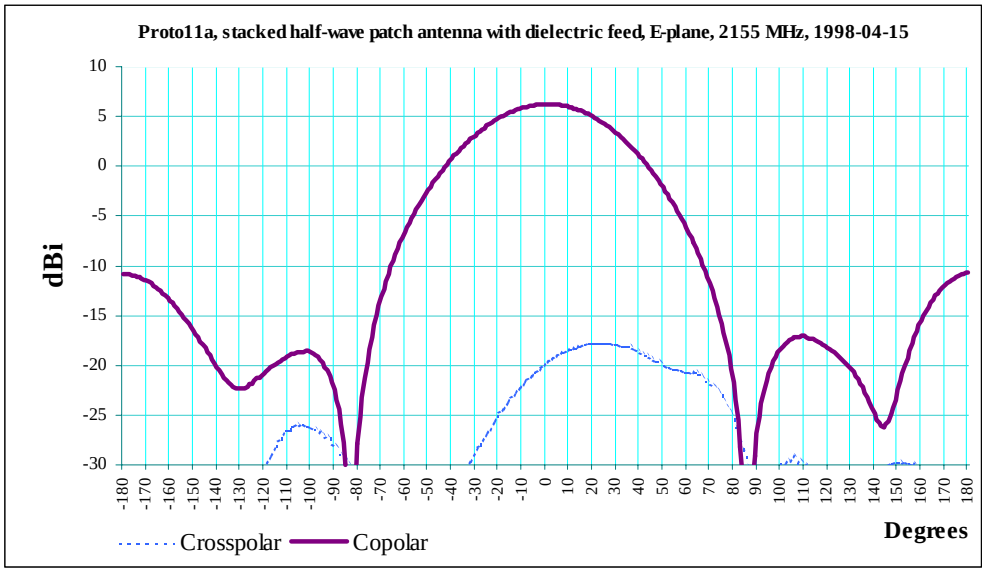

Figure 45. Measured radiation pattern in E-plane. The antenna has two dielectric feeds, and the feed for the other polarization is terminated with a 50Ω load The maximum cross-polarized level is -25.0 dB below copolar level in the z-direction. XPD>20 dB between -72°...+41° scanning angles.

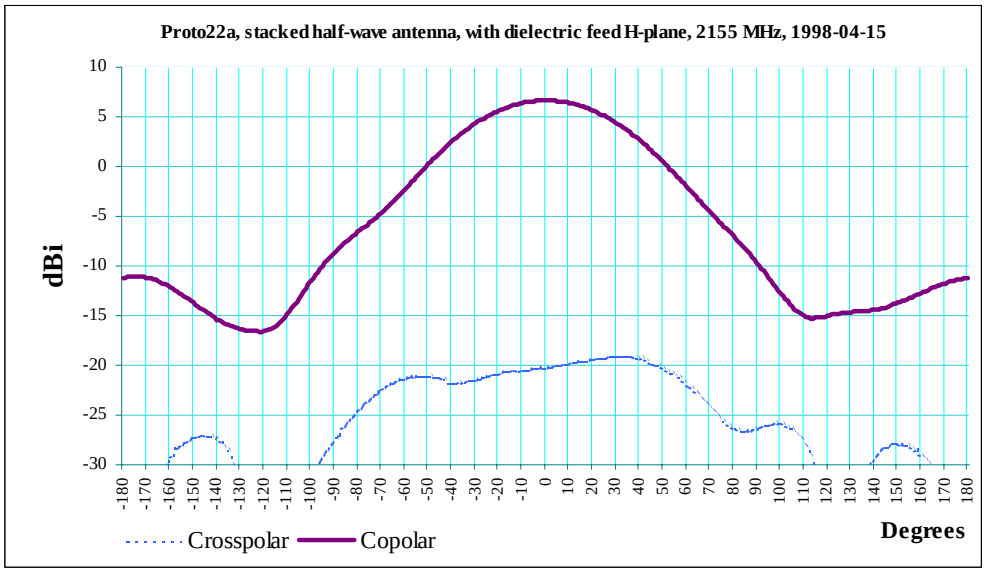

Figure 46. Measured radiation pattern in H-plane. Dielectric feeds, and the other feed is terminated with a 50Ω load The maximum cross-polarized level is –25.6 dB below copolar level of the z- direction. XPD>20 dB between -57°...+78° scanning angles.

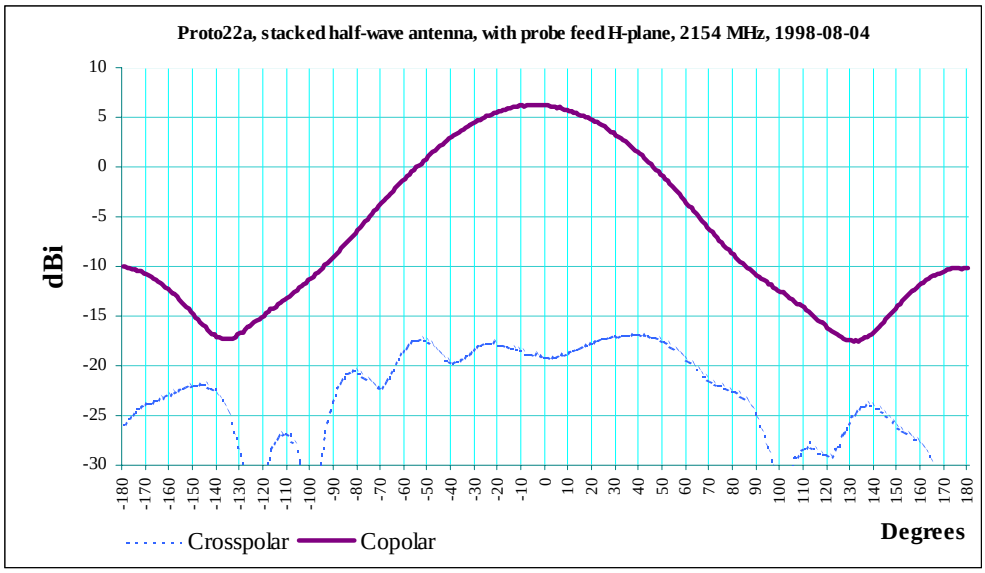

Figure 47. Measured radiation pattern in H-plane, ordinary probe feed. The other feed is terminated with a 50Ω load. The maximum cross-polarized level is –23 dB below copolar level of the boresight direction. XPD>20 dB between –48°...+33° scanning angles.

One can see that the dielectric feed decreases the maximum cross-polar level by 2.6 dB in the measured two similar antennas, Figure 46 and Figure 47. The prototype with dielectric feed in Figure 46 is 3.6 dB better than the simulated one in Figure 48. The probe-fed prototype in Figure 47 is 2 dB better than the simulated one in Figure 49.

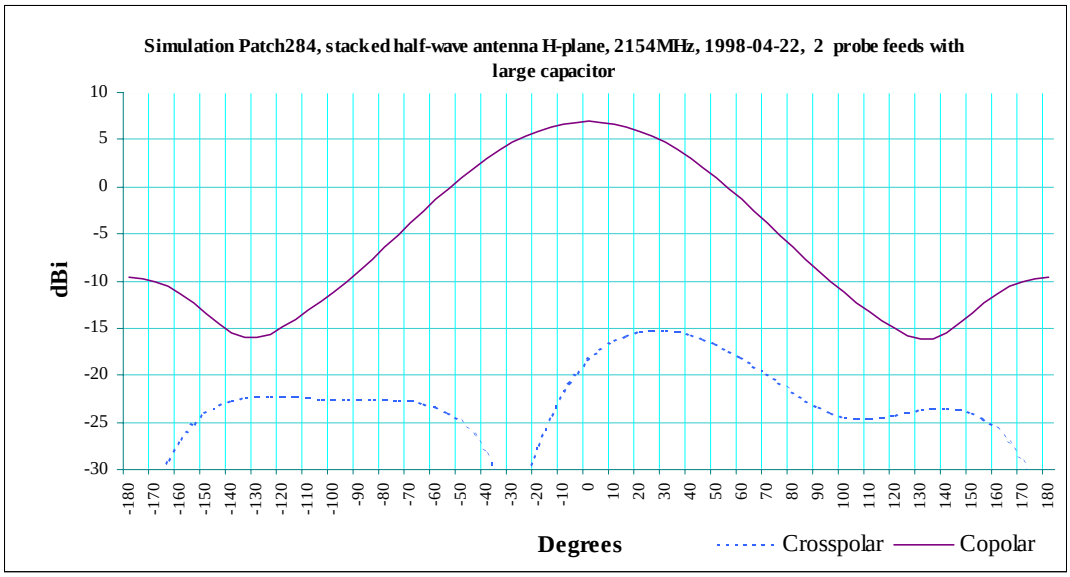

Figure 48. Simulated radiation pattern in H-plane. Dielectric feed, and the other feed is terminated with a 50Ω load The maximum cross-polarized level is –22 dB below copolar level of the boresight direction. XPD>20 dB between –65°...+30° scanning angles.

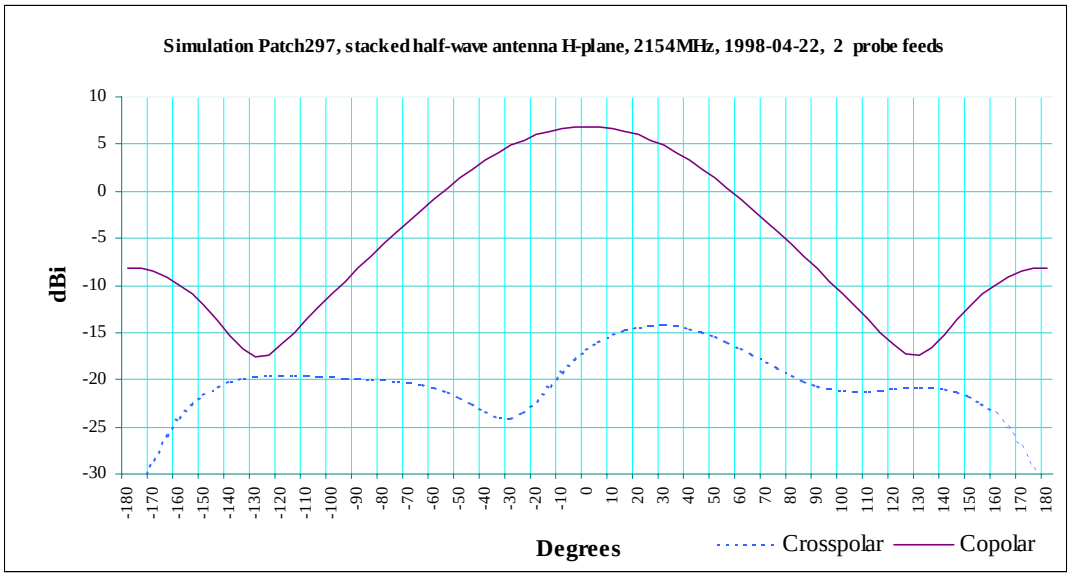

Figure 49. Simulated radiation pattern in H-plane, ordinary probe feed. The other feed is terminated with a 50Ω load The maximum cross-polarized level is –21 dB below copolar level of the boresight direction. XPD>20 dB between –60°...+25° scanning angles.

One can see that the capacitor feed decreases the maximum cross-polar level by 1 dB in the theoretical simulation for two similar antennas, Figure 48 and Figure 49.

The simulation with one dielectric feed shows (Figure 50) that the best cross-polarization separation is obtained with the single feed antenna arrangement.

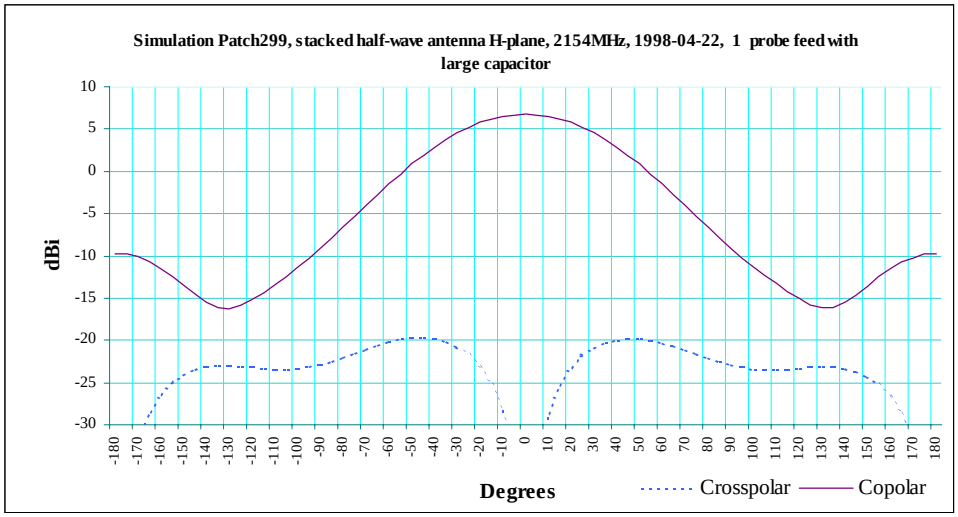

Figure 50. Simulated radiation pattern in H-plane, one dielectric feed. The maximum cross-polarized level is –26 dB below copolar level of the boresight direction. XPD>20 dB between -55°...+55° scanning angles.

4.7.1 Discussion

The dielectric feed increases the cross-polar discrimination 2.6 dB in the measured case and 1 dB in the simulation. The simulation predicts the behavior of the antenna. The increase is notable, but not incisive. The direct probe feed is mechanically rugged and therefore is preferred for the field use.

In order to get good cross-polarization separation, the dielectric feed should be relatively small and well centered.

In the normal operation, there is a matched receiver in the other feed, so the measurements and simulations are made so that the other feed has a 50Ω matched load. It will absorb cross-polar energy, and an equal amount of energy is radiated back (in matched case [42]), which fills the dip in the middle of the H-plane cross-polar radiation pattern.

Good impedance matching reduces the cross-polar component and also S_{21}, because more power is radiated, and less power is going to the other feed therefore also less power reradiates. It means that good impedance matching like L_{ret} > 20 dB is desirable especially at frequencies where the signal spectrum has strong components.

4.7.2 Findings

The dual-resonator patch with the lower resonator close to the ground plate results in low cross-polarized component. Using the idea of the dielectric feed the cross-polar component is further reduced, although the aperture feed is even better [94]. The probe feed is easy to manufacture for prototypes and is inherently sturdy, and the industry often favors galvanic contacts because components are connected using leads. The aperture feed is good for large scale manufacturing and is also mechanically stable. The dielectric feed is easy to manufacture for prototypes, but the electromechanical construction should be further developed. The stacked patch antenna with dielectric feed is feasible in the dual polarized arrays in the radio channel sounder project.

5. Array structures

Adaptive antenna systems need two or more antenna elements. The antennas can consist of a group of arbitrarily positioned elements, or more commonly, of an array. This chapter concentrates on array aspects: mutual coupling between elements and array structures.

One focus in this study is to develop antenna arrays that can separate two polarizations. This makes polarization diversity possible and hence adds one more dimension to be used in the adaptive processing.

The adaptive antenna process can adapt without previous knowledge of the signal path directions. Therefore studying the antenna array patterns might be seen unnecessary. Adapting after an arbitrary starting point can be however too slow in mobile communications. In contrast, if the antenna array pattern is known beforehand and the main beam is narrow, the adaptive system can quickly find the approximate direction of the signal by beam switching, and then the adaptive system can finish the full adaptive process much faster.

The level of the interfering signals can be higher than the desired signal. Therefore low sidelobe levels facilitate the finding of the desired signal. For the above mentioned reasons it is useful to design and optimize an array that has a narrow main beam and low sidelobes, Sections 5.3 and 5.4.

5.1 Antenna array configurations

The basic array configurations are introduced in this section. The structure dictates the available scanning angle, the achievable beamwidth and the sidelobe levels. Also the possibility for one-dimensional or two-dimensional scanning depends on the structure.

5.1.1 Linear arrays

Linear arrays are simple and the theory of them is well known. The linear array was not studied in this work, except as a benchmark for the cylindrical array. The scanning is one-dimensional. The available scanning angle is limited by the maximum allowed width of the main beam, and also by the maximum allowed grating lobes if element spacing over $0.5 \cdot \lambda$ is used.

5.1.2 Planar arrays

The planar array has elements in two dimensions on a flat surface. Two-dimensional scanning, in other words horizontal and vertical scanning can be done. The triangular antenna element in Figure 2 was designed for the array in Figure 51 having two polarizations. The idea was to minimize the mutual coupling by having maximum separation between the radiating ends of antennas by using the patch antenna in the corner of the ground plate.

If the elements are dual polarized, it is possible to minimize the cross-polarization of the array by suitable positioning of the antenna elements [91].

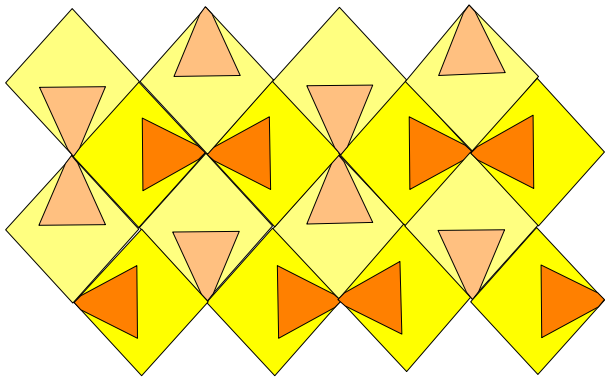

Figure 51. Planar array made of triangular patches on a square ground plate, two polarizations.

This array was not implemented since the level of the mutual coupling was still too high and the cross-polarization separation was not sufficient. In the further research a wider element spacing should be tested.

5.1.3 Cylindrical array

A cylindrical array might be feasible when the angular spread is large, especially in micro- and picocells (page 54, Table 1 in [65]). However, there are some problems to overcome. One is the difficulty to reach a narrow beamwidth. If the cylindrical array has few elements, it can be made small, but the beamwidth is large. For example a 40° beamwidth can be achieved by an 8 element array. Even with directional elements it is difficult to achieve a narrow beam, because the elements are pointing away from each other.

The effective width of the cylindrical array is smaller than in linear arrays with the same number of elements, because the projected spacing of the antenna elements shrinks from centre of the projection to the projected edges [58].

The sidelobe level of the cylindrical array tends to be high (- 10 dB), especially if the number of elements is low and the elements are omnidirectional. Yet, it is possible to design a cylindrical array with low sidelobes with high number of elements [77]. Increasing the element spacing beyond $\lambda/2$ quickly increases the sidelobe level. The bandwidth in the cylindrical array is limited, unless the elements are directive [58].

The cylindrical antenna array does basically one-dimensional scanning. It can also do limited vertical scanning as the ring antenna array [58]. Depolarization caused by the curvature of the surface is a problem [27]

Figure 52. The shape of a cylindrical array with patch elements.

5.1.4 Spherical array

A spherical array does basically two-dimensional scanning, particularly it can receive and separate signals equally in every 3-D direction. It can be useful for indoor communications where reflections come from ceilings, floors, and walls. It is useful in radio channel sounder applications. The array is difficult to manufacture and even antenna spacing can be achieved only if the number of antennas is 20 or less.

5.2 Reduction of the mutual coupling between array elements

When antenna elements are placed beside each other, there will inevitably be mutual coupling, which means that the antenna elements receive signals from the other antennas of the array. Normally mutual coupling is harmful and it should be minimized.

The mutual coupling was quite high in tentative measurements, especially with the triangular antenna with metal walls in Section 4.1. In order to reduce mutual coupling one has to know the mechanism of the mutual coupling. In the antenna used here the substrate is of air, so no surface waves should exist. The coupling is reactive or by space wave. But if the structure has many elements in a regular fashion, it corresponds a corrugated or periodic structure which can support surface waves [72]. The FDTD simulation can show the electromagnetic fields advancing as time series and therefore the FDTD simulation was used here to show the mechanism of the mutual coupling.

In the simulation an infinite array model would be best for this purpose. This would require the use of magnetic walls in the model, but this option was not available. Therefore the simulations were made with an antenna pair. The wall is on one side of the antenna only, because of the space limitations of the simulation. Two techniques for reducing the mutual coupling were tested: a metal wall or a dielectric wall between antennas.

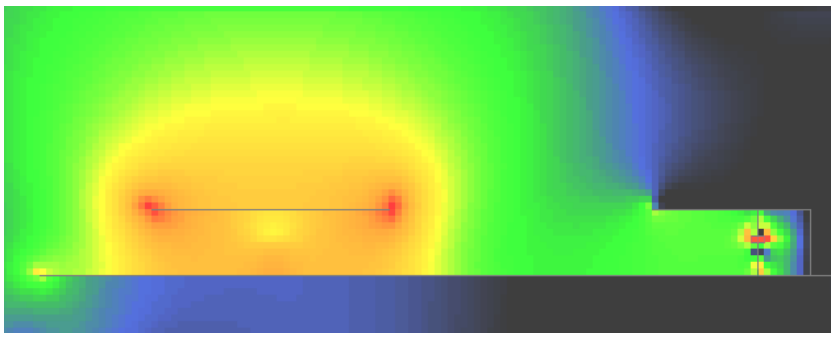

Figure 53.Illustration of an XFDTD simulation. In this picture the electric field strength in z-direction, E_z (Axes and antennas are same as in Figure 54, but no wall).

In Figure 53 there is an illustration how the electric field of a transmitting antenna element affects the nearby passive antenna element. In this case there is no wall between two patches. The mutual coupling $|S_{21}|$ = –20 dB.

5.2.1 Metal wall between two patches

The idea of using walls or cavities between elements to counteract the mutual coupling effects is suggested in [71] and [93]. Therefore a similar approach was

studied. The studied configuration is shown in Figure 54. The configuration simulates the array configuration in Figure 51 where the neighboring antennas have opposite polarities. The studied case corresponds to the worst case where the radiating ends are as close as possible. The shape of the patch and the dimensions are not same because the goal was to see whether the wall is effective. The ground plate dimensions are 140x140 mm, and there is a 10 mm high wall in the middle. The patches are similar, the patch width is 36 mm and length 24 mm, substrate thickness 10 mm. The probe is 8 mm from the short. The left patch is the transmitting patch, and the right hand side path is the receiving patch. The excitation is a vertical line excitation between the bottom end of the probe and the surface of the ground plane. The load corresponds to a vertical (z-directional) line made of a σ = 20 S/m material. In the 1 mm grid the length of the load is 1 mm long and the cross-section is 1 mm^2, which results to a 50Ω resistance. The load is in the corresponding place as the excitation (line feed) in the transmitting antenna: one end connected to the bottom end of the probe and the other end connected to the surface of the ground plane.

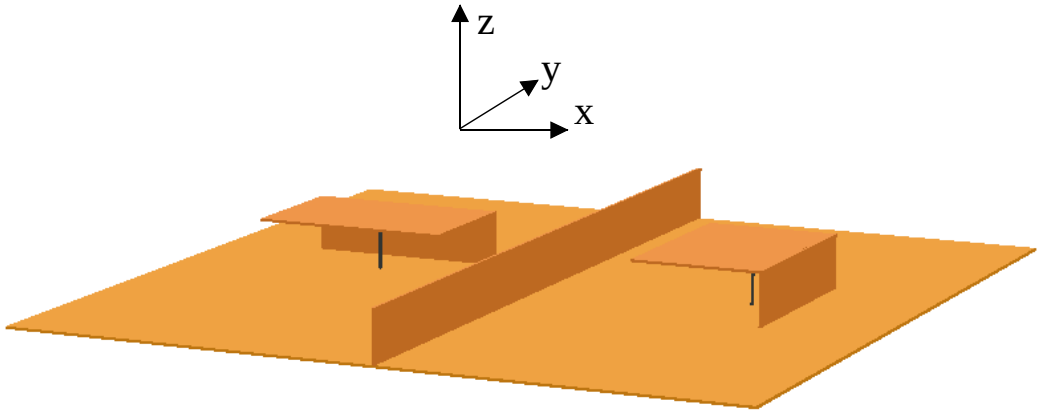

Figure 54. Schematic setup for the mutual coupling simulation and coordinates. Two similar patches, and a wall between the patches.

The mutual coupling is mainly between the side of one antenna and the radiating edge of the other antenna, as in a two-polarized antenna array, Figure 51. The spacing between antenna centers is 0.5· λ at 2154 MHz (35 mm). The metal wall is 10 mm high and it was modeled as PEC. The time point of the figures is at 1980 steps in simulation. The mutual coupling $|S_{21}|$ was calculated as -20 dB in the simulation.

The neighboring antenna element and the metal wall between elements change the radiation pattern and also increase the cross-polarized level, noticed from the radiation pattern from the simulation. Increasing the wall height decreases the bandwidth. Therefore the metal wall is not useful with this patch antenna, because the electrical field has a strong E_z component which travels to the next antenna element.

The electric field is shown in three figures, Figure 55, Figure 56, Figure 57. Each figure shows one component of the orthogonal fields.

In Figure 55, the electric field component E_y is parallel to the ground and parallel to wall horizontally, and the wall works efficiently. In Figure 56 the electric field

component E_x is parallel to the ground and perpendicular to the wall. The wall is not so efficient anymore. In Figure 57 the electric field component E_z is perpendicular to the ground and parallel to the wall vertically. For E_z the wall does not attenuate the propagation. The metal wall works well for dipole and slot antennas [27]. In those cases the direction of the electric field E is parallel to the ground plane.

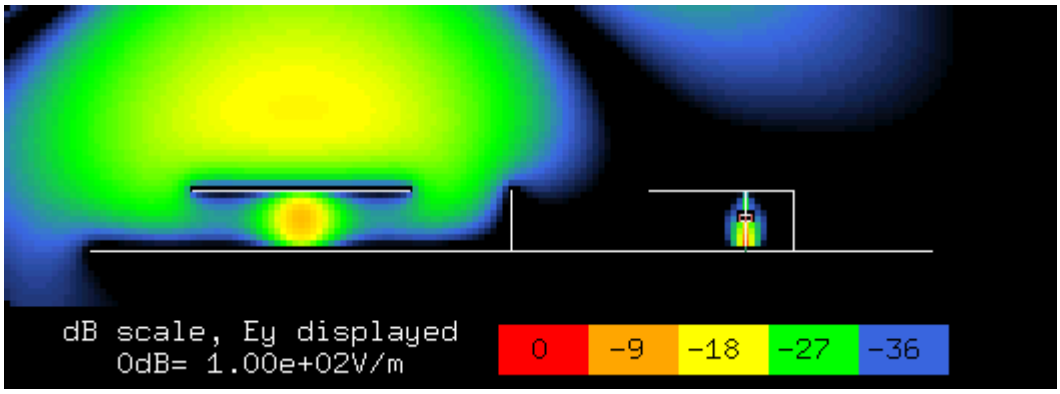

Figure 55. Simulation Patch172, electric field strength in y-direction.

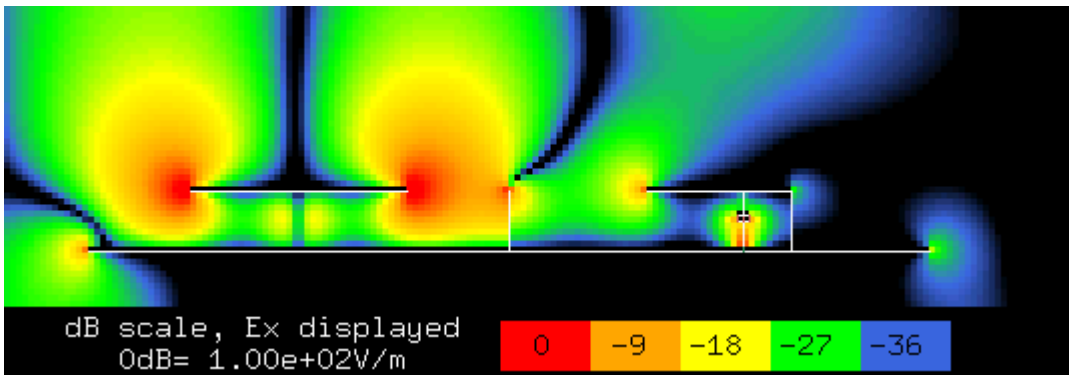

Figure 56. Simulation Patch172, electric field strength in x-direction.

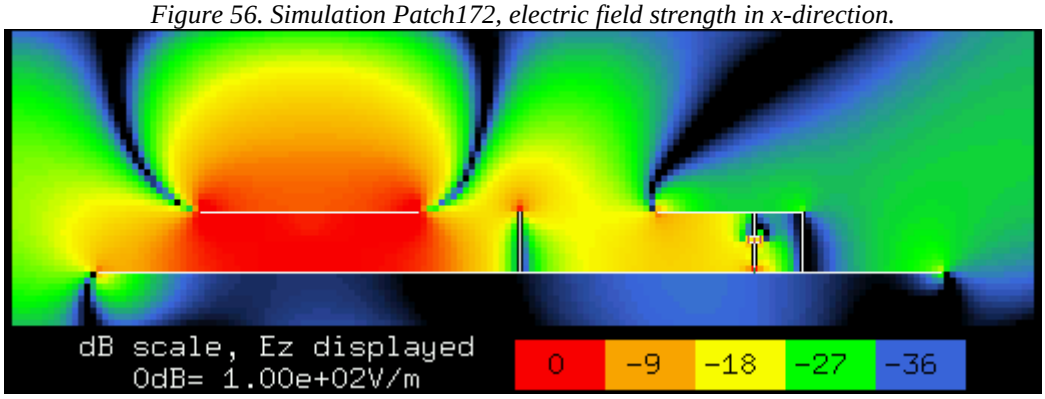

Figure 57. Simulation Patch172, electric field strength in z-direction.

5.2.2 Dielectric wall between two patches

In this case the configuration is as in Figure 54. Now the wall is 30 mm high dielectric wall, permittivity ε_r = 49, conductivity σ = 100 S/m. The wall has brown color. The time point of the figures is at 2000 steps in simulation. The mutual coupling $|S_{21}|$ is –34 dB.

The electric field is shown in three figures, Figure 58, Figure 59, Figure 60. Each figure shows one component of the orthogonal fields.

In Figure 58 the electric field component E_y is parallel to the ground and parallel to wall horizontally, and the wall works efficiently. In Figure 59 the electric field component E_x is parallel to the ground and perpendicular to the wall. The wall is not as efficient as in Figure 58. In Figure 60 the electric field component E_z is perpendicular to the ground and parallel to the wall vertically. The wall is better for E_z than for E_x but not as good as for E_y. Therefore the lossy dielectric wall is good in suppressing the mutual coupling, Table1. On the other hand, initial tests showed that the radiation pattern changes and the cross-polarization separation reduces. Therefore the advantages of the dielectric wall may be only marginal, and the wall was not used for antenna array prototypes.

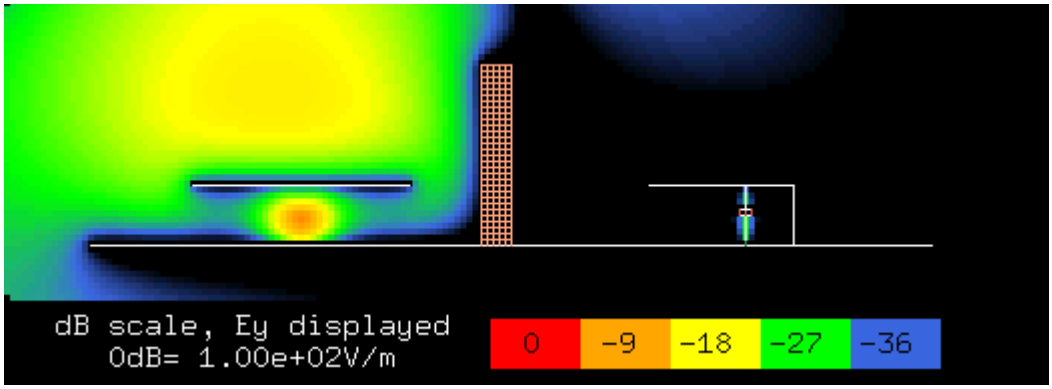

Figure 58. Simulation Patch186, electric field strength in y-direction.

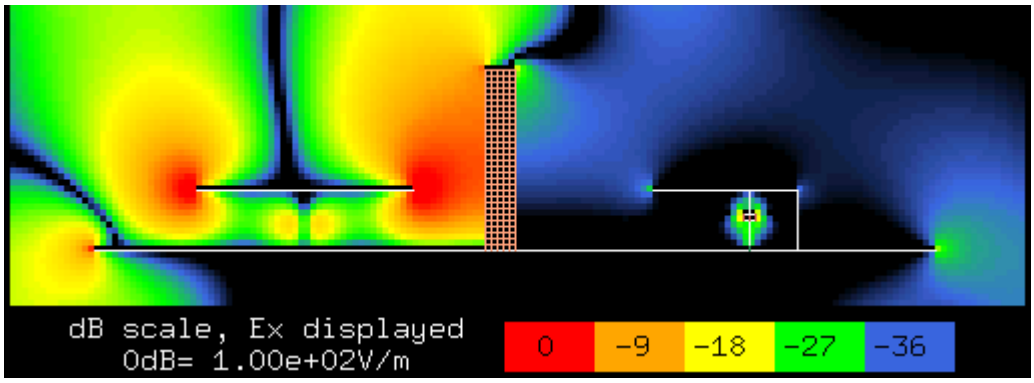

Figure 59. Simulation Patch186, electric field strength in x-direction.

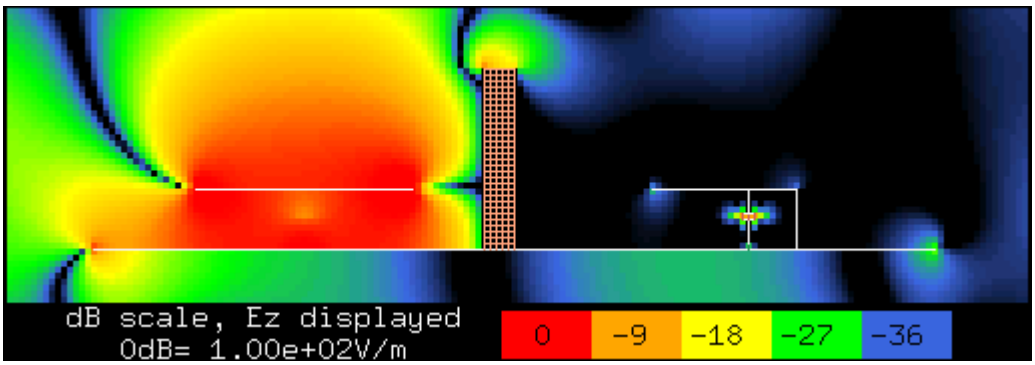

Figure 60. Simulation Patch186, electric field strength in z-direction.

Table 1. Dielectric wall between two patches, attenuation is compared to the case with no wall or metal wall.

ε_r	σ [S/m]	Height [mm]	Width [mm]	Attenuation [dB]
49	10	30	5	13
49	100	30	5	14
49	1000	30	5	16

All the parameters in Table 1. are theoretical. The relative permittivity ε_r = 49 was chosen in order to reduce the wavelength in the material to 20mm at 2154 MHz. Hence the thickness of the material is $\lambda/4$. Only the lowest conductivity σ =10 is realizable, but as it can be seen, increased conductivity increases the attenuation only a little.

5.2.3 Effect of spacing on mutual coupling

The level of mutual coupling depends on many aspects, but one can find some guidelines what can be expected. According to an example in [34] the mutual coupling between neighboring elements with $\lambda/2$ spacing is at worst -21.6 dB.

In this work the initial simulations and measurements the mutual coupling between patch antennas was between –20...-25 dB with element spacing $0.5\cdot \lambda$, depending on the positioning of the antennas. In the simulation with no wall between elements, two patches side by side separated by $0.7\cdot \lambda$, E-planes in parallel, the mutual coupling was about -30 dB. This indicates that increasing the spacing is very efficient. On the other hand, the sidelobe levels increase steeply when the spacing exceeds $0.7\cdot \lambda$.

Increasing the spacing between the antenna elements is the most efficient way to reduce the mutual coupling. Also the directivity of the antenna elements can reduce the mutual coupling.

One could increase the element spacing by putting the elements into two or more interleaved horizontal arrays, vertically separated. The radiation pattern in the horizontal plane corresponds to an array with small element spacing. The other choice is to use only a few antennas widely separated. The grating lobes are ignored assuming that the spatial channel model is diffuse and the grating lobes can be directed towards desired signal or away from interferers [78].

5.3 Cylindrical array with omnidirectional elements

As a general starting point, the cylindrical array can have any size and any number of elements with any element radiation pattern. The maximum radius and the maximum number of elements are often the given constraints, and the radiation pattern of the antenna element has some alternatives. Using the given constraints the antenna array radiation pattern can be optimized for narrowest beamwidth with a chosen sidelobe level. Other optimizations are also possible, for example related to number, depth and width of the nulls.

With omnidirectional element patterns the solution is not simple. Rather, it was

found that **there are certain optimal combinations of radius and element number** with omnidicrectional elements. That gives some constraints in the design of cylindrical array patterns. The directional element patterns have always some side and back radiation, therefore a similar set of optimal combinations is excepted with directional elements.

The number of active antenna elements was chosen to be 7, because it is an odd number and thus one antenna element can be considered as the center element. Sixteen elements were originally considered as the suitable number of elements, and seven elements fill a semi-circle of the 16-element array when the two elements at the ends of the semi-circle are ignored.

In this section the calculations were done using omnidirectional elements because then the sidelobe levels are high and the effect of the radius and the number of elements is easier to distinguish. The weight amplitudes were chosen as unity, in order to get the narrowest main beam. The weight phases were chosen so that the main beam is as narrow as possible, compensating the depth so that all the signals add in phase towards the main direction (0°).

The cost factor *CF* was calculated of the normalized radiation pattern so that sidelobes and above the desired sidelobe level E_d were added to the cost factor at one degree intervals, except at in the area of the desired main beam, equation (2). Vescovo is using a resembling approach: mean-square distance from a given radiation pattern [85].

$$CF = \sum_{i=i_a}^{i_b} (E_i - E_d), \quad E_i \text{ and } E_d \text{ are in [dB]}, \quad E_i > E_d \tag{2}$$

where E_i is the electric field strength towards the direction i in [dB], E_d is the desired electric field strength towards the direction i in [dB], i_a is the starting direction for the cost calculation around the main beam, i_b is the ending direction for the cost calculation around the main beam. Figure 61 shows and example of the intended radiation pattern (design goal) as dotted line: the main beam is 10° wide at -20 dB level and the maximum sidelobe level is –20 dB used in Section 5.4.3. The sidelobes exceeding the maximum level and the main lobe exceeding the desired width are shown as red slanted lines, which shows the area which is added to the cost factor.

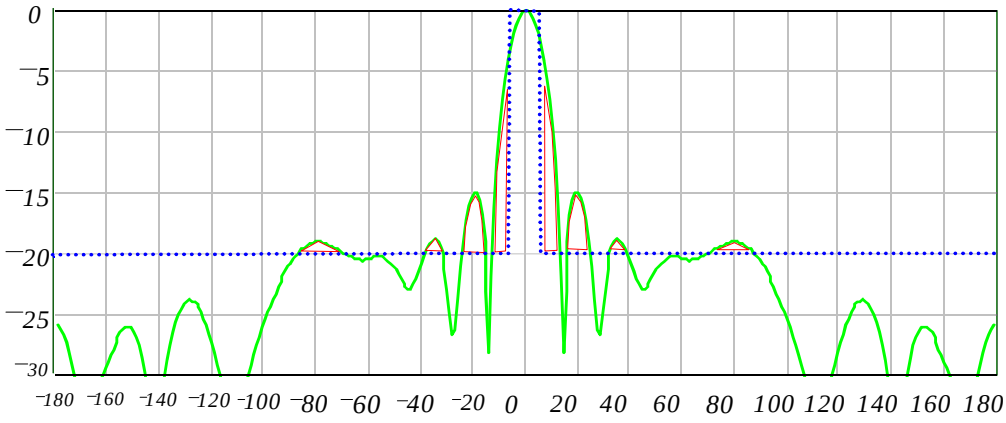

Figure 61. Example of the calculating of the cost factor: dotted line is the intended radiation pattern and the solid line is a real radiation pattern. The red areas show the areas that are added to the cost factor.

The code used in the calculations in this section and the results are in Appendix A and B. E_d = -15 dB, i_a =1, i_b = 360 because in the phasing always causes narrowest main beam with omnidirectional elements with the phasing that corresponds the depth.

Figure 62. Minimum (bottom line), average (middle line) and maximum (top line) cost factor caused by varying the number of elements at different radii (radius = x· 0.25· λ+0.25· λ)

When the radius stays constant and the number of elements varies between 16...49, one can find the maximum and minimum cost factors, and calculate the average cost factor for that radius. Putting that into a plot, Figure 62 shows maxima, averages and minima of the cost factor at different radii, the radius r = (x+1)· 0.25· λ. The starting point is radius r = 0.5· λ and it increases in 0.25· λ steps. When the radius is n· λ where the n is an integer (x=3,7,11...), the cost factor is low, which means low sidelobes and narrow main beam. When the radius is (n+$^1/_2$)· λ, the cost factor is high, which means high sidelobes and sometimes also a wide main beam. The figure suggests that the best antenna arrays have the radius r = 2· λ, 3· λ, 4· λ, or 5· λ.

Figure 63. Minimum (bottom line), average (middle line) and maximum (top line) cost factor caused by varying the radius, at different number of elements (number of elements = x+15)

When the number of elements stays constant and the radius varies between $0.5\cdot\lambda$...$8.75\cdot\lambda$, one can find the maximum and minimum cost factors, and calculate the average cost factor for that number of elements. Putting that into a plot, Figure 63 shows maxima, averages and minima of the cost factor at different numbers of elements. The number of elements $N = x+15$, N=16...49. from the bottom line we see that the local minima or optimal numbers of elements are 21, 26, 29, 30, 31, 32 and over 39 (x=6, 11, 14, 15, 16, from 24 onwards).

In Figure 64 the cost factor is shown in a color plot. It is a combination of Figure 62 and Figure 63. In the vertical axis the number of elements ($N=y+15$) is the variable, and in the horizontal axis the radius ($radius= x\cdot 0.25\cdot\lambda+0.25\cdot\lambda$) is the variable. The lowest cost factors are dark blue. One can see a clear pattern in the plot: the cost factor decreases when the radius grows, but periodically. With the numbers of elements the pattern is not so easy to distinguish, but the general tendency is that the cost factor decreases when the number of elements increases. One could sketch a line through deepest blue from (x = 3, y = 2) through (x = 11, y = 18)to (x = 19, y = 33) which corresponds element spacing changing from $0.48\cdot\lambda$....$0.63\cdot\lambda$.

Figure 64. Cost factor (color) versus number of elements (number of elements = $y+15$) and radius (radius = $x\cdot 0.25\cdot\lambda+0.25\cdot\lambda$). The red and yellow and green correspond to high cost factor and the deep blue corresponds to low cost factor.

Table 2. The combinations leading to lowest cost factors:

Number of elements	Radius	Element spacing	Weight1 phase	Weight2 phase	Weight3 phase
18	$1\cdot\lambda$	$0.37\cdot\lambda$	23°	87°	187°
26	$2\cdot\lambda$	$0.48\cdot\lambda$	21°	82°	179°
30	$3\cdot\lambda$	$0.63\cdot\lambda$	23°	93°	205°
40	$4\cdot\lambda$	$0.62\cdot\lambda$	18°	70°	155°

The Weight1 is the weight for the elements beside the central element, Weight2 for the next pair of elements, and Weight3 for the outermost elements.

From Table 2 one may conclude that the element spacing between 0.48...0.63· λ is the optimal spacing.

Table 2 indicates at least one element pair is approaching the 90° phase position when the cost function is at minimum. This observation leads to the design idea in section 5.4.2.

After several simulations it was clear the spacing near 0.5· λ is necessary in order to avoid too high sidelobe levels. Figure 65 shows the radiation pattern of one of the optimal array, second line in Table 2. The main beam is narrow and the sidelobe level between ±90° are below –10 dB but the backlobes are around –5dB. The conclusion is that with omnidirectional elements it is difficult to achieve low sidelobe or backlobe levels in a cylindrical array. In the non-optimal arrays the sidelobes are higher, Figure 66.

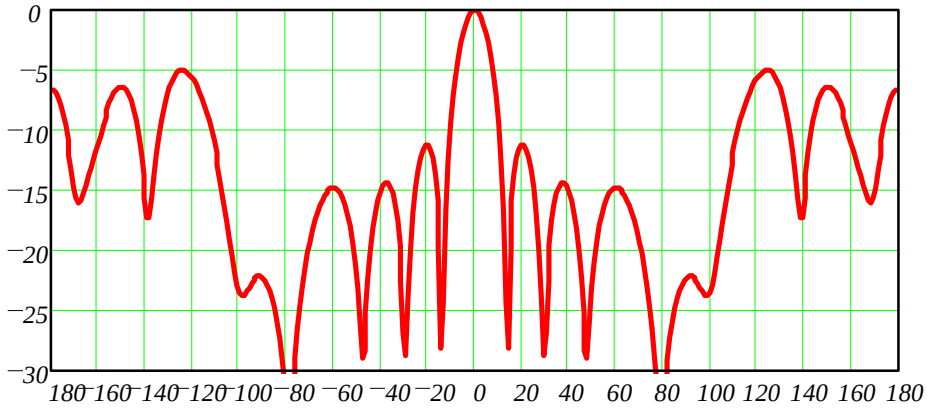

Figure 65. One of the optimal arrays: 30 omnidirectional elements, radius 3· λ., 7 active elements, 0.63· λ element spacing, equal amplitude, phase weighting for narrowest beamwidth. Beamwidth is 13°, but because the elements are omnidirectional, the backlobe level is high. Cost factor = 1083.

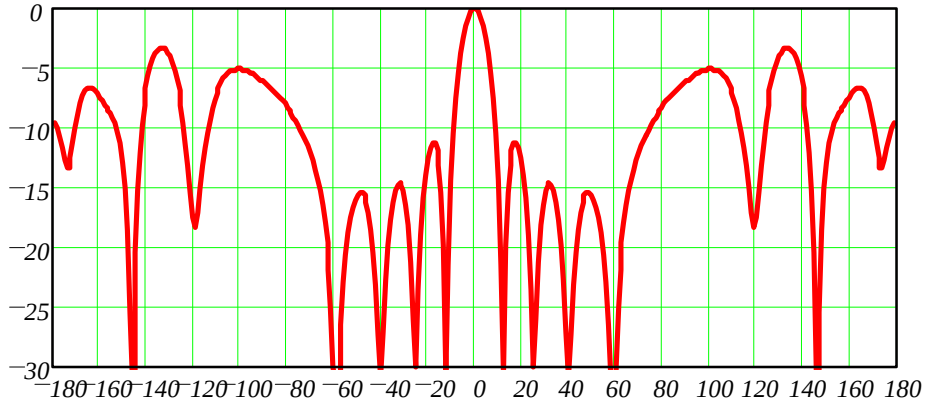

Figure 66. One of the non-optimal arrays: 30 omnidirectional elements, radius 3.5· λ., 7 active elements, 0.73· λ element spacing, equal amplitude, phase weighting for narrowest beamwidth. Beamwidth is 11°. Cost factor = 2493.

The directivity of the antenna array in Figure 65 is 8.9 dB. The directivity calculation was done using isotropic antenna elements with equal element amplitudes, Appendix F. As a comparison, a linear array of seven isotropic antenna elements with equal element amplitudes and λ/2 spacing produces a 8.5 dB directivity. Compared to that the optimal cylindrical antenna array in Figure 65 is slightly better, but the sidelobes are high. The cylindrical array with omnidirectional elements is not useful, but tit was shown that the sidelobes can be

reduced with suitable combinations of radius and element number. Therefore it is studied in the next section whether the cylindrical array pattern can be improved by using directional elements and by optimizing the element weights.

5.4 Narrowbeam cylindrical antenna array with directional elements

5.4.1 Introduction

This section describes an antenna array design method that makes use of the antenna spacing combined with directive antenna elements [89].

The proposed antenna array produces a narrow beam and relatively low sidelobe levels in a cylindrical antenna array configuration. The beamwidth is about 12° for a 35 element array having -20 dB sidelobe level. Omnidirectional coverage area is obtained by a combination of commutation and phasing. The array has less elements and smaller size than a respective array consisting of linear panels.

Simulated results are given with implementation examples for the center frequency of 2.15 GHz, which is the frequency of operation of the channel sounder system for adaptive array antennas developed at Helsinki University of Technology [37].

5.4.2 The principle

The cylindrical array normally has a wide main beam and high sidelobes [58] or it has a high number of elements [6] [77].

The idea is a combination of a $\lambda/4$ depth distance between array elements in the boresight direction in a cylindrical array and a 90° phase shift between them to cancel the grating lobes, while making the array as sparsely spaced as possible in order to produce a narrow beam and to reduce the complexity of the electronics.

To explain the principle used to enhance the properties of the cylindrical array, let's study a 6-element array (Figure 67):

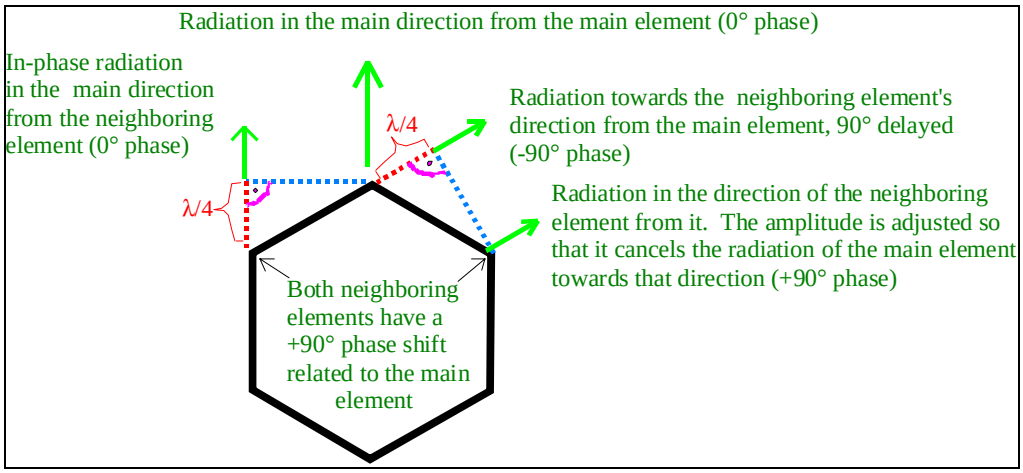

Figure 67. Operation principle of the proposed cylindrical array.

The idea makes use of the depth in the array, so that the appropriate spacing and phasing of the neighboring elements cause an additive pattern towards the main direction and a canceling pattern towards the direction of the neighboring element,

Figure 67. This principle can be applied in various ways, but the goal here is to provide a cylindrical antenna array for propagation measurement purposes and for adaptive antennas in mobile communications. In propagation measurements the horizontally omnidirectional scanning ability is useful. In adaptive antennas using digital beamforming, the minimizing of the number of the elements is desirable and low backlobe at the 180° is desired to attenuate the late reflection from the back. Whether this kind of array can provide wide deep nulls in adaptive operation needs research.

A similar effect happens if the phase difference caused by antenna depth is 270°. This effect is apparent when the same array is scanned in such a way that the main lobe is in the direction between two element directions. Then there is an even number elements activated and the 3rd weight has an about 270° depth phase, Figure 72.

5.4.3 Validation of the idea

In order to verify the idea, calculations were performed that give a cost factor (Figure 61) with various numbers of antenna elements and various array radii. The radiation pattern was calculated with a program that can have individually set radiation pattern, element weight (amplitude, phase), location and orientation of the antenna element. The theoretical background is in [84]. It calculates the cost factor indicating how much the pattern (in dB) of the real antenna differs from the desired array antenna pattern, same way as before in section 5.3.

In this example the element radiation pattern is assumed to have a horizontal behavior of $0.1+\cos(\varphi)^2$ within φ = -90°...90° and 0.1 elsewhere. A typical example of such an element is the stacked patch antenna. The 3 dB beamwidth of the element is then 70° in H-plane. (The element pattern was not normalized but the final antenna array pattern was normalized.) The code used in the calculations in this section and the results are in Appendix C and D. In this section the values for the equation (2) are E_d = -20 dB, i_a =6, i_b = 354. The 20 dB beamwidth is 10°. The sidelobe level is –20 dB which is a common requirement. The desired pattern corresponds the example in Figure 61.

Cylindrical arrays often make use only a part of the elements at a time to reduce the complexity of the pattern computation [58]. Then the cylindrical array resembles functionally an arc array. To produce similar patterns into various directions the active elements can be switched successively (rotated) along the cylinder surface. The beam can be also formed to the intermediate directions between switched directions by adjusting the weights, resulting in a similar radiation pattern (Figure 72).

This test is using 5 active elements of the whole array, because 3 elements quickly caused too wide element spacing. Wide element spacing like $1.3\cdot\lambda$ caused sidelobe levels of about -10...-15 dB, which was too high for the channel sounder but may be all right in microcellular base stations in congested areas. The optimal cylindrical array was first searched with equal amplitude excitation of the elements, and phasing adjusted so that it resulted in the narrowest main beam.

Combinations of various radii (0.5· λ...8.75· λ) and number of elements (8...41) were evaluated. Out of 1083 combinations, the combinations causing minimum cost factors at the smaller radii (1· λ...5· λ) are listed in Table 3.

One can see (Table 3) that the minimum combinations have the second weight (Weight2) close to 90° phasing except for the smallest radius 1· λ. This result is in agreement with the design principle described in section 5.4.2. With 1· λ radius it could be expected (based on the idea that the second weight is 90°) that the optimum number of antenna elements N = 17. The antenna spacing is low for 17 antenna elements which causes the beamwidth to be wide and therefore the cost factor is high. With 2· λ radius the expected number of elements is N = 25 and with 3· λ radius N = 30, which are close to the values in Table 3. With 4· λ the expected N =35 which holds. With 5· λ the expected N = 39, but the resulting optimum was at N = 42 which is again quite close. The case where the radius is 5· λ and N = 42 resembles a combination of 6 panels of linear arrays of 7 elements each, but has smaller diameter (140 cm compared to 147 cm at 2.15 GHz).

Table 3. Combinations causing minimum cost factors at various radii

Number of elements	Radius	Element spacing	$Weight_1$ phase	$Weight_2$ phase	Cost factor
14	1·λ	0.46·λ	36°	137°	1119
24	2·λ	0.52·λ	24°	96°	621
28	3·λ	0.67·λ	27°	107°	457
35	4·λ	0.73·λ	23°	93°	393
42	5·λ	0.75·λ	20°	80°	367

A comparison to Table 2 in Section 5.3 shows a surprising similarity, although the antenna elements are omnidirectional in Table 2. In Table 2 there are 26 elements at radius 2·λ, 30 elements at radius 3·λ and 42 elements at radius 4·λ, and corresponding element spacings are 0.48·λ, 0.63·λ and 0.63·λ and corresponding $Weight_2$ phases are 82°, 93°, and 70°. The optimality in the cylindrical array depends more on the array structure than on element pattern, although both affect the final result.

The calculations of the cost factor as a function of N are in Figure 68. As expected, the cost factor decreases when the number of the antenna elements increases, because then the main beam is sharper. But the minimum and maximum (achieved at each element number for different values of the radius) curves are not monotonous. When comparing to Figure 63 one can see that the cost factor is lower in Figure 63, which means that the sidelobes are lower. Also all the curves decrease in Figure 63 when the number of elements increases, which is caused by the directional elements.

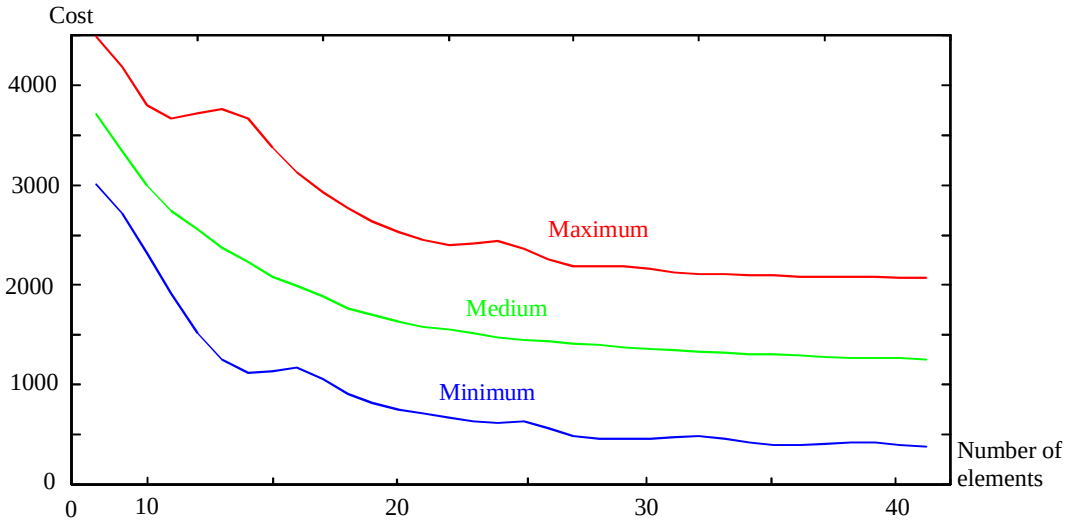

Figure 68. Minimum (bottom line), average (middle line) and maximum (top line) cost factor caused by varying the radius (between 0.5· λ...8.75· λ), at different number of elements. There are local minima at 14, 22, 27 and 34 elements. Compare to Figure 63.

The cost factor versus radius is in Figure 69. The minimum cost factors are located at where the radius is an integer number of wavelengths. Currently there is no explanation for that. Also the tests with the omnidirectional element pattern gave similar results in Section 5.3. In further research the step should be smaller than 0.25· λ in order to find possible lower minima. When comparing to Figure 58 one can see that the cost factor is lower, except maximum are clearly higher compared to minimums, which is caused by the directional elements pointing away from each other.

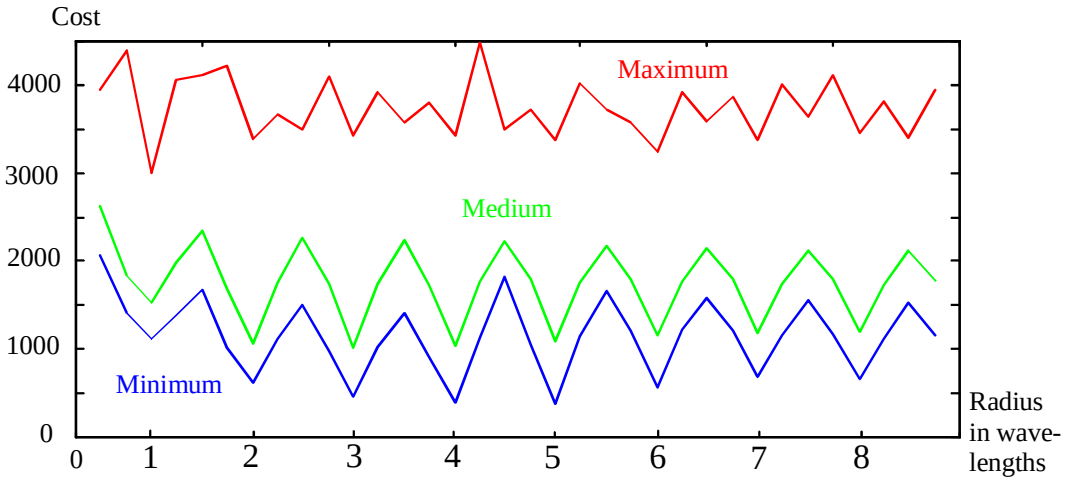

Figure 69. Minimum (bottom line), average (middle line) and maximum (top line) cost factor caused by varying the number of elements (betwwen 8...41) at different radii. The local minima are at 2, 3, 4 and 5· λ. Compare to Figure 62.

5.4.4 Calculated array patterns for a 35 element array

One of the arrays of Table 3 was taken for weight optimizing: 35 elements and radius 4· λ. (The 32 element array would be more suitable for the channel sounder, but its cost factor was 33% higher, which means that the sidelobes are higher. Using smaller increments in radius in order to optimize the 32 element array is left for further study.) The radiation pattern before optimizing is in Figure 70. The array weights were optimized to produce a final pattern that is as close to the

requirements as possible, 3 dB beamwidth 10° and 20 dB beamwidth 20°. The code for 7 elements (Figure 71) is in Appendix E. The code for 8 elements (Figure 72) is very similar. This optimization was done with 7 elements in order to get narrower main beam, although the calculations in 5.4.3 were done with 5 elements to save computing time. In case the 5 element pattern is the optimum, then the weights for the elements at the edge will become zero during the optimization process. Therefore optimizing with more elements here is not harmful. The 7 active elements of an array of 35 elements correspond to a 72° arc antenna. In the best case all the variables: radius, number of the elements and the element weights (amplitude, phase) should be optimized simultaneously, but currently it is a huge task.

The optimizing decreases the sidelobe levels. The narrower beamwidth in Figure 71 compared to Figure 70 is due to higher number of elements since decreasing the sidelobe levels increases the beamwidth.

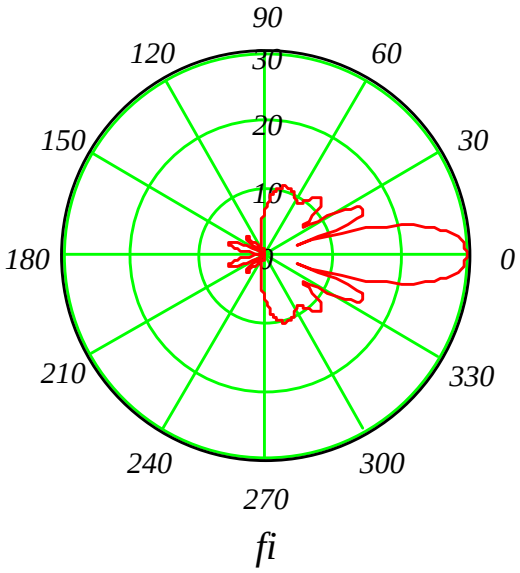

Figure 70. Radiation pattern in the horizontal plane for the 35 element cylindrical array after the first optimization for the cylinder radius and number of elements. 5 active elements are used with equal amplitudes , and phase weighting is for the narrowest beamwidth. Radius is 4· λ and element spacing 0.73· λ. 3 dB beamwidth is 14.7°. The same array with 7 active elements optimized in Figure 71.

By choosing the 35-element array and 4· λ radius, the diameter of he array is 113 cm at 2.15 GHz. In that array 7 or 8 adjacent elements are in use at a time (amplitude and phase are controlled) to produce a directional beam. By switching or commutating the selected elements, a coverage of 360 degrees can be obtained. In this example the element pattern is again $0.1+\cos^2(\varphi)$.

The 3 dB beamwidth of the array is close to 12° and the sidelobes are 20 dB or more below the main beam top (Figure 71 and Figure 72). The bandwidth of the structure is about 10 % (± 5 %) without significant degradation of the pattern. However, a ±10% change in the frequency causes significant changes in the radiation pattern. But even then the problem can be partly compensated by adjusting the weights at different frequencies.

The directivity of the array in Figure 71 is 16.5 dB, calculated with numerical integration, Appendix G. The directivity of the theoretical model of the stacked

patch element used in the array calculations is 9.5 dB. That gain is 2.9 dB higher than the measured gain in 4.7 because it is theoretical and the backlobe is assumed to be low in a cylindrical array having a large ground area.

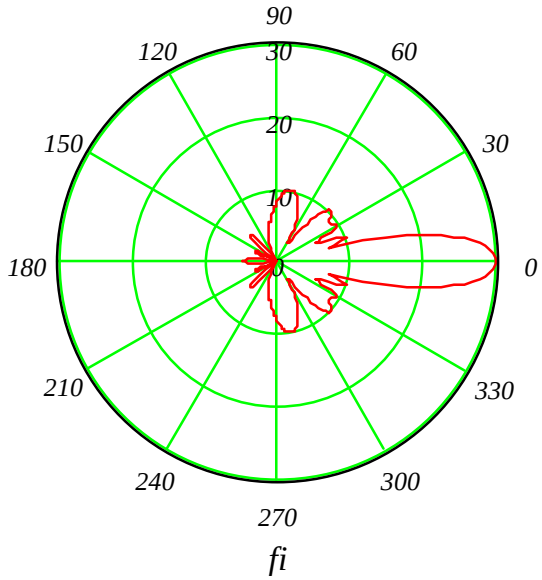

Figure 71. Radiation pattern in the horizontal plane for the 35 element cylindrical array. 7 active elements are used with optimized weights for –20 dB sidelobe level and narrow beamwidth. (W0 = 1 at 0°, W1 = 1 at 20°, W2 = 0.7 at 90°, W3 = 0.7 at 190°). Radius is 4· λ and element spacing 0.73· λ. 3 dB beamwidth is 12.1°.

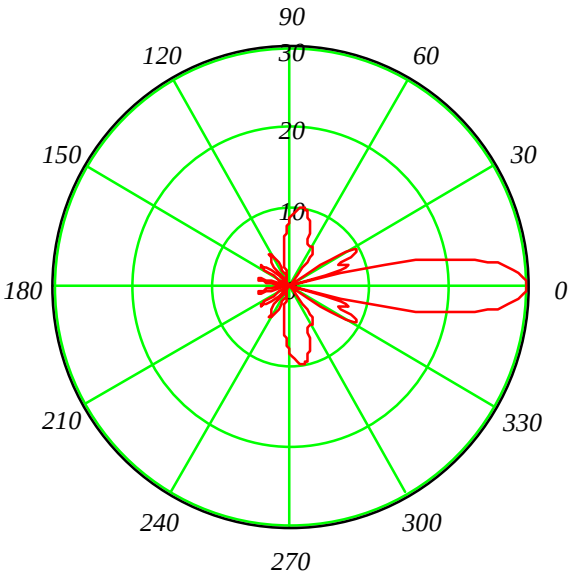

Figure 72. Radiation pattern for the 35 element cylindrical array. Now the boresight direction is in the middle of the 2 central active elements. 8 elements are active in order to get an even number of elements in this special case. The weights are optimized manually for –20 dB sidelobe level and narrow beamwidth. (W0 = 1 at 0°, W1 = 0.7 at 50°, W2 = 0.7 at 140°, W3 = 0.4 at 270°. The 270° depth has a similar effect as the 90° depth). Radius is 4· λ and element spacing 0.73· λ. 3 dB beamwidth is 11.5°.

The array in [85] is partially comparable with this antenna 32 elements, 17 active, radius 2· λ, element pattern 1+cos(φ). That array has a wider beamwidth (30°) and lower sidelobe level (-30 dB) than the array in this work, but the array pattern resembles the pattern in this work.

5.4.5 Comparison with the linear array

The linear array requires 6 panels, if one scans ±30°. The panel consists of a linear 7-element array, because it corresponds the number of the active array elements in the cylindrical array. It means that the 6 panels assembly has a total of 42 antenna elements and the diameter of the assembly is 124 cm. The element pattern is the same as above. Chebyshev weights are used in order to achieve -20 dB sidelobes and a sharp main beam [53].

The spacing is 0.60· λ because the 0.73· λ element spacing gives only ±16° scan angle if one wants to keep the grating lobes below -20 dB. One can notice that it is possible to use a 0.73· λ spacing with the cylindrical antenna, although it is not feasible in the comparable linear array. With the 0.73· λ spacing the 3 dB beamwidth of the linear panel is 11.1° when not scanned but when scanned to 30° the grating lobe would level be –6 dB. At 16° scan angle the 3 dB beamwidth is 11.5°. However, 360 degree coverage would require 12 panels of 7-element arrays, which would mean that the total antenna array would have a 276 cm diameter at 2.15 GHz.

The radiation patterns for the linear array suitable for scanning ±30° are below (Figure 73 and Figure 74). In this case the beamwidth is wider than for the cylindrical antenna: 13.5° when not scanned and 15.5° when scanned to ±30°.

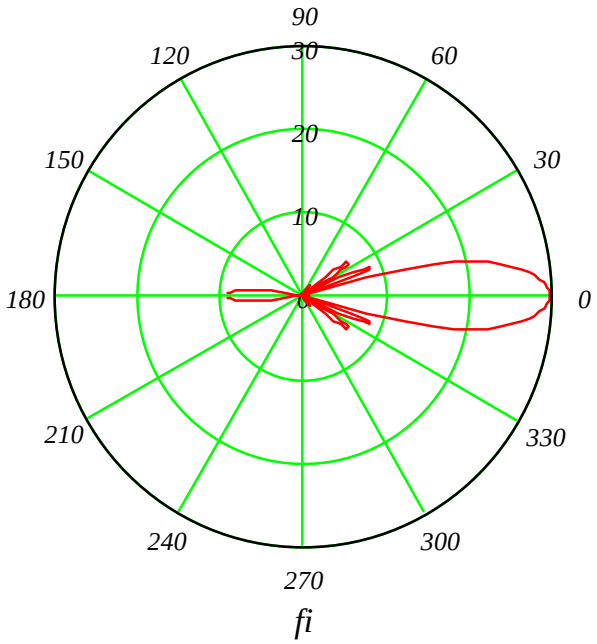

Figure 73. The radiation pattern in the horizontal plane for a linear 7-element array with 0.60· λ spacing, 0.1+cos^2(φ) element pattern, Chebyshev weights and 0° scan angle. (all weights have same phase, W0 = 1, W1 = 0.916, W2 = 0.694, W3 = 0.544) 3 dB beamwidth is 13.5°.

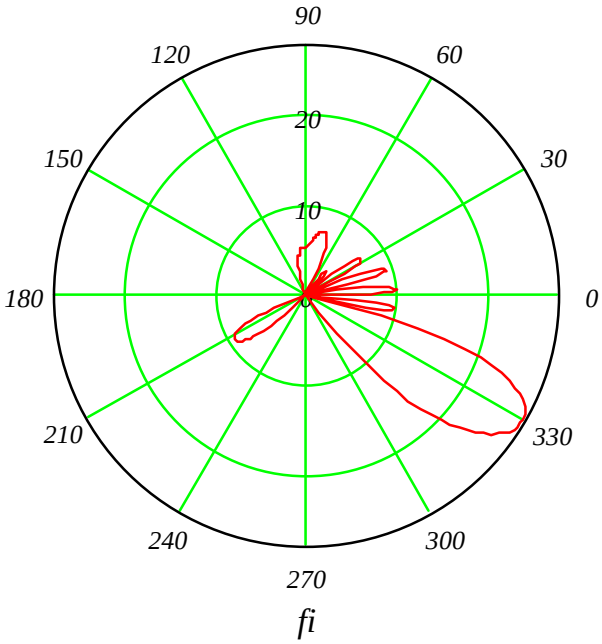

Figure 74. The radiation pattern in the horizontal plane for a linear 7-element array with 0.60· λ spacing, 0.1+cos2(φ) element pattern. Same Chebyshev weights as in Figure 73. Scanned to 30° scan angle. 3 dB beamwidth 15.5°.

The directivity of the linear array in Figure 73 is 16.2 dB, Appendix H. It is slightly less than the directivity of the cylindrical array (16.5 dB) in section 5.4.4. With constant weights the directivity of the linear array is 16.5 dB, but then the sidelobe levels are higher.

The backlobe of the linear antenna array of Figure 73 is –21.8 dBi and the backlobe of the cylindrical array of Figure 71 is –26.6 dBi.

5.4.6 Findings

The optimal cylindrical array has one active element pair at the $\lambda/4$ depth of the central active element or central active element pair, in addition to other active elements. It enables a smaller omnidirectionally scanning antenna array diameter and a smaller number of elements than linear array panels with comparable sidelobe levels. Also the comparably sized cylindrical array has narrower beamwidth.

The electronic scanning angle for the cylindrical array is small ($\pm\pi/N$, where N is the number of elements), and beyond that angle the beam steering is done by on commutating which simplifies the beam steering.

The optimized weights appear to be close to the Chebyshev weights with additional phasing proportional to the depth.

This array could be used in adaptive base station antennas or in 2D propagation channel measurements to obtain narrow beams with smaller number of antenna elements compared to a linear array.

6. Conclusions

In this thesis the goal was to find new designs for antenna elements that can be used in arrays, and to find new designs for arrays for adaptive antennas. The research subject of using adaptive antennas in cellular radio telecommunications is relatively new, therefore some basic literature research was performed in order to obtain a overview of the current level of technology and research, and to find the current opportunities and limitations regarding the antenna and array structures, in Section 2.

The mobile communications equipment need antennas that are small in size and have wide bandwidth. These are contradictory requirements. Of many possibilities, the designs and properties of microstrip patch antennas were chosen under study. The structure studied here was based on a microstrip patch antenna with a thick substrate of air. Thick air substrate does increase the bandwidth, but the analysis of that kind of antenna is not simple, because the relatively high probe inductance affects the matching of the antenna. Therefore a design method was developed for the patch antenna for with a thick substrate in Section 4.2. Also it was demonstrated that the FDTD method is a feasible method when designing antennas of complex shapes.

The rectangular quarter-wave patch antenna was studied, and the focus was on widening the bandwidth. A 35% bandwidth was achieved which is near the theoretical limit of an antenna of that size. The average cross-polar level of this antenna is 0 dB, so it is applicable to environments where the polarization separation is not the first priority, for example mobile handsets. Using two antennas of this kind in a handset located as far as possible from each other provides space diversity. Positioning the antenna so that the radiating ends point into opposite directions can offer some degree of polarization diversity and an adaptive signal processor can then further improve the reception based on the uncorrelated inputs.

Some initial study about the reduction of the mutual coupling between antenna elements was done. Two different structures were studied, metal wall and dielectric lossy wall. The metal wall between elements did not work for these types of antennas having an electrical field component perpendicular to the ground plane. The dielectric wall between antenna elements attenuates the mutual coupling well, but needs further study in order to avoid the problems with decreased efficiency, changes of radiation pattern and reduction of cross-polarization separation. The simplest way to reduce the mutual coupling, and also the method used in this research, was to increase the spacing between antenna elements from the commonly used $0.5 \cdot \lambda$. The spacing of $0.7 \cdot \lambda$ was found optimal so that the grating lobes do not raise above the sidelobe level while scanning ±30°.

Base station antennas can offer more space and therefore the ability to use two polarizations separately was included in the properties of antenna elements for the base station arrays. A probe-fed half-wave patch antenna was modified by using a dielectric feed replacing part of the probe to achieve good cross-polarization separation, and the result was XPD>20 dB between -57°...+78° scanning angles.

Using the stacked patch structure in that antenna element a sufficient 10% bandwidth was acquired.

The cross-polarization separation tends to decrease because of mutual coupling in the array. The wider element spacing of $0.7\cdot\ \lambda$ can help to alleviate this effect as well.

The array arrangement possibilities are almost endless. Utilizing the depth in a cylindrical antenna array was studied as a new viewpoint to the array problem. A cylindrical array has some inherent depth, therefore a cylindrical array was researched theoretically in this work. A convenient design was achieved by using $\lambda/4$ depth and 90° phasing between the selected elements.

The beamwidth of the cylindrical antenna array with of this study is 12° and the sidelobe level is –20 dB below the main beam. The backlobe is –26.6 dB. The directivity is 16.5 dB when the directivity of one element is 9.5 dB. The beamwidth and sidelobe level are comparable to a linear array with the same number of active elements, but the backlobe of the cylindrical array is 4.8 dB lower than in the linear array. The cylindrical array is 10% smaller than the comparable linear array. The optimal weight amplitudes of the cylindrical array resemble the Chebyshev amplitudes for a comparable linear array. The directivity of the comparable linear array is 16.2 dB. It was also shown that the radius of the cylindrical array cannot be chosen freely, and the optimum radii are $n\cdot\ \lambda$ where n is a positive integer.

The future base stations may not be on top of masts, and omnidirectionally scanning arrays are not needed except in rural areas. Most of the future base stations will be positioned on walls. Then an arc (or sector) array will be more suitable than the cylindrical array. The result of this research is applicable to the arc array. The cylindrical array with seven active elements can be modified to an arc array by removing the passive elements. Scanning the arc array cannot be done by commutating anymore, but the electronic scanning possibility is still available. Regarding the scanning the behavior can be different and is a subject for further research.

This research proposes several solutions to suitable antenna elements and convenient antenna arrays for mobile units and base stations for the third generation mobile radio systems utilizing the spatial properties of the radio channel by adaptive antennas.

7. References

[1] F. Amoroso, "Use Of DS/SS Signaling to Mitigate Rayleigh Fading in a Dense Scatterer Environment", *IEEE Personal Communications*, Vol. 3, no. 2, April 1996, pp. 52 - 61

[2] A.K. Bhattacharyya, "A Numerical Model for Multilayered Microstrip Phased-Array Antennas", *IEEE Transactions on Antennas and Propagation*, Vol. 44, no. 10, October 1996, pp. 1386-1394

[3] Hongming An, B. Nauwelaers, A. Van de Capelle "Broadband Microstrip Antenna Design", *IEEE Transactions on Antennas and Propagation*, Vol. 42, no. 2, Feb 1994, pp. 129-136

[4] F. Ananasso, F. Vatalaro, (editors) *Mobile and Personal Satellite Communications, Proceedings of the First European Workshop on Mobile/personal Satcoms (EMPS'94)* , London: Springer-Verlag, 1995, 335 p.

[5] J. Appel-Hansen, E.S. Gillespie, T.G. Hickman, J.D. Dyson, "Antenna Measurements", (Chapter 8 in the book: A.W. Rudge, K. Milne, A.D. Olver, P. Knight, *The Handbook of Antenna Design*, Vol.1) London: Peter Peregrinus, 1982, pp. 584-694

[6] F. Ares, S. Rengarajan, J. Ferreira, A. Trastoy, "Synthesis of Antenna Patterns of Circular Arc Arrays", *Proceedings of IEEE Antennas and Propagation Society International Symposium 1997*, Montreal, Canada, Jul 13-18 1997, pp. 2248-2251

[7] T.M. Au, K.F. Tong, K-M. Luk, "Performance of Aperture-Coupled Dual-Patch Microstrip Phase Arrays", *IEEE Transactions on Antennas and Propagation*, Vol. 44, no. 9, September 1996, pp. 1280-1297

[8] M. Barrett, R. Arnott "Adaptive Antennas for Mobile Communications", *Electronics and communication engineering journal*, Vol. 6, no. 4, August 1994, pp. 203-214

[9] K. Cho, K. Nishimori, T. Hori, "Adaptive Base Station Configuration for Street Microcells Considering Propagation Environment", *Proceedings of IEEE Antennas and Propagation Society International Symposium 1997*, Montreal, Canada, July 13-18 1997, pp. 346-349

[10] (CPK) Center for PersonKommunikation, "Tsunami 96", *Proceedings of EU-Tsunami (adaptive antennas) conference*, Aalborg University, Denmark , Jan 18, 1996, 129 p.

[11] R.E. Collin, *Antennas and Radiowave Propagation*, New York: McGraw-Hill, 1985, 508 p.

[12] R.E. Collin, F.J. Zucker, *Antenna Theory, Part 1*, New York: McGraw-Hill, 1966, 666 p.

[13] R.T. Compton Jr., *Adaptive Antennas, Concepts and Performance*, Englewood Cliffs: Prentice-Hall, 1988, 448 p.

[14] D.J. DeFatta , J.G. Lucas, W.S Hodkiss, *Digital Signal Processing: a System Design Approach*, Singapore: John Wiley & Sons, 1988, 661 p.

[15] R.C. Dixon, *Spread Spectrum Systems,* New York: John Wiley & Sons, 1994, 573 p.

[16] J. Doble, *Introduction to Radio Propagation for Fixed and Mobile Communications,* Norwood MA: Artech House, 1996, 189 p.

[17] R.B. Dybdal, S.J. Curry, "Adaptive Transmit Antenna", *Proceedings of IEEE Antennas and Propagation Society International Symposium 1997*, Montreal, Canada, July 13-18 1997, pp. 2410-2413

[18] P. Erätuuli, E. Bonek, "Diversity Arrangements for Internal Handset Antennas", *Proceedings of 8th IEEE International Symposium on Personal, Indoor and Mobile Radio Communications*, Helsinki, Finland, September 1-4 1997, pp. 589-593

[19] S. Eshira, E. Nishiyama, "Stacked Microstrip Antenna with Wide Bandwidth and High Gain", *IEEE Transactions on Antennas and Propagation*, Vol. 44, no. 11, November 1996, pp. 1533-1534

[20] G.E. Evans, *Antenna Measurement Techniques*, Boston-London: Artech House, 1990, 229 p.

[21] K. Fujimoto J.R. James (editors), *Mobile Antenna Systems Handbook*, Norwood, Massachusetts: Artech House, 1994, 617 p.

[22] V.K. Garg, L. Huntington "Application of Adaptive Array Antenna to a TDMA Cellular/PCS system", *Communications magazine*, Vol. 35, no. 10, October 1997, pp. 148-152

[23] R.N. Ghose, *Interference Mitigation*, New York, NY: IEEE Press, 1996, 274 p.

[24] R.M. Glorioso, F.C.C. Colón Osorio, *Engineering Intelligent Systems*, Bedford, Massachusetts: Digital Press, 1980, 472 p.

[25] L.C. Godara, "Applications of Antenna Arrays to Mobile Communications, Part 1: Performance Improvement, Feasibility, and System Considerations", *Proceedings of IEEE,* July 1997, pp. 1031-1060

[26] L.C. Godara, "Applications of Antenna Arrays to Mobile Communications, Part 2: Performance Improvement, Feasibility, and System Considerations", *Proceedings of IEEE,* August 1997, pp. 1195-1245

[27] R.C. Hansen, *Phased Array Antennas*, New York: John Wiley & Sons, 1998, 486 p.

[28] S. Haykin (editor), *Array Processing Applications to Radar*, Stroudsburg, Pennsylvania: Dowden Hutchinson & Ross, 1979, 362 p.

[29] G.C. Hess, *Handbook of Land-Mobile Radio System Coverage*, Norwood MA: Artech House, 1997, 346 p.

[30] K. Hirasawa, M. Haneishi *Analysis, Design, and Measurement of Small and Low-Profile Antennas,* Norwood, Massachusetts: Artech House, 1992, 253 p.

[31] J.E. Hudson, *Adaptive Array Principles*, London: Peter Peregrinus, 1991, 253 p.

[32] International Telecommunications Union, “ITU-R Recommendations”, *1994 Series Volume*, 1994, p. 128

[33] A. Jamalipour, *Low Earth Orbital Satellites for Personal Communication Networks*, Norwood MA: Artech House, 1997, 273 p.

[34] J.R. James, P.S. Hall (editors), *Handbook of Microstrip Antennas*, London: Peter Peregrinus, 1989, in 2 volumes 1295 p.

[35] J.R. James, P.S. Hall, C. Wood, *Microstrip Antenna Theory and Design*, London: Peter Peregrinus, 1981, 290 p.

[36] J.Joronen, “WCDMA tuo kaistaa” (“WCDMA conveys bandwidth”, in Finnish), *Prosessori*, May 1998, pp. 36 - 41

[37] K. Kalliola, P. Vainikainen, “Characterization System for Radio Channel of Adaptive Array Antennas”, *Proceedings of 8th IEEE International Symposium on Personal, Indoor and Mobile Radio Communications*, Helsinki, Finland, September 1-4 1997, pp. 95-99

[38] D.F. Kelley, W.L. Stutzmann “Array Antenna Pattern Modeling Methods that Include Mutual Coupling Effects”, *IEEE Transactions on Antennas and Propagation*, Vol. 41, no. 12, Dec 1993, pp. 1625-1631

[39] J. Kivinen, T. Korhonen, J. Hubach, P. Vainikainen, "Fast sounding of broadband radio channel at 2 GHz frequency range," *Proc. NRS'95*, 24-27 April 1995, Saltsjöbaden, Sweden, pp. 121-126

[40] R. Kohno, “Spatial and Temporal Communication Theory Using Software Antennas for Wireless Communications”, pp. 293-321 in S.G. Glisic, P.A. Leppänen *Wireless Communications TDMA Versus CDMA* London: Kluwer, 1997, 540 p.

[41] Päivi Koivisto, “Effects of Nearby Walls on Antenna Radiation Patterns: Comparison of Measurements and FDTD Calculations”, *Proceedings of Euro-COST 259 TD(97)*, Lisbon, September 24-261997, no 58

[42] J.D. Kraus, *Antennas*, Singapore: McGraw-Hill, 1988, 892 p.

[43] H. Krim, M. Viberg: “Two Decades of Array Signal Processing Research”, *IEEE Signal processing magazine*, Vol. 13, no. 4, July 1996, pp. 67-94

[44] K.S. Kunz, R.J. Luebbers, *Finite Difference Time Domain Method for Electromagnetics*, Boca Raton, Florida, CRC Press, 1993, 448 p.

[45] J. Laiho-Steffens, *Two-Dimensional Characterization of the Mobile Propagation Environment*, Licentiate thesis, Helsinki University of Technology, 3rd June 1996, 98 p.

[46] Eu-An Lee, Nelson Dorny “A Broadcast Reference Technique for Self-Calibrating of Large Antenna Phased Arrays”, *IEEE Transactions on Antennas and Propagation*, Vol. 37, no. 8, Aug 1989, pp. 1003-1010

[47] K.F. Lee, W.Chen, *Advances in Microstrip and Printed Antennas*, USA: Wiley, 1997, 599 p.

[48] W.C.Y. Lee, *Mobile Cellular Telecommunications: Analog and Digital Systems*, USA: McGraw-Hill, 2nd ed. 1995, 892 p.

[49] A. Lehto, A. Räisänen, *RF-ja mikroaaltotekniikka (RF and Microwave technology*, in Finnish), Helsinki Otatieto, 1994, 250 p.

[50] Z. Li, X. Yu, C. Wu, J. Litva, "A 4-Element Multibeam Microstrip Smart Antenna System", *Proceedings of IEEE Antennas and Propagation Society International Symposium 1997*, Montreal, Canada, July 13-18 1997, pp. 2-5

[51] J.C. Liberti, T.S. Rappaport, "Analysis of CDMA Cellular Radio Systems Employing Adaptive Antennas in Multipath Environments", *Proceedings of the IEEE 46th Vehicular Technology conference 1996 in Atlanta (VTC 96)*, 3 vols., May 1996, pp. 1076-1080

[52] H.P. Lin, S.S. Jeng, G. Xu, W.J. Vogel, "Experimental Studies of Using a Smart Antenna System in Low-Earth-Orbit Satellite Communications", *Proceedings of the IEEE 47th Vehicular Technology conference 1997 in Atlanta (VTC 97)*, 3 vols., May 1997, pp. 242-245

[53] I. Lindell, K. Nikoskinen, *Antenniteoria(Antenna theory*, in Finnish), Helsinki Otatieto, 3rd ed. 1995, 347 p.

[54] B. Lindmark, "A Novel Dual Polarized Aperture Coupled Patch Element with a Single Layer Feed Network and High Isolation", *Proceedings of IEEE Antennas and Propagation Society International Symposium 1997*, Montreal, Canada, July 13-18 1997, pp. 2190-2193

[55] J. Litva, T.K.-Y. Lo *Digital Beamforming in Wireless Communications*, Norwood MA: Artech House, 1996, 295 p.

[56] D. Löffler, F. Rostan, W. Wiesbeck, "Conformal Microstrip Patch Array for SDMA Applications", *Proceedings of IEEE Antennas and Propagation Society International Symposium 1997*, Montreal, Canada, July 13-18 1997, pp. 1533-1536

[57] M.T. Ma, *Theory and Application of Antenna Arrays*, New York: John Wiley & Sons, 1974, 413 p.

[58] R.J. Mailloux, *Phased Array Antenna Handbook*, Norwood MA, Massachusetts: Artech House, 1994, 524 p.

[59] J.S. McLean, "A Re-Examination of the Fundamental Limits On The Radiation Q of Electrically Small Antennas", *IEEE Transactions on Antennas and Propagation*, Vol. 44, no. 5, May 1996, pp. 672-676

[60] M.S. Mirotznik, "How to Choose EM Software", *IEEE Spectrum*, Vol. 34, no. 12, December 1997, pp. 53 - 58

[61] S. Moshavi, "Multi-User Detection for DS-CDMA Communications", *Communications magazine*, Vol. 34, no. 10, October 1996, pp. 124-136

[62] I. Nyström, D. Karlsson, "Reduction of Back Radiation and Cross-Coupling in Dual Polarized Aperture Coupled Patch Antennas", *Proceedings of IEEE Antennas and Propagation Society International Symposium 1997*, Montreal, Canada, July 13-18 1997, pp. 2222-2225

[63] G. Parker, Y.M.M. Antar, “A Dual Polarized Microstrip Ring Antenna with Good Isolation”, *Proceedings of IEEE Antennas and Propagation Society International Symposium 1997*, Montreal, Canada, July 13-18 1997, pp. 928-931

[64] R.L. Peterson R.E. Ziemer, D.E. Borth *Introduction to Spread-Spectrum Communications*, Englewood Cliffs NJ: Prentice-Hall, 1995, 688p.

[65] A.J. Paulraj, C.B. Papadias, “Space-Time Processing for Wireless Communications”, *IEEE Signal processing magazine*, Vol. 14, no. 6, November 1997, pp. 49-83

[66] D.M. Pozar, S.M. Duffy “A Dual-Band Circularly Polarized Aperture-Coupled Stacked Microstrip Antenna for Global Positioning Satellite”, *IEEE Transactions on Antennas and Propagation*, Vol. 45, no. 11, November 1997, pp. 1619-1625

[67] D.M. Pozar, D.H. Schaubert (editors), *Microstrip Antennas*, New York, NJ: IEEE Press, 1995, 431p.

[68] D.M. Pozar, D.H. Schaubert , S.D. Targonski, M.Zawadski, “A Dual-Band Dual Polarized Array for Spaceborne SAR” *Proceedings of IEEE Antennas and Propagation Society International Symposium 1998*, Atlanta, USA, June 21-26, 1998, pp. 2112-2115

[69] J.G. Proakis, *Digital Communications*, Singapore: McGraw-Hill, 1995, 928 p.

[70] T.S. Rappaport, *Wireless Communications*, Upper Saddle River NJ: Prentice-Hall, 1996, 641 p.

[71] C.J. Reddy, M.D. Deshpande, C.R. Cockrell, F.B. Beck, “Radiation Characteristics of Cavity Backed Aperture Antennas in Finite Ground Plane Using the Hybrid FEM/MoM Technique and Geometrical Theory of Diffraction”, *IEEE Transactions on Antennas and Propagation*, Vol. 44, no. 10, October 1996, pp. 1327-1333

[72] K.A. Remley, A. Weisshaar, H.R.Anderson, “A Comparative Study of Ray Tracing and FDTD for Indoor Propagation Modeling”, *Proceedings of the IEEE 48th Vehicular Technology conference 1998*, Ottawa (VTC 98), 3 vols., May 18-21 1998, pp. 865-869

[73] D.H. Schaubert, “A Class of E-Plane Scan Blindnesses in Single-Polarized Arrays of Tapered-Slot Antennas with a Ground Plane”, *IEEE Transactions on Antennas and Propagation*, Vol. 44, no. 7, July 1996, pp. 954 - 959

[74] K. Siwiak, *Radiowave Propagation and Antennas for Personal Communications*, Norwood MA: Artech House, 1995, 320p.

[75] H.L. Southall, “Direction Finding in Phased Arrays with a Neural Network Beamformer”, *IEEE Transactions on Antennas and Propagation*, Vol. 43, no. 12, Dec 1995, pp. 1369 - 1374

[76] H. Steyskal, J.S. Herd “Mutual Coupling Compensation in Small Array Antennas”, *IEEE Transactions on Antennas and Propagation*, Vol. 38, no. 12, Dec 1990, pp. 1971-1975

[77] J-C. Sureau, K.J. Keeping “Sidelobe Control in Cylindrical Arrays”, *IEEE Transactions on Antennas and Propagation*, Vol. 30, no. 5, September 1982, pp. 1027 – 1031

[78] M. Taromaru, M. Oishi and Y. Akaiwa, “Downlink Control Channel Transmission with Antenna Directivity Switching or Space Diversity at Base Stations”, *Proceedings of 8th IEEE International Symposium on Personal, Indoor and Mobile Radio Communications*, Helsinki, Finland, September 1-4 1997, pp. 599-603

[79] J.S. Thompson, P.M. Grant, B. Mulgrew “Smart Antenna Array for CDMA Systems”, *IEEE Personal Communications*, Vol. 3, no. 5, October 1996, pp. 16 – 25

[80] G. Tsoulos, “Approximate SIR and BER Formulas for DS-CDMA Based on Radiation Pattern Characteristics of Adaptive antennas,” *Electronics letters*, vol. 34, no. 19, 17th September 1998, pp. 1802-1803

[81] G. Tsoulos, M. Beach, J. McGeehan “Wireless Personal Communications for the 21st Century: European Technological Advances in Adaptive Antennas”, *Communications magazine*, Vol. 35, no. 9, September 1997, pp. 102-109

[82] G.A.E. Vandenbosch, “Capacitive Matching of Microstrip Antennas”, *Electronics letters*, Vol. 31, no. 18, 31st August 1995, pp. 1535-1536

[83] G.A.E. Vandenbosch, A.R. Van de Capelle “Study of the Capacitively Fed Microstrip Antenna Element”, *IEEE Transactions on Antennas and Propagation*, Vol. 42, no.12, December 1994, pp. 1648-1652

[84] L.I. Vaskelainen, “Iterative Least-Square Synthesis Methods for Conformal Array Antennas with Optimized Polarization and Frequency Properties”, *IEEE Transactions on Antennas and Propagation*, Vol. 45, no. 7, July 1997, pp. 1179-1185

[85] R. Vescovo, “Pattern Synthesis for Arc Arrays”, *Proceedings of IEEE Antennas and Propagation Society International Symposium 1997*, Montreal, Canada, July 13-18 1997, pp. 2256-2259

[86] V. Voipio “Adaptive Antennas”, *Practical aspects of antennas in mobile telecommunications systems*, Merito Forum TU100041U-VII, 21 p., Helsinki, 1998)

[87] V. Voipio: “Dual Half-wave Patch Antenna for Channel Measurements”, *Proceedings of the IRC Workshop 1997. Report IRC-5*, October 1997, p. 51-52.

[88] V. Voipio, J.Ollikainen, P.Vainikainen “Quarter-wave Patch Antenna with 35% Bandwidth”, *Proceedings of IEEE Antennas and Propagation Society International Symposium 1998*, Atlanta, USA, June 21-26, 1998, pp. 790-793

[89] V. Voipio, P.Vainikainen, “Narrowbeam Cylindrical Antenna Array with Sparse Antenna Spacing”, *Proceedings of the IEEE 48th Vehicular Technology conference 1998*, Ottawa (VTC 98), 3 vols., May 18-21 1998, pp. 465-469

[90] C. Ward, M. Smith, A. Jeffries, D. Adams, and J. Hudson, “Characterising the Radio Propagation Channel for Smart Antenna Systems”, *Electronics and Communication Engineering Journal*, Vol. 8, no. 4, August 1996, pp. 191-200

[91] K. Woelders, J. Granholm., “Cross-Polarization and Sidelobe Suppression in Dual Linear Polarization Antenna Arrays”, *IEEE Transactions on Antennas and Propagation*, Vol. 45, no. 12, December 1997, pp. 1727-1740

[92] R.B. Waterhouse, J.T. Rowley, K.H. Joyner, “Stacked Shorted Patch Antenna”, *Electronics Letters*, Vol 34 no 7, 2nd April 1998, pp.612-614.

[93] F. Zavosh, J.T. Aberle “Infinite Phased Arrays of Cavity-Backed Patches”, *IEEE Transactions on Antennas and Propagation*, Vol. 42, no. 3, March 1994, pp. 390-398

[94] J.F. Zürcher, F.E. Gardiol *Broadband patch antennas*, Norwood, Massachusetts: Artech House, 1995, 209 p.

Appendices

Appendix A: Radius/element optimizing code – omnidirectional

Matlab file Optarra1.m

```
clear; % clean the memory
CostMatrix(34,34)=0; %Cost function results
ElementSpacingMatrix(34,34)=0; %Writes down the element spacings

DesiredPattern(1:360)=-20;
for ii=1:10
   DesiredPattern(ii+175)=0;
end;

for NNN=1:34;
   NN=15+1*NNN% elements in the array
N=7; % number of active elements in the array
Alpha=2*pi/NN; % angular element spacing

for NRadius = 1:34 % antenna radius at the center of the element
Radius=NRadius*0.25+0.25; %generates the actual radius
ElementSpacing=2*sin(Alpha/2)*Radius/cos(Alpha/2);   %   width   of
plate elements
ElementSpacingMatrix(NNN,NRadius)=ElementSpacing;

NN
Radius
ElementSpacing

% Central element pattern:
for ii=1:360
   ElementPattern0(ii)=cos(pi+ii/360*2*pi)^2;
   end;
% First left element pattern:
for ii=1:360
   ElementPatternL1(ii)=cos(pi+ii/360*2*pi+Alpha)^2;
   end;
% First right element pattern:
for ii=1:360
   ElementPatternR1(ii)=cos(pi+ii/360*2*pi-Alpha)^2;
   end;
%**
% Second left element pattern:
for ii=1:360
   ElementPatternL2(ii)=cos(pi+ii/360*2*pi+2*Alpha)^2;
   end;
% Second right element pattern:
for ii=1:360
   ElementPatternR2(ii)=cos(pi+ii/360*2*pi-2*Alpha)^2;
   end;
%**
% Third left element pattern:
for ii=1:360
   ElementPatternL3(ii)=cos(pi+ii/360*2*pi+3*Alpha)^2;
   end;
```

```
% Third right element pattern:
for ii=1:360
   ElementPatternR3(ii)=cos(pi+ii/360*2*pi-3*Alpha)^2;
   end;
%**

% Weights - phase in radians
A0=1;
P0=Radius*2*pi;
A1=1;
P1=Radius*2*pi*cos(Alpha);
A2=1;
P2=Radius*2*pi*cos(2*Alpha);
A3=1;
P3=Radius*2*pi*cos(3*Alpha);

% Calculate the complex weights:
W0=A0*exp(-j*P0);
W1=A1*exp(-j*P1);
W2=A2*exp(-j*P2);
W3=A3*exp(-j*P3);

%Weighted element patterns, central element pattern no change
WeightedElementPatternL1=ElementPatternL1*W1;
WeightedElementPatternR1=ElementPatternR1*W1;
WeightedElementPatternL2=ElementPatternL2*W2;
WeightedElementPatternR2=ElementPatternR2*W2;
WeightedElementPatternL3=ElementPatternL3*W3;
WeightedElementPatternR3=ElementPatternR3*W3;

% Array pattern...

% Element pattern phases:
%Central:
for ii=1:360

ArrayElementPattern0(ii)=ElementPattern0(ii)*exp(j*(cos(pi+ii/360*
2*pi)*Radius*2*pi));
   end;
%First left:
for ii=1:360

ArrayElementPatternL1(ii)=WeightedElementPatternL1(ii)*exp(j*(cos(
pi+ii/360*2*pi+Alpha)*Radius*2*pi));
end;
%First right:
for ii=1:360

ArrayElementPatternR1(ii)=WeightedElementPatternR1(ii)*exp(j*(cos(
pi+ii/360*2*pi-Alpha)*Radius*2*pi));
end;
%Second left:
for ii=1:360

ArrayElementPatternL2(ii)=WeightedElementPatternL2(ii)*exp(j*(cos(
pi+ii/360*2*pi+2*Alpha)*Radius*2*pi));
end;
%Second right:
```

```
for ii=1:360

ArrayElementPatternR2(ii)=WeightedElementPatternR2(ii)*exp(j*(cos(
pi+ii/360*2*pi-2*Alpha)*Radius*2*pi));
end;
%Third left:
for ii=1:360

ArrayElementPatternL3(ii)=WeightedElementPatternL3(ii)*exp(j*(cos(
pi+ii/360*2*pi+3*Alpha)*Radius*2*pi));
end;
%Third right:
for ii=1:360

ArrayElementPatternR3(ii)=WeightedElementPatternR3(ii)*exp(j*(cos(
pi+ii/360*2*pi-3*Alpha)*Radius*2*pi));
end;

% Sum array pattern:
ArrayPattern=abs(ArrayElementPattern0+ArrayElementPatternL1+ArrayE
lementPatternR1+ArrayElementPatternL2+ArrayElementPatternR2+ArrayE
lementPatternL3+ArrayElementPatternR3);
ArrayPattern=20*log10(ArrayPattern);
Offset=max(ArrayPattern);
ArrayPattern=ArrayPattern-Offset;

% Comparison to the desired pattern
CostFunction=ArrayPattern-DesiredPattern; %Comparison itself
% Calculating the cost:
for ii=1:360
      if CostFunction(ii)<0
      CostFunction(ii)=0;
      end;

CostMatrix(NNN,NRadius)=CostMatrix(NNN,NRadius)+CostFunction(ii);
   end;
      CostMatrix(NNN,NRadius)

end; %end of NRadius
end; %end of NNN
```

Appendix B: Radius/element optimizing results – omnidirectional

Results from Matlab file `Optarra1.m`
Values must be multiplied with 1000
Rows 1....34 correspond to N=16...49
Columns 1....34 correspond to 0.5· λ...8.75· λ

Columns 1 through 7

2.4929	2.3740	1.8924	2.3670	3.7836	2.7327	1.5046
2.5038	2.5693	1.7401	2.3141	3.6802	2.8523	1.4054
2.4695	2.7672	1.7214	2.2560	3.3282	2.6760	1.5432
2.4065	2.8809	1.8270	2.3392	2.8282	2.3345	1.7185
2.3271	2.9361	1.9027	2.4336	2.8879	1.9471	1.7592
2.2410	2.9562	1.9873	2.4848	3.1502	1.8028	1.6802
2.1703	3.0368	2.0959	2.4552	3.3213	1.8660	1.6182
2.1253	3.0844	2.2232	2.3863	3.3699	1.9722	1.5171

2.1375	3.0995	2.3449	2.3140	3.3363	2.1181	1.3224
2.2450	3.0928	2.4421	2.2586	3.2804	2.2385	1.1632
2.3566	3.0717	2.5104	2.2258	3.2359	2.2936	1.0778
2.4726	3.0414	2.5524	2.2217	3.2321	2.3401	1.1808
2.5942	3.0061	2.5725	2.2437	3.2457	2.4282	1.2995
2.7240	2.9693	2.5755	2.2847	3.2510	2.4725	1.3911
2.8659	2.9338	2.5654	2.3343	3.2573	2.4892	1.4793
3.0305	2.9022	2.5451	2.3815	3.2686	2.4918	1.5587
3.2332	2.8769	2.5181	2.4192	3.2880	2.4921	1.5951
3.4092	2.8600	2.4869	2.4443	3.3149	2.5015	1.6042
3.5615	2.8537	2.4536	2.4555	3.3449	2.5598	1.5935
3.6946	2.8595	2.4207	2.4537	3.3763	2.6252	1.5690
3.8120	2.8788	2.3901	2.4406	3.4041	2.6987	1.5337
3.9164	2.9121	2.3641	2.4171	3.4268	2.7783	1.4965
4.0098	2.9594	2.3452	2.3849	3.4430	2.8596	1.4642
4.0940	3.0192	2.3355	2.3452	3.4506	2.9380	1.4685
4.1701	3.0896	2.3377	2.3051	3.4511	3.0097	1.5090
4.2392	3.1679	2.3543	2.2725	3.4440	3.0727	1.5498
4.3023	3.2512	2.3859	2.2420	3.4295	3.1258	1.5905
4.3601	3.3369	2.4310	2.2125	3.4098	3.1692	1.6301
4.4131	3.4229	2.4861	2.1839	3.3843	3.2031	1.6699
4.4620	3.5076	2.5484	2.1566	3.3554	3.2283	1.7096
4.5072	3.5897	2.6165	2.1314	3.3240	3.2457	1.7496
4.5490	3.6687	2.6903	2.1090	3.2891	3.2560	1.7914
4.5878	3.7441	2.7703	2.0903	3.2511	3.2601	1.8352
4.6240	3.8156	2.8587	2.0713	3.2112	3.2587	1.8851

Columns 8 through 14

2.2745	2.7162	1.9334	1.9509	2.3846	3.0239	2.2603
2.1042	2.7263	1.9817	1.4997	2.3115	2.5143	2.0302
1.9599	2.8657	1.8839	1.4667	1.8720	2.3665	1.8180
1.7899	3.0241	1.9813	1.6792	1.9684	2.7919	1.9965
1.7126	2.9634	2.3359	1.5071	2.1916	2.6475	2.0951
2.0083	2.9076	2.5403	1.4844	1.9553	2.7861	1.8191
2.4515	2.8652	2.6203	1.6886	1.7578	2.6511	1.6890
2.6146	2.5762	2.6325	1.9705	1.8500	2.6407	1.8137
2.5097	2.2752	2.5659	2.0335	2.0243	2.6241	1.9995
2.3072	2.0820	2.3447	1.8851	2.1878	2.5555	2.0236
2.1748	2.0559	2.1280	1.6818	2.2943	2.6879	1.9443
2.0886	2.2075	1.9093	1.4804	2.3149	3.0114	1.9964
2.1030	2.4747	1.7547	1.2932	2.2450	2.9891	2.2447
2.1377	2.4791	1.6783	1.1099	2.1102	2.6767	2.4971
2.2025	2.4557	1.6086	1.0833	1.9577	2.4932	2.5866
2.3013	2.4457	1.5403	1.0896	1.9030	2.4266	2.5892
2.4098	2.4920	1.4604	1.1083	1.8719	2.4422	2.6344
2.5056	2.6334	1.3912	1.1411	1.8485	2.5240	2.5850
2.5759	2.7840	1.3817	1.2106	1.8437	2.7159	2.4923
2.6202	2.9294	1.4549	1.2187	1.8503	2.9120	2.3379
2.6391	3.0542	1.5278	1.1830	1.8424	2.7805	2.1557
2.6369	3.1547	1.5960	1.1277	1.8189	2.6279	1.9467
2.6182	3.2236	1.6657	1.0793	1.7854	2.4609	1.7096
2.5865	3.2697	1.7413	1.0888	1.7547	2.3118	1.5071
2.5475	3.2971	1.8157	1.1178	1.7355	2.2344	1.4061
2.5036	3.3091	1.8759	1.1473	1.7400	2.2208	1.4236
2.4576	3.3121	1.9333	1.1748	1.7742	2.2486	1.4851
2.4113	3.3071	1.9894	1.2022	1.8337	2.3102	1.5641
2.3674	3.2977	2.0315	1.2255	1.9124	2.3975	1.6392

2.3285	3.2868	2.0622	1.2462	2.0143	2.5044	1.6992
2.2962	3.2768	2.0848	1.2644	2.1452	2.6261	1.7375
2.2717	3.2670	2.1018	1.2787	2.2484	2.7268	1.7571
2.2571	3.2638	2.1159	1.2919	2.3262	2.8093	1.7629
2.2512	3.2629	2.1302	1.3030	2.3831	2.8768	1.7642

Columns 15 through 21

1.8344	1.9687	2.0361	2.0074	1.5630	2.2837	3.1076
1.7630	1.6131	2.4458	2.2368	1.8767	2.0665	2.7973
1.8735	1.9562	2.6583	2.2955	1.5893	1.8336	1.9223
1.6981	2.2486	2.2581	2.5151	1.8605	1.6948	2.8650
1.9031	2.5271	2.5500	2.2602	1.8041	2.0334	2.5618
1.8155	2.5350	2.1472	2.1389	1.6476	1.8801	2.5666
1.5972	2.3149	2.6618	2.2507	1.4110	1.7664	2.4054
1.5533	2.2260	2.1536	2.0672	1.6693	1.6147	1.9868
1.5827	2.3481	2.5251	1.8165	1.9215	2.0110	2.5111
1.5596	2.3390	2.7404	1.7215	1.8037	2.2894	2.6346
1.5281	2.2542	2.7357	1.7168	1.4939	2.0894	2.4578
1.5446	2.1282	2.7487	1.8198	1.4699	1.8638	2.3876
1.5869	2.1223	2.7669	1.8518	1.6579	1.9302	2.1099
1.6304	2.1594	2.8256	1.8312	1.7692	2.2082	2.1249
1.6626	2.2252	2.9067	1.8949	1.7671	2.2919	2.3825
1.6725	2.2149	2.8983	1.9800	1.7112	2.2682	2.5888
1.7070	2.1054	2.7664	2.0186	1.6776	2.1978	2.5821
1.6983	1.9572	2.1650	2.0523	1.6908	2.2340	2.5258
1.6266	1.9043	1.8538	2.0759	1.7353	2.3397	2.5830
1.5070	1.9846	1.8885	2.0922	1.7863	2.4537	2.7422
1.3802	2.0797	2.1655	2.2424	1.8143	2.4795	2.7791
1.2399	2.1361	2.4245	2.4099	1.7670	2.4017	2.4030
1.1004	2.1767	2.6569	2.5055	1.6662	2.2374	2.1177
0.9986	2.1843	2.9075	2.5476	1.5407	2.0294	1.9175
0.9816	2.1607	3.1427	2.5396	1.4327	1.8390	1.8098
1.0008	2.1093	3.3482	2.4958	1.3692	1.6814	1.8099
1.0097	2.0281	3.2710	2.4139	1.3351	1.6926	1.9322
1.0160	1.9270	3.1620	2.2952	1.3137	1.8438	2.2325
1.0175	1.8167	3.0368	2.1456	1.2948	2.0733	2.6211
1.0188	1.7064	2.9014	1.9755	1.2514	2.2232	2.9763
1.0205	1.6087	2.7584	1.8233	1.1858	2.3057	3.2918
1.0243	1.5586	2.6161	1.6869	1.1025	2.3339	3.3657
1.0265	1.5408	2.4787	1.5640	1.0137	2.3206	3.3611
1.0211	1.5279	2.3565	1.4969	0.9324	2.2770	3.3315

Columns 22 through 28

2.3317	1.7791	2.2004	2.2460	2.2811	2.0729	1.9005
2.2216	1.7678	2.0905	2.2516	2.2347	1.8019	2.1221
1.6492	1.6831	2.4255	2.8452	1.7794	1.6477	2.0705
2.3174	1.7739	2.3808	2.3562	2.1132	1.5238	2.0905
2.0579	1.5802	2.2984	2.5135	1.9224	1.6417	2.0844
2.0709	1.1446	1.8387	2.7083	1.7942	1.7559	2.3684
2.3836	1.6677	1.8452	2.8557	2.2513	1.6737	2.4343
2.2320	1.6772	1.8962	2.4633	2.0979	1.7386	2.2050
2.2570	1.6880	1.6063	2.2728	2.0872	1.4837	2.1789
2.2161	1.7453	1.8606	2.0071	2.4195	1.7225	2.1008
1.7049	1.5427	2.0362	2.2631	2.3746	1.7605	1.8105
1.8023	1.4183	2.1005	2.9728	2.5424	1.7548	1.8287
1.9012	1.6507	2.0343	2.8729	2.5182	1.9052	1.8295

1.7070	1.6698	2.0374	2.5378	2.2907	1.9528	2.1187
1.5160	1.5414	2.0645	2.1897	1.9460	1.7595	2.2191
1.5062	1.3649	1.8997	2.1015	1.7099	1.5232	2.1146
1.6489	1.3869	1.8124	2.1290	1.8213	1.6339	2.0386
1.7759	1.6293	1.9476	2.1723	1.8294	1.8323	2.0676
1.7688	1.7420	2.1826	2.3173	1.7112	1.7422	1.9749
1.7010	1.7227	2.2534	2.4231	1.5407	1.5494	1.8099
1.6662	1.6451	2.2542	2.4829	1.5005	1.4813	1.7958
1.7408	1.6040	2.2217	2.4797	1.5588	1.5815	1.9313
1.9166	1.6408	2.2402	2.4350	1.6251	1.7266	2.1555
2.0091	1.7658	2.3126	2.4159	1.6345	1.7535	2.3641
2.1340	1.8938	2.3936	2.2275	1.5831	1.7072	2.4005
2.2816	1.9621	2.4361	2.0376	1.5261	1.6222	2.3726
2.3644	1.9586	2.4050	1.9356	1.5278	1.5818	2.3164
2.4039	1.8992	2.3389	1.8887	1.6018	1.6183	2.2777
2.4128	1.8112	2.2474	1.8948	1.8457	1.7189	2.2811
2.4100	1.7003	2.1354	1.9288	2.1036	1.8426	2.3149
2.3926	1.5735	2.0151	2.0043	2.2662	1.9262	2.3396
2.3622	1.4442	1.8901	2.1206	2.3811	1.9710	2.3512
2.3158	1.3313	1.7813	2.2806	2.4445	1.9774	2.3370
2.2510	1.2360	1.7048	2.4821	2.4717	1.9522	2.3037

Columns 29 through 34

2.5274	2.0458	1.4425	2.2328	2.0014	2.0730
2.1683	1.9073	1.4355	2.0974	2.3575	1.8854
2.3564	2.1520	1.8477	2.2579	2.5619	2.2854
2.7705	2.2538	1.8075	2.1490	2.5676	2.1768
2.7303	2.1440	1.7339	1.7357	2.4778	2.1940
1.9026	2.0471	1.9075	2.1690	2.5414	2.3446
2.5728	1.7846	1.8374	2.1259	2.0549	2.2418
2.8840	2.1965	1.6928	2.3458	2.2696	2.2903
2.7433	2.0605	1.9726	2.5347	2.6977	2.1649
2.7324	2.1837	1.9828	2.6255	2.4215	2.0585
2.1047	2.0711	1.7333	2.3095	2.8647	2.2931
2.0577	2.0201	1.7939	2.4588	2.7825	2.3024
2.3299	2.2834	1.6362	2.3342	2.4480	2.2346
2.5465	2.5112	1.5959	2.0176	2.1394	2.2320
2.9638	2.6557	1.6557	1.8628	2.3730	2.1059
3.2463	2.8302	2.0493	1.9088	2.5744	2.2057
3.0498	2.8043	2.1987	2.1996	2.5361	2.2246
2.6831	2.5093	2.0125	2.4690	2.7268	2.5499
2.2799	2.0568	1.6919	2.4301	2.8989	2.9472
2.0801	1.9187	1.5453	2.2465	3.1105	3.0264
2.0694	2.0823	1.7970	2.0131	3.2365	2.8376
2.0987	2.1344	1.9789	1.9291	2.8194	2.5527
2.2178	1.9688	1.9141	1.9295	2.4111	2.2304
2.3976	1.7163	1.7601	1.8596	2.3562	2.1261
2.5150	1.5971	1.6164	1.7248	2.3487	2.3069
2.5130	1.6173	1.6273	1.8377	2.2406	2.3558
2.4309	1.6062	1.7400	2.1029	2.1248	2.2373
2.1950	1.5710	1.8472	2.3850	2.2134	2.0223
1.9335	1.5377	1.8462	2.4958	2.3443	1.7527
1.7858	1.5145	1.7980	2.4968	2.4533	1.7081
1.7287	1.4679	1.7376	2.4415	2.2831	1.7148
1.7611	1.5323	1.6838	2.3685	1.9572	1.7140
1.8103	1.6471	1.6712	2.3067	1.7149	1.6780
1.8768	1.7816	1.7193	2.2930	1.6232	1.5560

Appendix C: Radius/element optimizing code – directional

Matlab file Opt5arr2.m

```
clear; % clean the memory
CostMatrix(34,34)=0; %Cost function reesults
%elementSpacingMatrix(34,34)=0; %Writes down the element spacings

DesiredPattern(1:360)=-20;
for ii=1:10
   DesiredPattern(ii+175)=0;
end;

for NNN=1:34;
   NN=7+1*NNN% elements in the array
N=5; % number of active elements in the array
Alpha=2*pi/NN; % angular element spacing

for NRadius = 1:34 % antenna radius at the center of the element
Radius=NRadius*0.25+0.25; %generates the actual radius
ElementSpacing=2*sin(Alpha/2)*Radius/cos(Alpha/2);   %   width   of
plate elements
%ElementSpacingMatrix(NNN,NRadius)=ElementSpacing;

NN
Radius
ElementSpacing

% Central element pattern:
for ii=1:360
   ElementPattern0(ii)=cos(pi+ii/360*2*pi);
   if ElementPattern0(ii)<0.1
      ElementPattern0(ii)=0.1;
      else
      ElementPattern0(ii)=0.1+ElementPattern0(ii)^2;
      end;
   end;
% First left element pattern:
for ii=1:360
   ElementPatternL1(ii)=cos(pi+ii/360*2*pi+Alpha);
   if ElementPatternL1(ii)<0.1
      ElementPatternL1(ii)=0.1;
      else
      ElementPatternL1(ii)=0.1+ElementPatternL1(ii)^2;
      end;
   end;
% First right element pattern:
for ii=1:360
   ElementPatternR1(ii)=cos(pi+ii/360*2*pi-Alpha);
   if ElementPatternR1(ii)<0.1
      ElementPatternR1(ii)=0.1;
      else
      ElementPatternR1(ii)=0.1+ElementPatternR1(ii)^2;
      end;
   end;
%**
```

```
% Second left element pattern:
for ii=1:360
   ElementPatternL2(ii)=cos(pi+ii/360*2*pi+2*Alpha);
   if ElementPatternL2(ii)<0.1
      ElementPatternL2(ii)=0.1;
      else
      ElementPatternL2(ii)=0.1+ElementPatternL2(ii)^2;
      end;
   end;
% Second right element pattern:
for ii=1:360
   ElementPatternR2(ii)=cos(pi+ii/360*2*pi-2*Alpha);
   if ElementPatternR2(ii)<0.1
      ElementPatternR2(ii)=0.1;
      else
      ElementPatternR2(ii)=0.1+ElementPatternR2(ii)^2;
      end;
   end;
%**

% Weights - phase in radians
A0=1;
P0=Radius*2*pi;
A1=1;
P1=Radius*2*pi*cos(Alpha);
A2=1;
P2=Radius*2*pi*cos(2*Alpha);

% Calculate the complex weights:
W0=A0*exp(-j*P0);
W1=A1*exp(-j*P1);
W2=A2*exp(-j*P2);

%Weighted element patterns, central element pattern no change
WeightedElementPatternL1=ElementPatternL1*W1;
WeightedElementPatternR1=ElementPatternR1*W1;
WeightedElementPatternL2=ElementPatternL2*W2;
WeightedElementPatternR2=ElementPatternR2*W2;

% Array pattern...

% Element pattern phases:
%Central:
for ii=1:360

ArrayElementPattern0(ii)=ElementPattern0(ii)*exp(j*(cos(pi+ii/360*
2*pi)*Radius*2*pi));
   end;
%First left:
for ii=1:360

ArrayElementPatternL1(ii)=WeightedElementPatternL1(ii)*exp(j*(cos(
pi+ii/360*2*pi+Alpha)*Radius*2*pi));
end;
%First right:
for ii=1:360
```

```
ArrayElementPatternR1(ii)=WeightedElementPatternR1(ii)*exp(j*(cos(
pi+ii/360*2*pi-Alpha)*Radius*2*pi));
end;
%Second left:
for ii=1:360

ArrayElementPatternL2(ii)=WeightedElementPatternL2(ii)*exp(j*(cos(
pi+ii/360*2*pi+2*Alpha)*Radius*2*pi));
end;
%Second right:
for ii=1:360

ArrayElementPatternR2(ii)=WeightedElementPatternR2(ii)*exp(j*(cos(
pi+ii/360*2*pi-2*Alpha)*Radius*2*pi));
end;

% Sum array pattern:
ArrayPattern=abs(ArrayElementPattern0+ArrayElementPatternL1+ArrayE
lementPatternR1+ArrayElementPatternL2+ArrayElementPatternR2);
ArrayPattern=20*log10(ArrayPattern);
Offset=max(ArrayPattern);
ArrayPattern=ArrayPattern-Offset;

% Comparison to the desired pattern
CostFunction=ArrayPattern-DesiredPattern; %Comparison itself
% Calculating the cost:
for ii=1:360
      if CostFunction(ii)<0
      CostFunction(ii)=0;
      end;

CostMatrix(NNN,NRadius)=CostMatrix(NNN,NRadius)+CostFunction(ii);
   end;
      CostMatrix(NNN,NRadius)

end; %end of NRadius
end; %end of NNN
```

Appendix D: Radius/element optimizing results – directional

Results from Matlab file `Opt5arr2.m`
Values must be multiplied with 1000
Rows 1....34 correspond to N=8...41
Columns 1....34 correspond to 0.5· λ...8.75· λ

Columns 1 through 7

3.9490	4.3984	3.0139	4.0665	4.1116	4.2255	3.3888
3.6984	3.3677	2.9303	3.7505	3.5857	4.1822	2.7152
3.6580	2.4632	2.4865	3.5682	3.5158	3.3970	2.3518
3.6657	2.0513	1.9607	3.2675	3.4156	3.2236	1.9132
3.7227	2.1312	1.5509	2.9886	3.0750	2.8876	1.5113
3.7582	2.2288	1.2567	2.6599	3.0532	2.5120	1.4645
3.6720	2.2255	1.1186	2.3163	3.2359	2.1944	1.5179
3.3764	2.1562	1.1400	2.0183	3.2186	2.0619	1.4133
3.1309	2.0545	1.1763	1.7329	3.0832	2.0397	1.2337
2.9287	1.9399	1.2094	1.4913	2.8760	1.9188	1.0497

2.7647	1.8244	1.2353	1.3894	2.6392	1.7437	0.9061
2.6345	1.7155	1.2523	1.4380	2.3013	1.5432	0.8139
2.5312	1.6176	1.2609	1.4860	1.9805	1.3407	0.7571
2.4492	1.5354	1.2648	1.5315	1.7480	1.1795	0.7153
2.3832	1.4740	1.2675	1.5740	1.7897	1.1245	0.6761
2.3298	1.4345	1.2737	1.6123	1.8342	1.1501	0.6373
2.2859	1.4128	1.2861	1.6440	1.8778	1.1732	0.6208
2.2498	1.4063	1.3049	1.6677	1.9190	1.1923	0.6400
2.2197	1.4108	1.3277	1.6845	1.9567	1.2065	0.6583
2.1948	1.4234	1.3526	1.6953	1.9923	1.2159	0.6753
2.1738	1.4406	1.3782	1.7009	2.0238	1.2226	0.6911
2.1560	1.4613	1.4037	1.7031	2.0375	1.2250	0.7056
2.1412	1.4838	1.4287	1.7025	2.0354	1.2234	0.7190
2.1286	1.5066	1.4532	1.7008	2.0213	1.2173	0.7314
2.1180	1.5296	1.4769	1.6983	1.9983	1.2074	0.7429
2.1090	1.5517	1.4997	1.6957	1.9697	1.1945	0.7535
2.1015	1.5732	1.5215	1.6936	1.9366	1.1781	0.7639
2.0952	1.5941	1.5426	1.6920	1.9006	1.1586	0.7741
2.0902	1.6138	1.5627	1.6907	1.8628	1.1370	0.7844
2.0860	1.6328	1.5820	1.6905	1.8242	1.1132	0.7954
2.0823	1.6509	1.6004	1.6910	1.7855	1.0894	0.8077
2.0793	1.6680	1.6179	1.6919	1.7472	1.0650	0.8224
2.0766	1.6844	1.6347	1.6938	1.7102	1.0404	0.8428
2.0742	1.6998	1.6507	1.6965	1.6745	1.0168	0.8651

Columns 8 through 14

3.6631	3.4490	4.1106	3.4249	3.9233	3.5787	3.4340
3.1478	3.4916	4.0302	2.9570	3.3461	3.3360	3.6412
2.9147	3.3597	3.7205	2.3278	2.9260	3.2783	3.8042
3.0567	2.9727	3.1127	2.0136	2.9223	2.9996	3.0734
3.0076	3.1592	2.7835	1.7232	2.4327	3.0805	2.7838
2.3138	3.0886	2.5659	1.6372	2.5306	2.6380	2.6595
2.1693	2.6289	2.3786	1.2502	2.4210	2.5853	2.2313
2.3725	2.4164	2.1830	1.1343	2.0901	2.6673	2.0874
2.3730	2.6331	1.9390	1.1803	2.0175	2.5304	2.1720
2.1784	2.7781	1.8332	1.0600	1.9583	2.3491	1.9595
1.9166	2.6856	1.8357	1.0452	1.7895	2.1578	1.6560
1.7056	2.5241	1.8345	1.0555	1.7746	2.1010	1.5482
1.5896	2.4480	1.8148	1.0505	1.7818	2.1741	1.5489
1.5268	2.4154	1.7592	1.0268	1.7607	2.1968	1.5620
1.4829	2.4055	1.6656	0.9749	1.7239	2.1731	1.5655
1.4415	2.4122	1.5491	0.8874	1.6771	2.1432	1.5556
1.3976	2.4368	1.4216	0.7790	1.5999	2.1330	1.5414
1.3416	2.3621	1.2942	0.6690	1.5169	2.1474	1.5310
1.2758	2.2552	1.1762	0.5704	1.4445	2.1711	1.5144
1.2075	2.1272	1.0803	0.4942	1.3872	2.1864	1.4910
1.1480	1.9864	1.0150	0.4565	1.3422	2.1941	1.4577
1.1172	1.8387	0.9786	0.4577	1.3063	2.1908	1.4121
1.1423	1.6911	0.9939	0.4645	1.2759	2.1622	1.3526
1.1705	1.5682	1.0183	0.4735	1.2472	2.1049	1.2821
1.1973	1.5005	1.0413	0.4904	1.2189	2.0405	1.2078
1.2230	1.5277	1.0627	0.5062	1.1890	1.9701	1.1343
1.2474	1.5548	1.0827	0.5223	1.1573	1.8958	1.0625
1.2700	1.5808	1.1012	0.5373	1.1235	1.8193	0.9975
1.2912	1.6050	1.1174	0.5515	1.0922	1.7415	0.9447
1.3104	1.6273	1.1322	0.5662	1.0639	1.6632	0.9121
1.3282	1.6475	1.1448	0.5793	1.0414	1.5865	0.9230

1.3437	1.6657	1.1557	0.5928	1.0292	1.5150	0.9437
1.3580	1.6814	1.1640	0.6048	1.0435	1.4538	0.9636
1.3702	1.6948	1.1706	0.6169	1.0643	1.4122	0.9828

Columns 15 through 21

3.4359	4.4855	3.4905	3.5813	3.3834	4.0242	3.7273
3.0034	3.2712	3.1368	3.6930	2.9174	3.6810	3.1485
2.3852	2.8769	3.1234	3.7217	2.4544	2.8908	2.9793
2.0309	2.7324	3.0688	3.2340	2.1396	2.6389	2.8506
1.8991	2.4559	3.0052	2.9456	1.8562	2.4251	2.7590
1.4260	2.3529	2.6238	2.4693	1.7125	2.2995	2.8796
1.4904	2.2745	2.8024	2.4837	1.4097	2.2778	2.5813
1.2571	2.0641	2.3031	2.2036	1.3408	2.0144	2.5397
1.2184	1.9748	2.4184	1.9662	1.1951	2.0366	2.5275
1.1988	1.9030	2.2947	1.8730	1.0740	1.8152	2.4147
0.9998	1.7852	2.2075	1.8273	1.0737	1.6682	2.1498
0.9237	1.7295	2.2331	1.8014	1.1015	1.6607	2.1222
0.8783	1.7004	2.1800	1.6996	1.0417	1.6788	2.0161
0.8831	1.6110	2.0717	1.4626	0.8719	1.6342	2.0836
0.9124	1.5259	1.9079	1.3663	0.7875	1.5133	2.1434
0.9255	1.5671	1.8631	1.3687	0.8057	1.4087	2.0364
0.9255	1.5932	1.9063	1.3406	0.8091	1.3895	1.8448
0.9046	1.6018	1.9547	1.3686	0.8025	1.3949	1.6677
0.8663	1.5917	1.9969	1.3970	0.8271	1.3917	1.6773
0.8184	1.5532	2.0280	1.4181	0.8453	1.4154	1.7057
0.7634	1.4925	2.0300	1.4345	0.8564	1.4454	1.7381
0.7052	1.4222	2.0063	1.4366	0.8576	1.4708	1.7817
0.6462	1.3574	1.9690	1.4219	0.8441	1.4875	1.8188
0.5843	1.3095	1.9448	1.3956	0.8170	1.4910	1.8711
0.5242	1.2795	1.9468	1.3662	0.7748	1.4767	1.9124
0.4658	1.2618	1.9657	1.3382	0.7217	1.4384	1.9464
0.4176	1.2489	1.9898	1.3105	0.6643	1.3790	1.9482
0.3934	1.2363	2.0057	1.2822	0.6090	1.3082	1.9214
0.4009	1.2222	2.0073	1.2528	0.5588	1.2390	1.8772
0.4097	1.2067	1.9894	1.2227	0.5121	1.1861	1.8336
0.4173	1.1899	1.9600	1.1883	0.4720	1.1590	1.8151
0.4261	1.1726	1.9202	1.1481	0.4353	1.1524	1.8195
0.4382	1.1545	1.8723	1.1032	0.4013	1.1550	1.8398
0.4501	1.1360	1.8183	1.0551	0.3768	1.1580	1.8550

Columns 15 through 21 – addition from tmp.m, N=41...45

0.4501	1.1360	1.8183	1.0551	0.3768	1.1580	1.8550
0.4635	1.1169	1.7599	1.0063	0.3668	1.1593	1.8641
0.4746	1.0977	1.6999	0.9596	0.3734	1.1577	1.8663
0.4880	1.0783	1.6409	0.9185	0.3821	1.1531	1.8604
0.4994	1.0581	1.5833	0.8878	0.3881	1.1458	1.8463

Columns 22 through 28

3.5800	3.2456	3.9160	3.5901	3.8650	3.3719	3.4956
3.2800	2.9163	3.6387	3.3124	2.9951	3.0726	4.0107
3.3437	2.5938	3.0007	2.8857	3.1199	2.7195	3.2132
3.1532	2.2483	2.6695	2.8942	3.0862	2.1932	2.6634
2.9683	1.9353	2.3878	2.7545	2.9228	1.9373	2.2794
2.5551	1.6539	2.4366	2.6665	2.6924	1.6410	2.1995
2.3773	1.5613	2.0874	2.5401	2.2955	1.4407	2.2604

2.1660	1.3312	2.1413	2.5605	2.1855	1.3881	2.0357
2.1040	1.2618	1.9330	2.3518	2.0893	1.3407	1.9740
2.0505	1.2280	1.8193	2.3098	1.9433	1.2019	1.9335
1.6933	1.1039	1.8586	2.2364	1.8318	1.2108	1.7645
1.7429	0.9880	1.7749	2.4457	1.8364	1.0411	1.7559
1.6211	0.9893	1.5553	2.0958	1.7386	1.0538	1.5818
1.6286	0.9531	1.5839	2.0336	1.5514	1.0312	1.7146
1.6705	0.9313	1.4992	2.1111	1.5722	0.9373	1.6055
1.6555	0.9354	1.4350	1.9586	1.5595	0.9432	1.4747
1.4997	0.9009	1.4629	1.9542	1.4987	0.9141	1.4948
1.2835	0.7703	1.4692	2.0343	1.4973	0.8481	1.4643
1.2646	0.7238	1.3747	2.0819	1.5370	0.8146	1.3334
1.2703	0.7371	1.2399	1.9621	1.5417	0.8008	1.3217
1.2596	0.7477	1.2228	1.7418	1.4118	0.7763	1.3470
1.2515	0.7552	1.2552	1.5804	1.2355	0.7021	1.3462
1.2815	0.7713	1.2853	1.6066	1.2080	0.6876	1.2747
1.3123	0.7888	1.3158	1.6288	1.2175	0.6980	1.1694
1.3398	0.8030	1.3435	1.6514	1.2190	0.7061	1.1616
1.3590	0.8115	1.3679	1.6687	1.2109	0.7198	1.1910
1.3669	0.8102	1.3880	1.7066	1.2149	0.7386	1.2197
1.3622	0.8065	1.4021	1.7509	1.2442	0.7530	1.2465
1.3442	0.7900	1.4090	1.7879	1.2696	0.7628	1.2715
1.3160	0.7595	1.4057	1.8259	1.2900	0.7745	1.2932
1.2846	0.7191	1.3893	1.8499	1.3056	0.7800	1.3123
1.2552	0.6704	1.3548	1.8677	1.3142	0.7816	1.3276
1.2302	0.6162	1.3027	1.8721	1.3152	0.7741	1.3392
1.2104	0.5624	1.2390	1.8460	1.3071	0.7655	1.3454

Columns 29 through 34

3.6444	4.1209	3.4541	3.5856	3.4042	3.9468
3.1617	3.0108	2.9755	3.8124	3.2131	3.0649
2.7543	2.8203	2.8067	3.2387	2.7953	2.5737
2.7721	3.0626	2.2656	2.6371	2.5817	2.8395
2.7630	2.8293	2.0743	2.4817	2.7321	2.8065
2.6965	2.5429	1.8522	2.1643	2.7487	2.6540
2.5373	2.3625	1.5583	2.1921	2.7375	2.4178
2.5747	2.2988	1.4481	2.1080	2.5070	2.1812
2.3445	2.0774	1.2776	1.9068	2.4059	1.9981
2.3812	1.8527	1.2105	1.9332	2.2186	1.9316
2.1053	1.8955	1.1516	1.7340	2.3028	1.9267
2.2046	1.7378	1.0943	1.7855	2.0643	1.6779
2.1100	1.8044	1.0966	1.6078	2.1237	1.7134
2.1261	1.6387	1.0728	1.6653	2.0088	1.6259
2.1933	1.5135	0.9052	1.5614	2.1503	1.6502
1.9539	1.5470	0.9307	1.4553	2.0143	1.6502
1.9391	1.4658	0.9359	1.5603	1.9321	1.4336
2.0415	1.4983	0.8946	1.4746	1.9751	1.3851
2.0170	1.4967	0.8979	1.4063	1.8399	1.4006
1.8762	1.4530	0.8802	1.4248	1.8731	1.4201
1.9109	1.4152	0.8216	1.4234	1.9397	1.4369
1.9683	1.4024	0.7493	1.3370	2.0078	1.4498
1.9977	1.4447	0.7185	1.2468	1.8706	1.4308
1.9026	1.4442	0.7044	1.2535	1.8256	1.3840
1.7264	1.3420	0.6835	1.2576	1.8363	1.3479
1.5545	1.2065	0.6543	1.2522	1.9248	1.3341
1.5675	1.1802	0.6606	1.2087	1.9392	1.3523
1.5889	1.1886	0.6721	1.1331	1.8583	1.3495

1.6031	1.1932	0.6815	1.1227	1.7249	1.2739
1.6211	1.1947	0.6961	1.1481	1.5650	1.1785
1.6370	1.1892	0.7108	1.1725	1.5347	1.1648
1.6627	1.1983	0.7255	1.1957	1.5654	1.1740
1.6981	1.2207	0.7385	1.2185	1.5847	1.1823
1.7275	1.2399	0.7461	1.2392	1.5960	1.1835

Appendix E: Antenna pattern optimizing code for 7 active element antenna

Matlab file Moreal06.m

```
clear; % clean the memory
NN=35; % elements in the array
N=7; % active elements in the array
Alpha=2*pi/NN; % angular element spacing
Radius=(0.25/(1-cos(Alpha)))*0.26; % antenna radius at the center
of the element
     % this will cause a 90 degree phase shift for the first side
elements
ElementSpacing=2*sin(Alpha/2)*Radius/cos(Alpha/2);   %   width   of
plate elements

% The desired pattern: (please check the range and central
values!!!)
DesiredPattern=[1:360];
for ii=DesiredPattern
   DesiredPattern(ii)=-20;
   end;
%for ii=1:340
%   DesiredPattern(ii+10)=-20;
%   end;
for ii=1:20
   DesiredPattern(ii+170)=-3;
   end;
for ii=1:10
   DesiredPattern(ii+175)=0;
end;

% Central element pattern:
ElementPattern0=[1:360];
for ii=ElementPattern0
   ElementPattern0(ii)=cos(pi+ii/360*2*pi);
   if ElementPattern0(ii)<0.1
      ElementPattern0(ii)=0.1;
      else
      ElementPattern0(ii)=0.1+ElementPattern0(ii)^2;
      end;
   end;
%**
% First left element pattern:
ElementPatternL1=[1:360];
for ii=ElementPatternL1
   ElementPatternL1(ii)=cos(pi+ii/360*2*pi+Alpha);
   if ElementPatternL1(ii)<0.1
      ElementPatternL1(ii)=0.1;
      else
      ElementPatternL1(ii)=0.1+ElementPatternL1(ii)^2;
```

```
      end;
   end;

% First right element pattern:
ElementPatternR1=[1:360];
for ii=ElementPatternR1
   ElementPatternR1(ii)=cos(pi+ii/360*2*pi-Alpha);
   if ElementPatternR1(ii)<0.1
      ElementPatternR1(ii)=0.1;
      else
      ElementPatternR1(ii)=0.1+ElementPatternR1(ii)^2;
      end;
   end;

%**
% Second left element pattern:
ElementPatternL2=[1:360];
for ii=ElementPatternL2
   ElementPatternL2(ii)=cos(pi+ii/360*2*pi+2*Alpha);
   if ElementPatternL2(ii)<0.1
      ElementPatternL2(ii)=0.1;
      else
      ElementPatternL2(ii)=0.1+ElementPatternL2(ii)^2;
      end;
   end;

% Second right element pattern:
ElementPatternR2=[1:360];
for ii=ElementPatternR2
   ElementPatternR2(ii)=cos(pi+ii/360*2*pi-2*Alpha);
   if ElementPatternR2(ii)<0.1
      ElementPatternR2(ii)=0.1;
      else
      ElementPatternR2(ii)=0.1+ElementPatternR2(ii)^2;
      end;
   end;
%**
% Third left element pattern:
ElementPatternL3=[1:360];
for ii=ElementPatternL3
   ElementPatternL3(ii)=cos(pi+ii/360*2*pi+3*Alpha);
   if ElementPatternL3(ii)<0.1
      ElementPatternL3(ii)=0.1;
      else
      ElementPatternL3(ii)=0.1+ElementPatternL3(ii)^2;
      end;
   end;

% Third right element pattern:
ElementPatternR3=[1:360];
for ii=ElementPatternR3
   ElementPatternR3(ii)=cos(pi+ii/360*2*pi-3*Alpha);
   if ElementPatternR3(ii)<0.1
      ElementPatternR3(ii)=0.1;
      else
      ElementPatternR3(ii)=0.1+ElementPatternR3(ii)^2;
      end;
   end;
```

```
%**
MinCost=100000; % Initializing MinCost
OptimumW1=1; % Initializing optimum weight
OptimumW2=1; % Initializing optimum weight
OptimumW3=1; % Initializing optimum weight

% Weights...please check the steps and end values!!!!
% Outer loop weight part A1
for A1=0.8:0.1:1.5
   %A1
% Outer loop weight part P1
for P1=10:10:40
   %P1
% Mid loop weight part A2
for A2=0.5:0.1:1.2
   %A2
% Mid loop weight part P2
for P2=70:10:110
   %P2
% Inner loop weight part A3
for A3=0.0:0.2:1.2
   A1
   P1
   A2
   P2
   A3
   %A3
% Inner loop weight part P3
for P3=0:30:330
   %A1
   %P1
   %A2
   %P2
   %A3
   %P3
% Central element - the value is fixed:
Amplitude0=1;
Phase0=0; % the phase is 0

% Set values for first left:
AmplitudeL1=A1;
PhaseL1=P1*2*pi/360; %the value is in degrees

% Set values for first right:
AmplitudeR1=A1;
PhaseR1=P1*2*pi/360; %the value is in degrees

% Set values for second left:
AmplitudeL2=A2;
PhaseL2=P2*2*pi/360; %the value is in degrees

% Set values for second right:
AmplitudeR2=A2;
PhaseR2=P2*2*pi/360; %the value is in degrees

% Set values for third left:
AmplitudeL3=A3;
PhaseL3=P3*2*pi/360; %the value is in degrees
```

```
% Set values for third right:
AmplitudeR3=A3;
PhaseR3=P3*2*pi/360; %the value is in degrees

% Calculate the complex weights:
W1=AmplitudeL1*exp(j*PhaseL1);
W2=AmplitudeL2*exp(j*PhaseL2);
W3=AmplitudeL3*exp(j*PhaseL3);

%Weighted element patterns, central element pattern no change
WeightedElementPatternL1=ElementPatternL1*W1;
WeightedElementPatternR1=ElementPatternR1*W1;
WeightedElementPatternL2=ElementPatternL2*W2;
WeightedElementPatternR2=ElementPatternR2*W2;
WeightedElementPatternL3=ElementPatternL3*W3;
WeightedElementPatternR3=ElementPatternR3*W3;

% Array pattern...

% Element pattern phases:
%Central:
for ii=1:360

ArrayElementPattern0(ii)=ElementPattern0(ii)*exp(j*(cos(pi+ii/360*
2*pi)*Radius*2*pi));
   end;
%First left:
for ii=1:360

ArrayElementPatternL1(ii)=WeightedElementPatternL1(ii)*exp(j*(cos(
pi+ii/360*2*pi+Alpha)*Radius*2*pi));
end;
%First right:
for ii=1:360

ArrayElementPatternR1(ii)=WeightedElementPatternR1(ii)*exp(j*(cos(
pi+ii/360*2*pi-Alpha)*Radius*2*pi));
end;
%Second left:
for ii=1:360

ArrayElementPatternL2(ii)=WeightedElementPatternL2(ii)*exp(j*(cos(
pi+ii/360*2*pi+2*Alpha)*Radius*2*pi));
end;
%Second right:
for ii=1:360

ArrayElementPatternR2(ii)=WeightedElementPatternR2(ii)*exp(j*(cos(
pi+ii/360*2*pi-2*Alpha)*Radius*2*pi));
end;
%Third left:
for ii=1:360

ArrayElementPatternL3(ii)=WeightedElementPatternL3(ii)*exp(j*(cos(
pi+ii/360*2*pi+3*Alpha)*Radius*2*pi));
end;
%Third right:
```

```
for ii=1:360

ArrayElementPatternR3(ii)=WeightedElementPatternR3(ii)*exp(j*(cos(
pi+ii/360*2*pi-3*Alpha)*Radius*2*pi));
end;

% Sum array pattern:
ArrayPattern=abs(ArrayElementPattern0+ArrayElementPatternL1+ArrayE
lementPatternR1+ArrayElementPatternL2+ArrayElementPatternR2+ArrayE
lementPatternL3+ArrayElementPatternR3);
ArrayPattern=20*log10(ArrayPattern);
Offset=max(ArrayPattern);
ArrayPattern=ArrayPattern-Offset;

% Comparison to the desired pattern
if ArrayPattern(180)==0
CostFunction=ArrayPattern-DesiredPattern; %Comparison itself
% Calculating the cost:
Cost=0; % Initialize Cost
for ii=1:360
   if CostFunction(ii)<0
      CostFunction(ii)=0;
      end;
   Cost=Cost+CostFunction(ii);
   end;
if MinCost>Cost
   MinCost=Cost;
   OptimumW1=W1;
   OptimumW2=W2;
   OptimumW3=W3;
   end;
end;

%A1
%P1
%OptimumW1

end; % end of inner loop weight part P3
end; % end of innerr loop weight part A3

end; % end of mid loop weight part P2
end; % end of mid loop weight part A2

end; % end of outer loop weight part P1
end; % end of outer loop weight part A1

%** Print out data:
MinCost
abs(OptimumW1)
angle(OptimumW1)*360/(2*pi)
abs(OptimumW2)
angle(OptimumW2)*360/(2*pi)
abs(OptimumW3)
angle(OptimumW3)*360/(2*pi)

%Optimal pattern:
WeightedElementPatternL1=ElementPatternL1*OptimumW1;
WeightedElementPatternR1=ElementPatternR1*OptimumW1;
```

```
WeightedElementPatternL2=ElementPatternL2*OptimumW2;
WeightedElementPatternR2=ElementPatternR2*OptimumW2;
WeightedElementPatternL3=ElementPatternL3*OptimumW3;
WeightedElementPatternR3=ElementPatternR3*OptimumW3;

% Element pattern phases:
%Central:
for ii=1:360

ArrayElementPattern0(ii)=ElementPattern0(ii)*exp(j*(cos(pi+ii/360*
2*pi)*Radius*2*pi));
   end;
%First left:
for ii=1:360

ArrayElementPatternL1(ii)=WeightedElementPatternL1(ii)*exp(j*(cos(
pi+ii/360*2*pi+Alpha)*Radius*2*pi));
end;
%First right:
for ii=1:360

ArrayElementPatternR1(ii)=WeightedElementPatternR1(ii)*exp(j*(cos(
pi+ii/360*2*pi-Alpha)*Radius*2*pi));
end;
%Second left:
for ii=1:360

ArrayElementPatternL2(ii)=WeightedElementPatternL2(ii)*exp(j*(cos(
pi+ii/360*2*pi+2*Alpha)*Radius*2*pi));
end;
%Second right:
for ii=1:360

ArrayElementPatternR2(ii)=WeightedElementPatternR2(ii)*exp(j*(cos(
pi+ii/360*2*pi-2*Alpha)*Radius*2*pi));
end;
%Third left:
for ii=1:360

ArrayElementPatternL3(ii)=WeightedElementPatternL3(ii)*exp(j*(cos(
pi+ii/360*2*pi+3*Alpha)*Radius*2*pi));
end;
%Third right:
for ii=1:360

ArrayElementPatternR3(ii)=WeightedElementPatternR3(ii)*exp(j*(cos(
pi+ii/360*2*pi-3*Alpha)*Radius*2*pi));
end;

% Sum array pattern:
ArrayPattern=abs(ArrayElementPattern0+ArrayElementPatternL1+ArrayE
lementPatternR1+ArrayElementPatternL2+ArrayElementPatternR2+ArrayE
lementPatternL3+ArrayElementPatternR3);
ArrayPattern=20*log10(ArrayPattern);
Offset=max(ArrayPattern);
ArrayPattern=ArrayPattern-Offset;

%**
```

```
%Plot ArrayPattern:
x=-179:180;
figure(1);
plot(x,ArrayPattern,'r','Linewidth',3);
hold on;
plot(x,DesiredPattern,'b','Linewidth',1);
axis([-180 180 -40 0])
axis('on')
xlabel('Degrees in horizontal plane')
ylabel('Relative gain, offset=')
set(gca,'GridLineStyle',':')
set(gca, 'xtick',[-180 -150 -120 -90 -60 -30 0 30 60 90 120 150
180])
grid on


%Plot ArrayPattern, enlarged:
x=-29:30;
for ii=1:60
   PlotArrayPattern(ii)=ArrayPattern(ii+150);
   end;
figure(2);
plot(x,PlotArrayPattern,'r','Linewidth',3);
axis([-30 30 -10 0])
axis('on')
xlabel('Degrees in horizontal plane')
ylabel('Relative gain, offset=')
set(gca,'GridLineStyle',':')
set(gca, 'xtick',[-30 -20 -10 0 10 20 30])
set(gca, 'ytick',[-10 -9 -8 -7 -6 -5 -4 -3 -2 -1 0])
grid on
```

Appendix F: Gain for the cylindrical array and isotropic elements

Appendix G: Gain for the cylindrical array and directional elements

Appendix H: Gain for linear array and directional elements